TALLINN UNIVERSITY OF TECHNOLOGY
School of Information Technologies

Waqas Rashid, 184604IVEM

Piezoelectric Based MEMS Accelerometer Design and Optimization

Master's Thesis

Supervisor: Mehadi Hassan Ziko
(Ph.D.)

Co. Supervisor: Ants Koel
(Assoc. Professor)

Tallinn 2021

TALLINNA TEHNIKAÜLIKOOL
Infotehnoloogia teaduskond

Waqas Rashid, 184604IVEM

Piesoelektrilise mems-kiirendusanduri disain ja optimeerimine

Magistritöö

Juhendaja: Mehadi Hasan Ziko
(Doktorikraad)

Kaasjuhendaja: Ants Koel
(Seostada Professor)

Tallinn 2021

Author’s declaration of originality

I hereby certify that I am the sole author of this thesis. All the used materials, references to the literature and the work of others have been referred to. This thesis has not been presented for examination anywhere else.

Author: Waqas Rashid

04.01.2021

Abstract

Accelerometers are electromechanical devices used to sense the acceleration, orientation, vibration and shock of a body. Their use in defence, medical and consumer electronics has increase very rapidly in recent times and is expected to grow in the same manner. Piezoelectric base MEMS accelerometer has got great attention in the recent years, due to its self-generating properties such as long-term stability and higher band width, although the use of Lead (Pb) containing hazardous materials is still a problem. The advancement in MEMS technology transformed the accelerometers use as it can be manufactured at much smaller scale more like a microelectronics.

The objective of the thesis is to design a MEMS accelerometer using AlN (Aluminium Nitride) piezoelectric material to achieve better overall efficiency and an environmentally friendly solution. One single axis and one tri-axial accelerometer was designed, total of 23 geometrical structures were designed of which 15 were for the single axis design and rest of 8 were for the tri-axial design. MATLAB were used for the mathematical analysis and COMSOL Multiphysics were used to perform FEM model simulations. Design parameters were optimized for both accelerometers and from the design of optimized parameter of single axis accelerometer the voltage sensitivity on sensing axis was 1.04mv, deflection in beam was 10.44nm and 586Hz eigenfrequency was recorded with acceleration of 1g. And for three axis accelerometer deflection for x, y, z axis with acceleration of 1g was 38.01nm, 5.39nm, 4.46nm, as the voltage signal for the x, y axis acceleration is only on their respective sensing beams so it was recorded to be 1.09mv for x and 1.01mv for y and for z axis acceleration both directional beams collect a signal hence we got 6.11 mv at x-directional and 7.4 mv at y-directional beams, while the eigenfrequency was recorded to be 2.5 KHz.

This thesis is written in English and is 86 pages long, including 6 chapters, 74 figures and 28 tables.

List of abbreviations and terms

DETF	Double-ended tuning- fork
TBTFs	Triple beam tuning forks
FEM	Finite element modelling
AlN	Aluminium nitride
PZT	Lead zirconate titanate
MEMS	Microelectromechanical system
MST	Microsystem technology
Pb	Lead
IBM	International Business Machines Corporation
DC	Direct Current
CPR	Cardiopulmonary resuscitation
ZnO	Zinc oxide
LiNbO3	Lithium niobate
SNR	Signal to Noise Ratio
Si	Silicon
SiO2	Silicon dioxide
CMOS	Complementary metal-oxide-semiconductor

Table of contents

List of figures

List of tables

1 Introduction

MEMS or microelectromechanical system is field of research [1], where mechanical elements like membranes or cantilevers had been manufactured at a scale more alike the microelectronics circuits than to the standard machining mechanisms. Terms like micromachining and microsystem technology (MST) are used in the Japan and Europe respectively to describe the same technology. Although microelectronics and MEMS had some similarities, but they are two completely different field. MEMS structures have cavities, cantilevers, holes, membranes, channels, etc, while electronics circuits are solid structures in its nature. Size of these devices are below 100µm, to machine all these features inside such as small size the machining technique called micro-fabrication technology is used instead of standard machining. Some very popular components in market utilizing the MEMS technology are inertial and pressure sensors, MEMS accelerometers, bio-MEMS, optical MEMS, RF MEMS etc[2][3].

Accelerometers are electronics devices that can sense and measure the acceleration and orientation of an object. They are basically transducers which convert mechanical acceleration into an electrical signal. These sensors can measure different types of acceleration such a vibratory acceleration (variation with time), linear acceleration, constant acceleration, (gravitational, quasi static(tilt)). It can be classified by their sensing capabilities, such as single axis and multiple axis accelerometers. Single-axis accelerometer can sense the acceleration in just one direction and is the most used accelerometer. Similarly, as the named indicates multiple axis accelerometer is capable of sensing acceleration in multiple directions. Accelerometer with multiple axis acceleration sensing capabilities take more footprint and costs more.

Different transducing techniques such capacitive, piezoresistive, piezoelectric, thermal, optical and many other are used to design an accelerometer. Among all the different transduction techniques mentioned, piezoelectric transducers because of its advantages such as self-generating, wide frequency range, good linearity, low output noise, and easy to integrate in electronic circuits, is the most promising and hence more popular in the researchers in recent times[4][5].

Market of accelerometer and gyroscope is forecasted to reach USD 3.50 Billion by 2022. High end market is expected to increase at a Compound annual growth rate of 3.8% between 2016 and 2022, to increase from USD 1.59 Billion in 2015 to USD 2.07 Billion by year 2022. Market

is driven by the increasing defence budgets globally and a huge demand for the use of these inertial sensors in the consumer electronics industries, strict regulations on the automotive industries, advancement and cheapness of MEMS technology, trend of automations in homes and industries, figure 1.1 shows the market trend.

In this thesis we had design and optimized a single and three axis accelerometers based on the piezoelectric transduction technique, using a Lead (Pb) free material AlN (aluminium nitride) for the piezoelectric transduction.

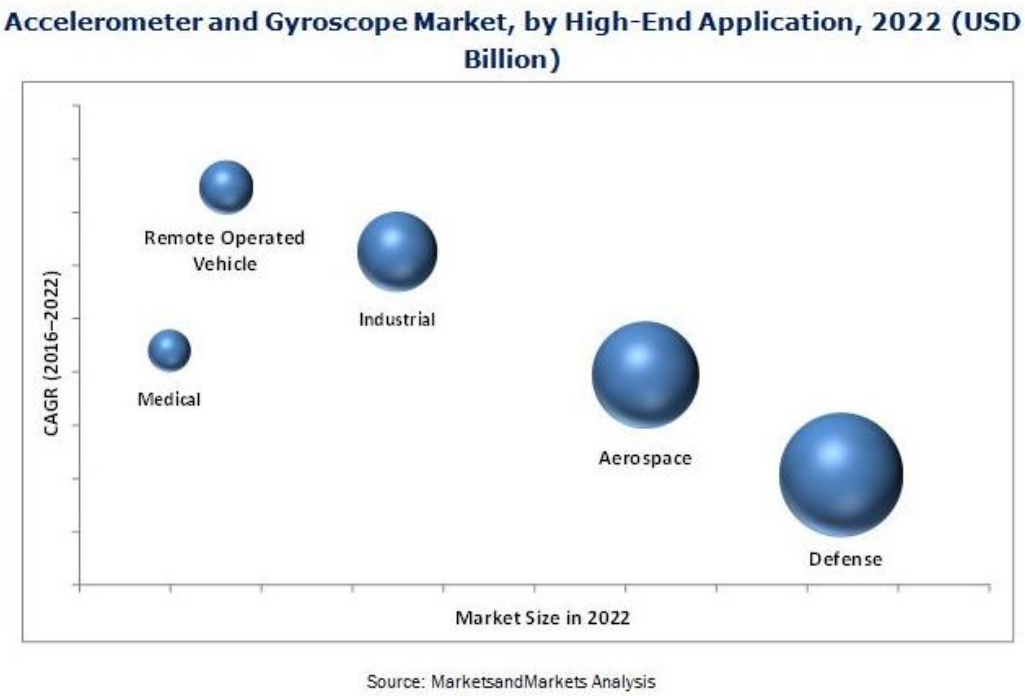

Figure 1. 1. Shows the trend of market till 2022 (source: marketsandmarkets)

1.1 Motivation behind the thesis

Market forecasting of accelerometers is very promising, Its used in defence, medical and consumer electronics increase very rapidly and is expected to continue in the same manner. Accelerometer can be design using different techniques such as optical technique, Thermal technique, piezoelectric technique, piezoresistive technique, capacitive technique, all these methods are discussed in detail in next chapter.

Among all these different available methods Piezoelectric base MEMS accelerometer has got great attention in the recent years, so we decided to base our work on this technique. The reasons for the acceptance of piezoelectric based accelerometers are its properties; self-

generating and no need for external power source to function, has a wide frequency range, good linearity, low output noise and is can be easily integrated in electronic circuits.

As the previous research are mostly done on PZT material, but because of its hazards natural as it contains elements like Lead, according to the European union ‘’ Restriction of Hazardous Substances Directive’’ which is also known as ‘’ lead free directive’’ Union member states are directed to not used a list of ten substances and lead is one of them. It is expected that a governmental regulation on PZT usage maybe introduced in next 8 to 10 years, which will pose a significant threat to piezoelectric industries which is mostly PZT. Hence this will create an opportunity or need for more research in preparing alternative piezoceramics for the piezoelectric device market.

AlN (aluminium nitride) is consider for this research to have an environmentally friendly solution to minimize the use of material which contains the Lead (Pb).

1.2 Problem statement

Accelerometer are electromechanical device used to sense the acceleration, orientation, vibration and shock in a body. Piezoelectric base MEMS accelerometer has got great attention in the recent years, due to its self-generating properties such as long-term stability and higher band width. Although Improvement in the overall efficiency of the device while using the environment friendly (lead free) materials is needed.

In this research we will design a MEMS accelerometer using AlN (Aluminium Nitride) piezoelectric material to achieve better overall efficiency and an environmentally friendly solution.

Structure of thesis

Chapter 1: Introduction

This chapter is about the general introduction of the topic, problem statement, motivation behind this research and market forecast.

Chapter 2: State of the art review

In this chapter a details study about the accelerometer's different types, its transduction methods and MEMS technology, with piezoelectric materials and piezoelectric based accelerometers with its different bending structure of Unimorph and bimorph and its mode d31 and d33 with its application are described. Research papers review is reported after ward with discussion about the common trends in the market and it end of the chapter materials properties of aluminium nitride (AlN) and its comparison with PZT is reported.

Chapter 3: Static analysis

Concept design was chosen for single axis accelerometers and static analysis were performed for that designs using MATLAB to get the optimal design parameters.

Chapter 4: Finite element modelling (FEM)

Both 1-axis and 3-axis accelerometers were design using COMSOL Multiphysics. Accelerometer were design initially with the preliminary parameter we selected from literature study and FEM analysis were performed on those design and optimized design parameters were chosen.

Chapter 5: Discussions of the mathematical and FEM modelling

Data we got from mathematical modelling and FEM model's simulations were examined and final design parameters were derived from those data based on the best performance of the accelerometers**.**

Chapter 6: Conclusion and future work

This chapter includes conclusion of the thesis and recommends the future works which can be performed in this research.

2 State of the art review

This chapter represents the research conducted in the field MEMS and accelerometers and advancement or progress made over time. The advantage and the possibilities that make it useful and its large number of applications, different method and techniques used by researcher in the past and the benefits and challenges those techniques carry along with them. The comparison of the different techniques used and their advantages and disadvantages.

2.1 MEMS technology advantages

It is understood that the development cost of MEMS components is way more compare to conventional electronics or its other competitors and cannot be ignored, but the technology is capable to offer some unique benefits. The motivating factors to use the MEMS can be classified into three big classes[6].

1. **Miniaturization of the existing devices:** For example, the gyroscope which weighted in several kg's and volume of 1000cm^2 is reduced into a chip of few grams with volume of 0.5cm^3 after its silicon production.
2. **Using physical principles that do not work at larger scale:** A typical example is given by the biochips where electric field are used to pump the reactant around the chip. This so called electro-osmotic effect based on the presence of a drag force in the fluid works only in channels with dimension of a fraction of one mm, that is, at micro-scale [1].
3. **Developing tools for operation in the micro-world:** In 1986 H. Rohrer and G. Binnig at IBM were awarded the Nobel prize in physics for their work on scanning tunnelling microscope. This work heralded the development of a new class of microscopes (atomic force microscope, scanning near-field optical microscope...) that shares the presence of micromachined sharp microtips with radius below 50 nm. This micro-tool was used to position atoms in complex arrangement, writing Chinese character or helping verify some prediction of quantum mechanics [1].

It is certain that miniaturization is a very important driver behind the MEMS development. Normally miniaturization is considered good in term of cost reduction as by decreasing the use of materials and batch fabrication, but even more important is the increase in the applicability.

As the reduction in mass and volume of the MEMS device make is possible to place it in many places where due to size constraint the traditional components are not possible to used.

Apart from the importance of miniaturization and benefits its offers, it is not enough to justify the development of MEMS. Microfabrication process cannot compete with other conventional production methods. If the traditional bulky components are cheap and reliable and small enough to be used, then there is no need to make it small.

MEMS technology enables something different and more important, at the time you make things small you can also make it smarter. For example, some non-MEMS airbag crash sensor are based on a spring or a magnetic field retaining a metal ball, with the rapid deacceleration the ball moves and connects two point inside the sensor. The method is simple and cheap, but connection can be contaminated, or the ball may have been blocked, it is not easy to find out that the sensor will work on not. While on the other hand the MEMS device can be design in way to have a build-in self-testing mechanism, so the system can check its functionality every you start the engine.

Another advantage of the MEMS is the integration of the system. Instead of having a series of external components (sensor, inductor...) connected by wire or soldered to a printed circuit board, the MEMS on silicon can be integrated directly with the electronics. Whether it is on the same chip or in the same package it results in increased reliability and decreased assembly cost, opening new application opportunities. MEMS technology not only makes things smaller but often makes them better[1].The rapid advancement of the microelectromechanical systems (MEMS) technology in the past decades or so, enables the researchers/engineers to design different sensors with a low footprint which consume low power.

2.2 Different transduction technics used for accelerometers

Different methods which are used to convert the displacement of the body due to acceleration into a signal which is measurable, transducing technics such capacitive, piezoresistive, piezoelectric, thermal, optical and many other are used to design an accelerometer. More common of those technics are described here.

2.2.1 Capacitive technique

Capacitor can be used both as sensors and actuators, capacitive transduction technic is the one more research has been done upon, because of its advantages like high sensitivity, low temperature sensitivity, low noise, linearity and small footprint. In this technique the sensing relies on the change of capacitance produced by the change in geometry of the plates when a system had change in the velocity and is independent of the on base material used[7]. Figure 2.1 shows the Implementation of the band change accelerometer with its equivalent circuit diagram.

Because of its outstanding overall sensitivity and low sensitivity to the temperature made it one of favourite choice of the researchers [8][9].

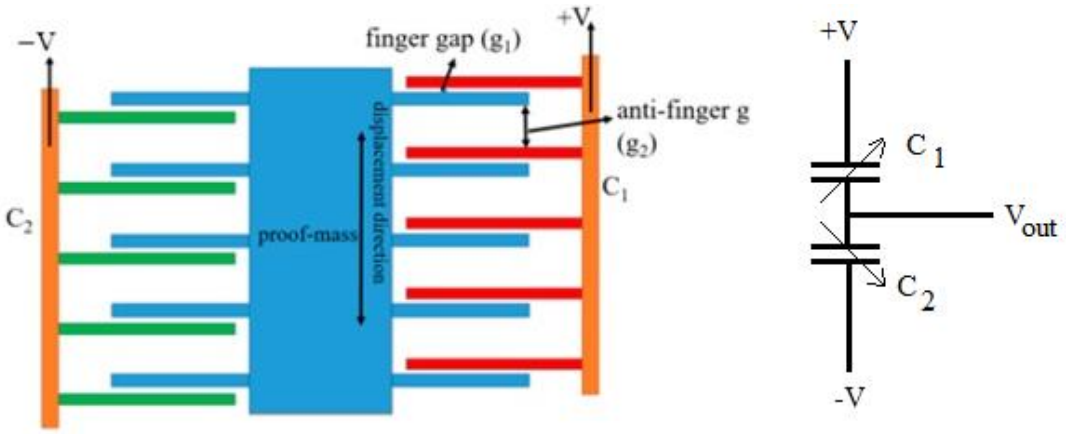

Figure 2. 1. Gap-change capacitive accelerometer and its equivalent circuit.

2.2.2 Piezoresistive technique

This technique uses the effect exhibited by various materials, which under the applied pressure exhibit a change in its resistivity [10]. Contrary to the capacitance change sensing technique in the seismic mass, piezoresistive accelerometer use the properties of the resistance change of the piezoresistive materials to convert the mechanical strain into the DC output power. Figure 2.2 shows a design of piezoresistive technique deployment [11][12][13].

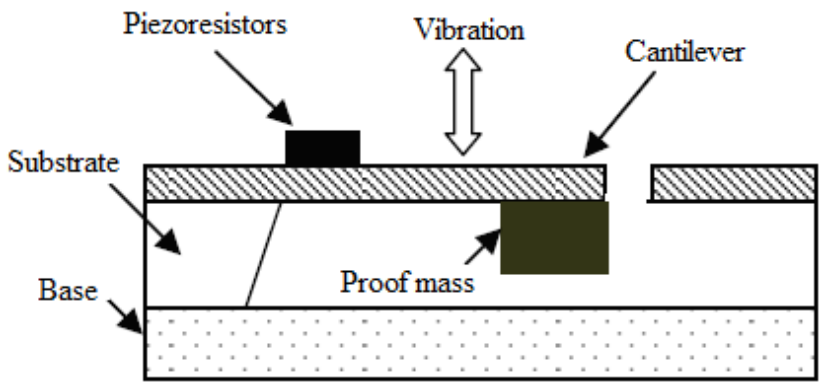

Figure 2. 2 A typical piezoresistive accelerometer using cantilever design

2.2.3 Piezoelectric technique

This actuation technique is based upon the piezoelectric effect of the piezoelectric materials. A common structure of the piezoelectric based accelerometer is shown in figure 2.3 A cantilever beam is fixed at the one end and having a proof mass attached at the free. A piezoelectric active material is located on the surface of the fixed end of the beam. When the structure experience pressure or acceleration, it will cause a displacement in the proof mass which will eventually produce a deformation in beam. Thus, the piezoelectric film located on surface of the beam will experience tensile or compressive stress which will lead to generation of the electric charges on its surface due to its unique piezoelectric effect[14][15].

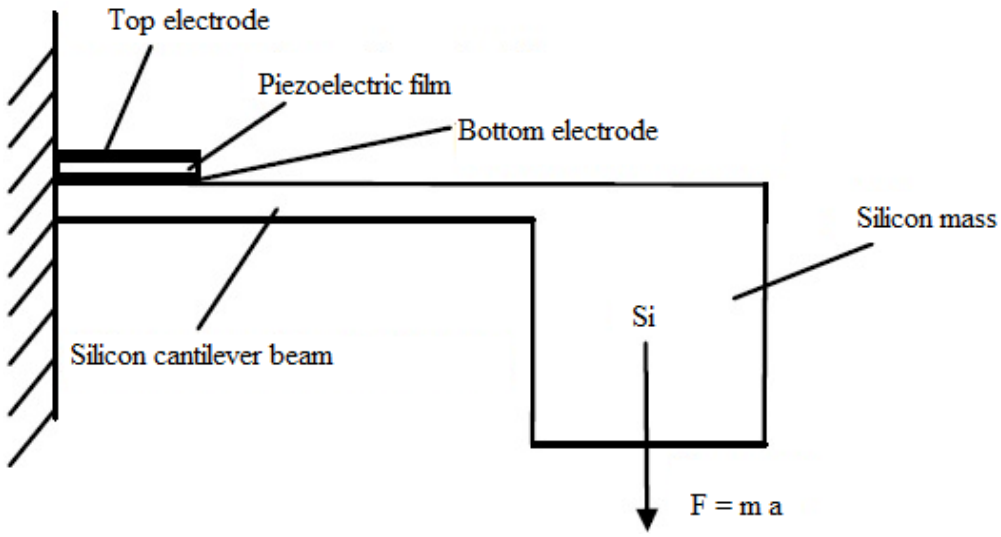

Figure 2. 3. Principle schematic of piezoelectric accelerometer

2.2.4 Thermal accelerometer technique

This is a comparatively new technique, which is based on the principle of convection of the heated gas molecules within as sealed cavity. A general structure of single axis thermal accelerometer is shown figure 2.4(a). A symmetrically placed temperature sensor read the same temperature under no acceleration condition, when it experience an acceleration in one direction it causes the temperature to skew as shown in figure 2.4(b). As the temperature starts to increase on one side and decrease on other, sensors begin to read different temperature as shown in figure 2.4(c). The difference in the reading of the both sensor(ΔT) is then used to measure the acceleration of the object [16][17][18].

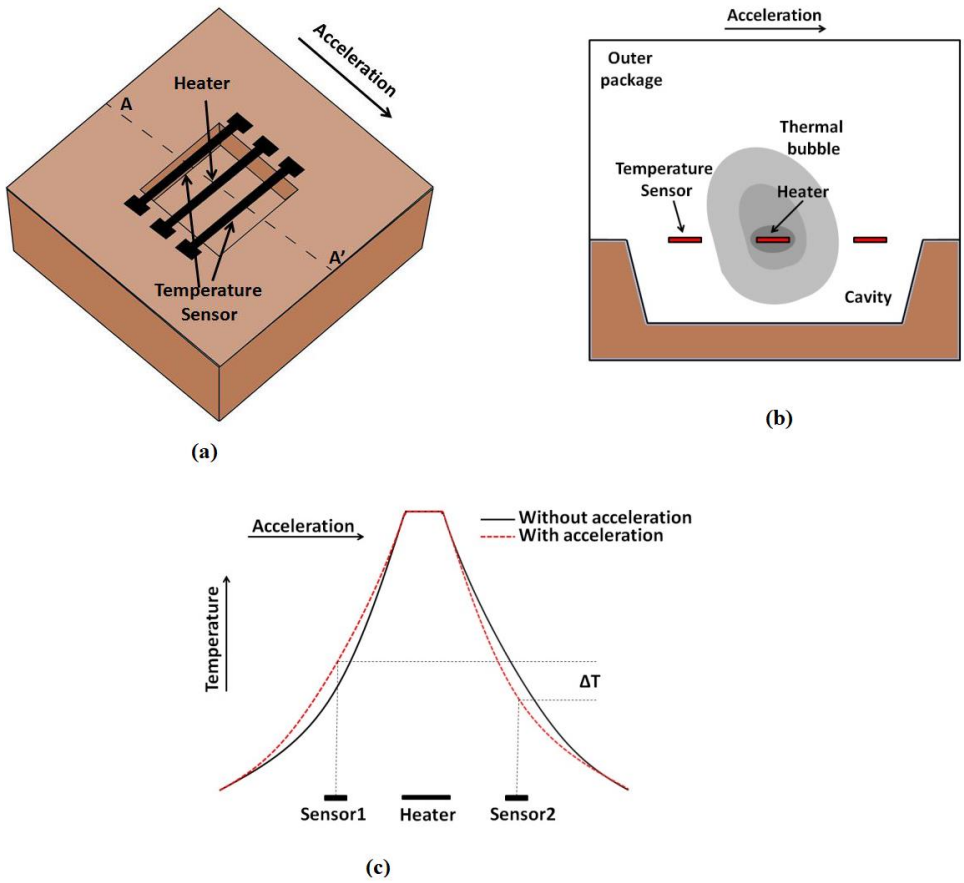

Figure 2. 4. (a) Schematic view of thermal accelerometer, (b) cross-sectional view along AA′ line, and (c) temperature profile along AA′.

2.2.5 Optical accelerometer

In the technique an optical signal is passed through a waveguide from one end and is detected through a photodetector at the other side. In between the light source and the photodetector, a graphene (mostly used) finger is place connect to seismic mass[19]. When acceleration in the

direction of the waveguide is applied the seismic push the finger into the waveguide which absorb the light and the photodetector detect less light as shown in figure 2.5 The reading of the photodetector is used for the acceleration measurement, in the same manner when the acceleration in from the opposite direction the waveguide is freer and photodetector detect more light which shows the direction of the opposite acceleration [20][21][22].

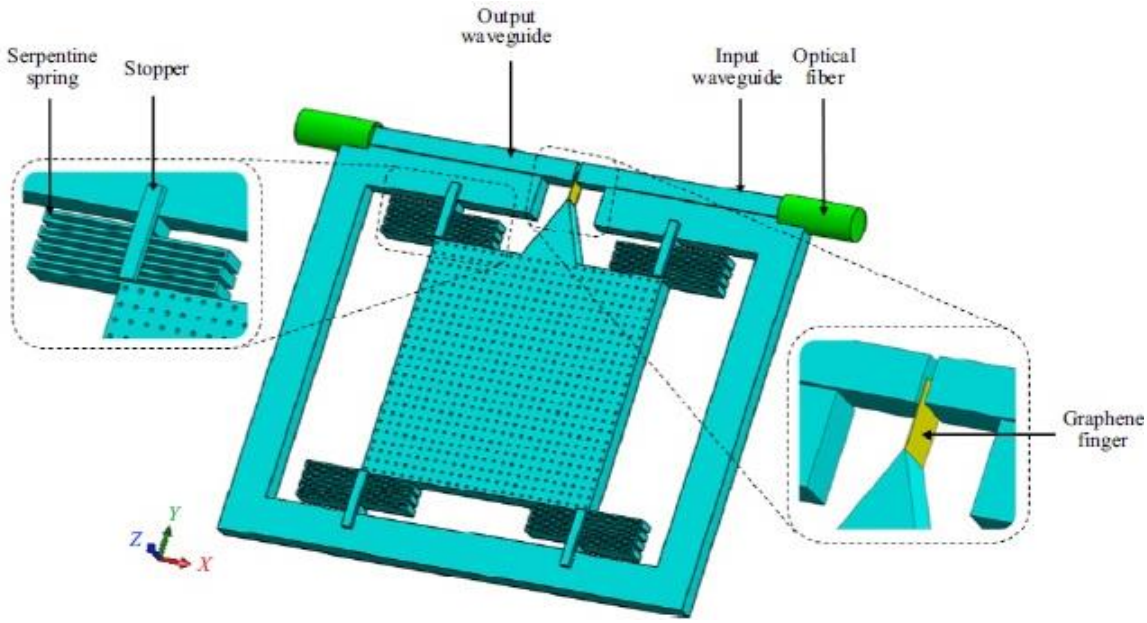

Figure 2. 5. Structure of optical microelectromechanical systems accelerometer

2.3 Piezoelectricity

The electric charge produces from the piezoelectric materials in response to the applied stress is known as piezoelectricity.

2.3.1 Physics of Piezoelectricity

It is a phenomenon which occurs in materials when they come under an external pressure and experience an induced strain, they generate electric charge or voltage on their surface due the change in its polarization produced by externally applied strain, the phenomenon is known as piezoelectric effect. Similarly, if an external field is applied across the material will disturb the

electric charges polarization and will eventually result in an elastic strain, this property of material is known as inverse piezoelectric effect.

The piezoelectric effect is exhibit in those materials which have no centre of symmetry in its structure. When such type of crystals is applied with a stress (compression or expansion) its separation between the opposite charges get disrupted in each elementary cell and form a new polarization at the crystal surface (lead to piezoelectric effect). Likewise, if such crystal is applied with an electric potential across its surface, will lead to a change in the polarization of positive and negative charges and it will cause an increase or decrease its length according to the orientation of the applied electric field (Converse piezoelectric effect). Both effects are demonstrated in following Figure 2.6.

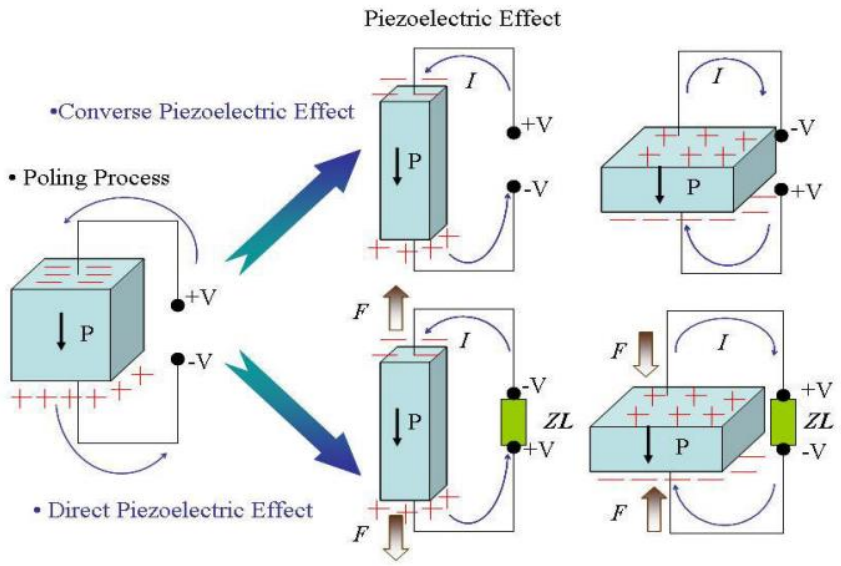

Figure 2. 6. Demonstrate the piezoelectric effects. Figure from[23].

2.3.2 Piezoelectric effect (Basic mathematic formulation)

As explained previously when a piezoelectric material is mechanically strained, it became polarized and the induced charge can be collected if electrodes are attached on the surface. The density of the generated charge $\boldsymbol{E}$ directly depends on the piezoelectric coefficient $\boldsymbol{d}$ and external stress it is experiencing $\boldsymbol{T}$.

$$\boldsymbol{E} = \boldsymbol{d} \times \boldsymbol{T} \tag{2.1}$$

In reverse affect when a potential is applied across piezo material, it induces a strain $\boldsymbol{S}$ in the material which is directly proportional to the applied potential $\boldsymbol{E}$ and material piezo-electric coefficient $\boldsymbol{d}$.

$$S = \boldsymbol{E} \times \boldsymbol{d} \tag{2.2}$$

2.3.3 History of piezoelectric materials

Two brothers Jacques Curie (1856-1941) and Pierre Curie (1859-1906) discovered a unique property of certain materials as tourmaline, quartz, topaz, cane sugar and Rochelle salt. It was realised that some materials generate electric charge of electric potential on their surface when they experience tension or compression from an external source, which is proportional to the applied load [24].

Piezoelectricity is a Greek word which mean the electricity produced by the pressure (Greek word piezo means pressure). After the discovery of the direct piezoelectric effect the Gabriel Lippman predicted that there must be converse effect to this on the basses of the thermodynamics principles. In 1881 the brothers Curies confirmed the converse effect experimentally, by demonstrating that through exposing these materials which shows direct piezoelectric effect to an electric field and found them changing its dimensions according to the orientation of the electric field applied.

Piezoelectric was introduced to global market in 1945 with the discovery of the mixed oxide compound barium titanate BaTiO3. Today piezoelectric transducers are used in a high range of application, Consumer electronics, military application, aeronautics, automobile industries, robotics, and many other industrial applications [24].

2.4 Piezoelectric base accelerometer

In piezoelectric based accelerometer the actuation technique is based upon the phenomena discovered by Pierre and Jacques Curie at the end of 18th century. They found that some specific materials are having a unique property that they produce electrical charges on their surface whenever they come under an external pressure, which is commonly known as piezoelectric effect. And similarly, when they are applied with an electric field the materials expand or contracts, also known as inverse piezoelectric effect. The materials work as a natural transducer

between mechanical and electrical and are commonly known as piezoelectric materials. Thus, they have been used in many different types of mechanical sensors and actuators, and because of their high-power density and relatively large force for small volume they get more attention for use in the micro-scale actuation [1].

2.4.1 Different bending structures of piezoelectric transducers

Unimorph and bimorph benders are piezoelectric bending mode elements, and both can be used for sensing and actuation in many different applications. When used as actuators these devices convert the applied electric field into a mechanical output. When used as sensing element they convert external mechanical energy into electrical signal or electrical charge.

Unimorph Structure

Unimorph is the most common structure and simple structure of the piezoelectric bending transducer, also known as monomorph. The structure is consisting two layers bonded together, one layer is called active layer (which is consist of the piezoelectric material i.e. AlN, PZT, Quartz) and other one is known as passive layer which is made of a material which don't possess the piezoelectric properties usually made of: Silicon, steel, aluminium etc. The side view of the Unimorph structure is shown in Figure 2.7. when an electric potential is applied to the electrode of the active layer, the piezoelectric material shows reaction according due its unique properties and result in deflection of bending of the beam. Similarly, when an external pressure is applied on the structure which cause it to bend, the active layer generates an electric energy.

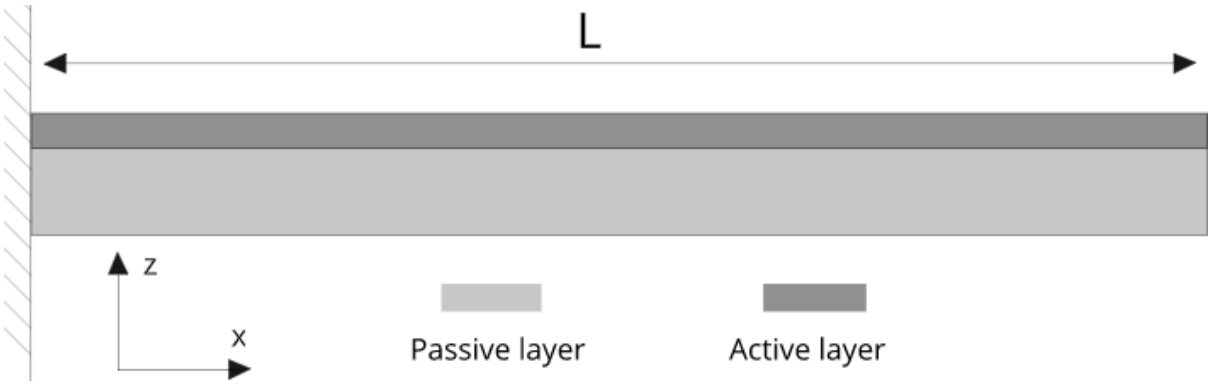

Figure 2. 7. Side view of Unimorph structure of piezoelectric actuator [24].

Bimorph structure

Bimorph structure consists of two active layers (two piezoelectric layer), bonded together or by a separation of a passive layer. The basic working principle of Bimorph is same as Unimorph structure transducers. The side of this type of structure is shown in Figure 2.8 (a)(b).

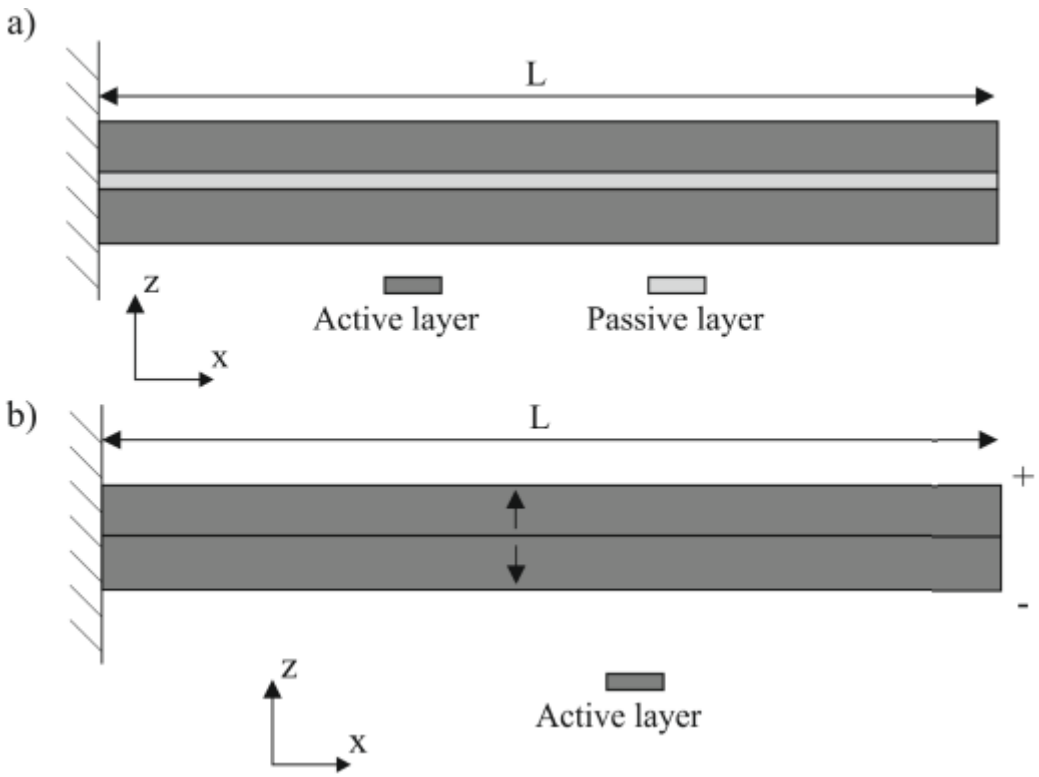

Figure 2. 8. Side view of bimorph structure: (a) with centre passive layer (b) just active layers [24].

In case of a single non-attached piezoelectric elements, the contraction and expansion are free in any direction. But when two elements are joined along one surface, where one is in contraction form while other is in expansion form, this is the case of bimorph. When a piezoelectric bimorph is joined together in a way that when an electric potential is applied one layer expands and the other one contracts, hence the motion restriction along the one side generate moment which produce the curling of bimorph [24].

2.4.2 Comparison of d_{33} and d_{31} modes

In MEMS transducers, the configuration of piezoelectric transductions is mostly applied in two different types and are called d_{31} and d_{33}. In case of d_{31} mode arrangement when a horizontal strain is applied to the piezoelectric film, it creates a vertical electrical field Fig. 2.9. The electrical potential resulted from the electric field can be detected through the upper and lower

metallic electrode. As shown in Fig. 2.10 is a device in its typical d_{33} mode configuration, the this an electric field is generated in horizontal direction when a stain is applied in the horizontal direction[25][26][27].

In this arrangement a set of ITD electrodes were used to detect the generated charges.

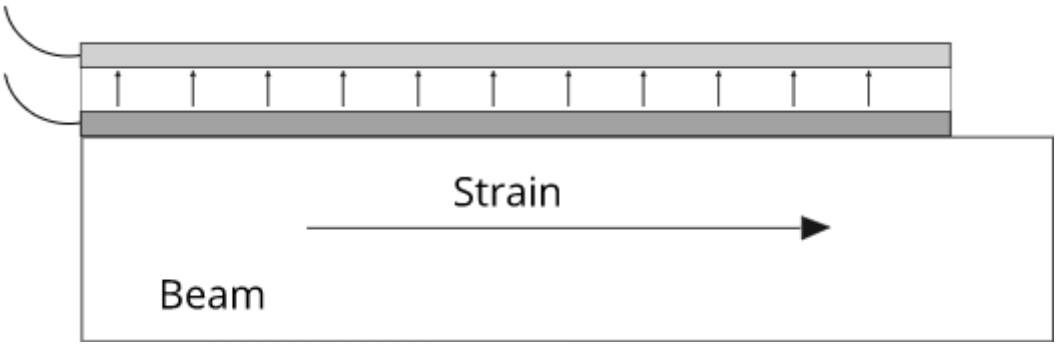

Figure 2. 9. d_{31}: horizontal strain produced electric field in vertical direction.

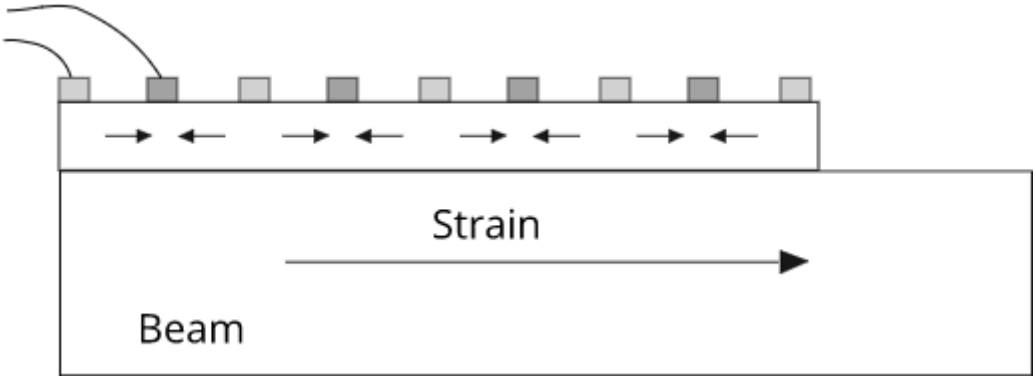

Figure 2. 10. d_{33}: horizontal strain produced electric field in horizontal direction.

2.4.3 Piezoelectric based accelerometers advantages

- Self-generating and need no external power to perform its functions
- Has wide frequency range
- Good linearity
- Output noise is low
- Can easily integrated in circuits

2.5 Equivalent electronic circuit model for 1-axis and 3-axis piezoelectric accelerometers

This section describes the basic theory of the piezoelectric accelerometer and present a general equivalent electronic circuit of the sensor. As basic design block of both our single and three axis accelerometers is same, the equivalent circuit described here represent a general equivalent circuit for both single and three axis accelerometers.

The base of the piezoelectric accelerometer is piezoelectricity, the property of some materials which converts stress into voltage whenever they come under an external pressure, the phenomena is also called piezoelectric transduction and is the main block element of a piezoelectric accelerometer. The amount of charge generated is directly related to applied mechanical stress and piezoelectric charge constant “d” [28].

To design an equivalent circuit for the accelerometer sensor, we need to represent a charge source in our circuit, which we cannot in standard circuit diagrams, but we can use a current source for that purpose because the charge generated by the piezoelectric transducer is when connected to a circuit is mover and became current. As current (Amperes) is the amount of electric charge (Coulombs) that pass through a specific point in one second [29]. Or the rate of change of the charges over the time is called current, which mathematically is the derivative of charge and can be express as:

$$I = \frac{\mathrm{d}Q}{\mathrm{d}t}$$

The charge generated by the piezoelectric material which in our case is the AlN (Aluminium nitride) is pass to the circuit which the help of two electrode (top electrode and bottom electrode) which is a sandwich along AlN in between the two electrodes shown in figure 2.11.

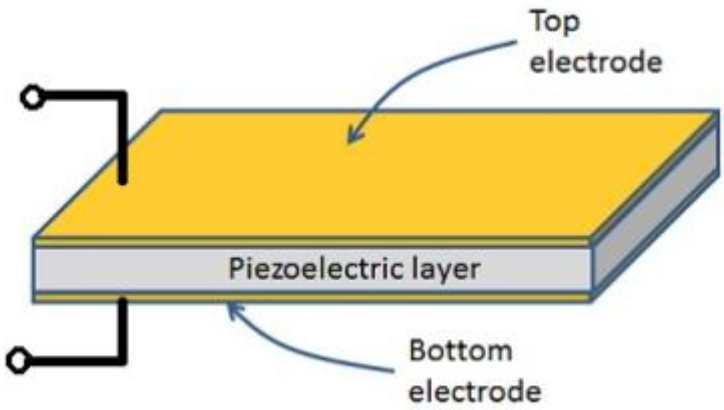

Figure 2. 11. Basic design of piezoelectric transducer (www.allaboutcircuits.com)

From the design shown in figure 2.11 we can see that these electrodes together with the piezoelectric material in the middle form a capacitor, from here we can incorporate capacitance into our electronic equivalent circuit of accelerometer.

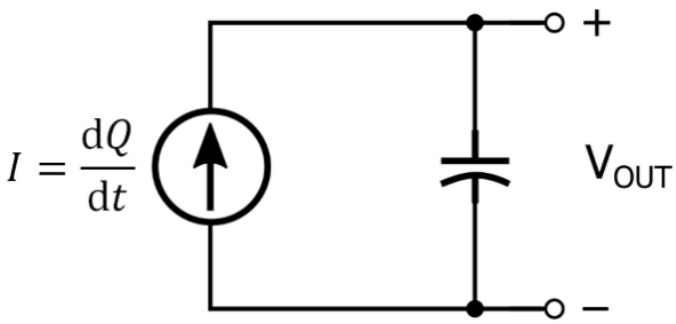

Figure 2. 12. Electronic equivalent circuit of the basic piezoelectric accelerometer design (www.allaboutcircuits.com)

To calculate the output of the equivalent circuit Vout, we can use the relationship of current and voltage for capacitive circuits. The integral of current with respect to time divided by capacitor is equal to voltage:

$$V_{out} = \frac{1}{C}\int I\, dt \tag{2.3}$$

As we can replace the current with the derivate of charge with respect to time, we get the equation

$$V_{out} = \frac{1}{C}\int \frac{dQ}{dt}\, dt = \frac{Q}{C} \tag{2.4}$$

Here C is value of the capacitor in parallel.

2.6 Applications of accelerometers

Accelerometers are inertial sensor which senses the acceleration in an object and is used for many different applications in several industries and products. Application based on different domains are mention here.

Engineering

Accelerometers are used to measure acceleration in vehicles, are used to find the inclination, machine vibrations, vibrations in trucks, processes control systems, safety installations. Also used in the scientific research projects of earthquakes.

Biology

Scientist are using accelerometer to track the record of the animal's behaviours when they are out of the visible range, the approach is mostly used to study the marine animals because of its difficulty of the visible analysis[30].

Industrial machines

Accelerometer are used in the many industrial machines to watch over the fitness of the machine to schedule the maintenances and calibrations of the machines to avoid bad quality product and breakdown of the systems.

Medical applications

Accelerometers are used in many medical applications such as, monitoring blood pressure, to measure the CPR chest compressions, sports watches to measure the footsteps, speed, distance travelled and time of activity of runners.

Navigation systems

Accelerometers are used in inertial navigations systems which is consist of a computer and accelerometers to monitor a moving object continuous, tracking its speed, orientations, position and do not need any external reference for that.

Automobiles

Most common used of accelerometer in automobiles are the MEMS accelerometers use in airbags which offer several advantages over the previously used technologies, other applications are monitoring of noise, harshness and vibration that can be an indicator of a mechanical fault.

Consumer electronics

It is used to detect the orientation of the screen in many smart devices, also used as free fall sensor which protect the device to against the hard crash from memory loss, also used to calculate the distance from which the device is dropped and is useful in monitoring the handling operation in shipping of containers.

Military application

Accelerometer is used in several different military equipment like the guided missiles, drone, Helicopters, submarines and on the soldiers.

2.7 Papers review of different materials and designed based piezoelectric accelerometers

Table 2. 1. Compiled key information from the different piezoelectric based accelerometer

Accelerometer type	**Charge Sensitivity Theoretical and measured**	**Resonant frequency theoretical and measured**	**Fabrication process & Active material**	**Design parameters**	**References**
Simple Cantilever Sensor (1 axis)	Theoretical= 0.95 fC/g Measured = 0.21 fC/g (mV/g)	Theoretical = 3.9KHz Measured = 3.3 KHz	Sacrificial oxide process: Zinc oxide (ZnO)	L(length)= 1000um B(width)= 50um tsi = 2.1 um tzno = 0.5 um d31= 2.3 pC/N	[31]
Cantilever Sensor with Integrated Proof Mass (1 axis) Design#1	Theoretical= 12.8fC/g Measured = 13.3fC/g (mV/g)	Theoretical = 1.95 KHz Measured = 2.23 KHz	Sacrificial oxide process: Zinc oxide (ZnO)	Design# 1 L = 500 um b= 30 um Lm= 500um bm= 500 um te = 2.0 um Tp= 0.7 um	
Cantilever Sensor with Integrated Proof Mass (1 axis) Design#2	Theoretical= 39.8 fC/g Measured = 44.7fC/g (mv/g)	Theoretical = 0.78 KHz Measured = 1.03KHz	sacrificial oxide process: Zinc oxide (ZnO)	Design # 2 L = 1000 um b= 30 um Lm= 500um bm= 500 um te = 2.0 um Tp= 0.7 um	
Single-Axis Piezoelectric Bimorph accelerometer with a proof mass	***Theoretical*** Voltage sensitivity = 8.3 mV/g Charge Sensitivity on one electrode = 231 fC/g ***Measured*** Voltage sensitivity = 7 mV/g Charge Sensitivity on one electrode = unknown	Theoretical = 131 Hz Measured = 98 Hz	Bulk-micromachined Zinc oxide (ZnO)	Beam length(um) = 140 Beam width(um) = 1000 Al thickness(um) = 0.4 Al elctrde lngth(um) = 40 Al electrode width(um) = 1000 Zno thickness(um) = 0.3 PECVD SixNy thicknees(um) = 0.1 Parylene thickness(um) = 3.7 Proof mass length(um)=2150 Proof mass width(um) = 1200 Proof mass thickness(um) = 330	[32]
Tri-Axis Piezoelectric Bimorph accelerometer with a proof mass	***Theoretica***l Sensitivity at **x-axis** voltage = 1.59mV/g Charge = 38.5fC/g At **Y-axis** voltage = 1.59mV/g Charge = 38.5fC/g At **z-axis** voltage = 10.89mV/g Charge = 111.7fC/g ***Measured*** Sensitivity at **x-axis** voltage = 0.93mV/g **Y-axis** voltage = 1.13mV/g **z-axis** voltage = 0.88mV/g	Theoretical = Unknown Measured = Unknow	Bulk-micromachined Zinc oxide (ZnO)	Beam length(um) = 340 Beam width(um) = 300 Al thickness(um) = 0.4 Al elctrde lngth(um) = 130 Al electrode width(um) = 250 Zno thickness(um) = 0.3 PECVD SixNy thicknees(um) = 0.1 Parylene thickness(um) = 2.1 Proof mass length(um)=1700 Proof mass width(um) = 1700 Proof mass thickness(um) = 400	

Accelerometer type	Charge Sensitivity Theoretical and measured	Resonant frequency theoretical and measured	Fabrication process & Active material	Design parameters	References
Single-axis simple cantilever accelerometer Design#1 with L=100um	***Theoretical*** Voltage sensitivity = 0.884 mV ***Measured*** Voltage sensitivity = 1.93 mV	Theoretical = Unknown Measured = Unknow	Bulk micromachining technique Lead zirconate titanate (PZT)	Length of beam=L= 100um Thickness of beam = t=0.9um Platinum thickness = 0.2um ZnO thickness(active) =0.5um Width of beam= W= 20um Acceleration=g= 9.8m/s^2	
Single-axis simple cantilever accelerometer Design#2 with L=150um	***Theoretical*** Voltage sensitivity = 2.21 mV ***Measured*** Voltage sensitivity = 8.05 mV	Theoretical = Unknown Measured = Unknow	Bulk micromachining technique Lead zirconate titanate (PZT)	Length of beam=L= 150um Thickness of beam = t=0.9um Platinum thickness = 0.2um ZnO thickness(active) =0.5um Width of beam= W= 20um Acceleration=g= 9.8m/s^2	[33]
Single-axis simple cantilever accelerometer Design#2 with L=200um	***Theoretical*** Voltage sensitivity = 3.930 mV ***Measured*** Voltage sensitivity = 19.51 mV	Theoretical = Unknown Measured = Unknow	Bulk micromachining technique Lead zirconate titanate (PZT)	Length of beam=L= 200um Thickness of beam = t=0.9um Platinum thickness = 0.2um ZnO thickness(active) =0.5um Width of beam= W= 20um Acceleration=g= 9.8m/s^2	
Single-axis T-shape resonant accelerometer	***Theoretical*** Unknow ***Measured*** 1.11 Hz/g (i.e., 68.9 ppm/g)	Theoretical = Unknow Measured = 16.10925 kHz	Bulk micromachining Technique Aluminium Nitride (Active material)	Length of beam (AB) = 450um Width of beam (AB) = 20um Length of beam (CD) = 528um Width of beam (CD) = 14um Length of electrode = 300um Width of electrode = 4.5 um Width of proof mass = 350um The sides of releasing hole = 50um Thickness of structure = 2.05um	[34]
Triaxial accelerometer based on d_{33} mode	***Measured*** 4.55mV/g (Vertical acceleration) 0.497 mV/g (horizontal acceleration)	Theoretical = Unknow Measured = 13485Hz	PZT (Active material)	Thickness of cantilever beam = 55um Thickness of PZT = 2.1um Beam width = 500um Length of cantilever beam = 500um – 2500um d_{33} = 168pC/N	[35]
In-plane Resonant accelerometer (2D) with DETF beam	***Theoretical*** Unknow ***Measured*** 201ppm/g	Theoretical = Unknow Measured = 141KHz	AlN (active material)	Size of proof mass = 1000x1000um^2 Size of DETF beam = 1330x32 um^2 L1, power arm of first stage leverage = 1050um l1, resisting arm of first stage leverage = 100um L2, power arm of first stage leverage = 90um	

Accelerometer type	Charge Sensitivity Theoretical and measured	Resonant frequency theoretical and measured	Fabrication process & Active material	Design parameters	References
				Size of input beam = 135x10um^2 Size of pivot beam 1 = 155x5um^2 Size of connection beam = 135x5um^2 Size of pivot beam 2 = 135x20um^2 With of leverage = 150um Thickness of the structure = 10um	[36]
DETF Aluminium Nitride Resonating Accelerometer (In-plane)	***Theoretical*** Unknow **FEM analysis** Sensitivity = 89ppm/g Experimental Sensitivity = 54.5ppm/g	**FEM analysis** Base frequency = 348.6KHz Experimental based frequency = 332.1KHz	AlN (active material)	Design Parameters Beam dimensions = 6 µm x 300 µm Thickness of AlN = 2um Thickness of platinum = 100nm Proof mass dimensions = 800 µm x 800 µm	[37]
ALUMINUM NITRIDE ON SILICON RESONANT MEMS ACCELEROMETER (TBTF)	***Theoretical*** Unknow ***Experimental*** Sensitivity = 387 ppm/g	Theoretical = Unknow Simulated frequency = 137.6 kHz	AlN (active material)	Design Parameters Length of each tine (Lt) = 760um Width of each tine (Wt) = 40um Thickness of silicon layer (t_{si}) = 10um Thickness of piezoelectric-AlN layer (t_{AlN}) = 0.5 um Thickness of metal (Al) layer (t_{Al}) = 1 um Mass of each tine (m_t) = 0.7ugm Seismic mass (m_s) = 81.59ugm Resonant frequency (f_o-simulated) = 136.3 Khz	[38]
TRI-AXIAL MICRO PIEZOELECTRIC ACCELEROMETER (single proof mass)	***Theoretica***l Z-axis= 22.12pC/g, ***FEM Analysis*** Z-axis= 23.85 pC/g X-axis = 4.62 pC/g Y-axis = 4.62 pC/g	***Calculated*** Natural frequency = 207.47Hz. ***FEM Analysis*** Natural frequency = 230.46 Hz.	PZT (active material)	Design Parameters Length of cantilever beam = 1700um Width of cantilever beam =250um Thickness of cantilever beam = 3.2um Thickness of PZT film = 0.9um	[39]

Accelerometer type	Charge Sensitivity Theoretical and measured	Resonant frequency theoretical and measured	Fabrication process & Active material	Design parameters	References
PZT Thick-Film Triaxial Accelerometer (single proof mass)	***Theoretical*** **Design # 1** Sv_v= 2.75 mV/g Sv_h= 2.75 mV/g SQ_v= 0.0275 mC/g SQ_h= 0.0275 mC/g **Design # 2** Sv_v= 0.927 mV/g Sv_h= 0.927 mV/g SQ_v= 0.0463 mC/g SQ_h= 0.0463 mC/g ***FEM Analysis*** **Design # 1** Sv_v= 2.85 mV/g Sv_h= 2.87 mV/g SQ_v= 0.0285 mC/g SQ_h= 0.0287 mC/g **Design # 2** Sv_v= 0.950 mV/g Sv_h= 0.930 mV/g SQ_v= 0.0475 mC/g SQ_h= 0.0465 mC/g	***Calculated*** **Design # 1** f_v = 25khz **Design #** 2 f_v = 25khz ***FEM Analysis*** **Design # 1** f_v = 23.65khz f_h = 22.2 khz **Design # 2** f_v = 24.58 khz f_h =22.7 khz	PZT (active material)	Design Parameters Design # 1 H = 10um H_p = 14.2um H_m = 1000um W_m = 1872um W = 261 um L = 193um Design # 2 H = 10um H_p = 14.2um H_m = 1000um W_m = 1413um W = 758um L = 331um	[40]
A High Sensitivity Piezoelectric MEMS Accelerometer Based on Aerosol Deposition Method (single axis)	***Experimental*** **Design 1:** SQ_1 = 25.6 pc/g Sv_1 = 5.43 mv/g **Design 2:** SQ_2 = 25.5 pc/g Sv_2 = 7.30mv/g **Design 3:** SQ_3 = 41.4 pc/g Sv_3 = 9.32 mv/g **Design 4:** SQ_4 = 23.9 pc/g Sv_4 = 7.54 mv/g	**Experimental** ***Resonant frequencies*** **Design 1**= 769.01 Hz **Design 2**= 572.25 Hz **Design 3**= 573.59 Hz **Design 4**= 723.25	PZT (active material)	Design Parameters These parameters are same for all 4 designs: Te = 0.22um Tp = 11um Tb = 0.1mm Tm = 1mm lb = 2.5mm lm = 2mm width of mass $_{1,2,4}$ = 4.2mm width of mass $_3$ = 6.2 mm (heavy mass)	[41]
High-Sensitivity Piezoelectric Microelectromechanical Systems Accelerometers (One axis good sensitivity)	***Theoretical*** **Design 1:** SQ_1 = 7.60 pc/g **Design 2:** SQ_2 = 1.45 pc/g **Design 3:** SQ_3 = 1.06 pc/g **Design 4:** SQ_4 = 0.77pc/g ***FEM analysis*** **Design 1:** SQ_1 = 7.45 pc/g **Design 2:** SQ_2 = 2.10 pc/g **Design 3:** SQ_3 = 1.18 pc/g **Design 4:** SQ_4 = 0.84pc/g	**Theoretical** Resonant frequencies **Design 1**= 3.7 KHz **Design 2**= 17.4 KHz **Design 3**= 27.5 KHz **Design 4**= 35.3 KHz	PZT (active material)	Design Parameters Parameters are not recorded in detail, but they were all same except the thickness of Silicon membrane Design 1: 6.1 um Design 2: 21.2 um Design 3: 36.8 um Design 4: 44.4 um	[42]

2.7.1 Review of different design approaches and its affects

Literature study shows that different designs approaches are used by researchers for both single-axis and three-axis accelerometers and every design showed its own advantages and disadvantage. Some researches preferred simple cantilever beam for designing mostly single-axis accelerometers [33], where other researcher come up with a different design by making a slight change to design by adding a proof mass on the tip of the cantilever beam, and using multiple cantilever beam instead of a single cantilever beam [31], this approach showed improved sensitivity and resonant frequency. A similar kind of design approach is used by some researchers with proof mass and a single cantilever beam with larger width [43]. Other designs mainly used are DETF (double-ended tuning- fork) [44], TBTFs (triple beam tuning forks) [38], T-shape designs with two proof mass attached [34], some design had a proof mass while others doesn't.

For three-axis accelerometer most commonly used design is a single proof mass suspended by four symmetric beam which are connected to an outer frame [39][40][35][45][46][32]. A trampoline type design is also reported having a suspended proof mass at the junction of crossed beam and beams are connected to a circular mounting frame [42], Similar types four of designs are reported in this paper with different beam for all the four designs [47].

Unimorph or Bimorph types of beam design methods are used in all the design for both single-axis or tri-axial accelerometer, with different piezoelectric materials used as active materials (mostly PZT, ZnO, and AlN). Transductions configuration of piezoelectric can mostly applied in d_{31} mode. It is observed that the deployment of piezoelectric (active material) at places where the structure experience is important during the design process of the accelerometers.

2.8 Piezoelectric material properties review:

Material properties of different piezoelectric materials commonly used by researchers for designing accelerometers, such as PZT (Lead zirconate titanate), ZnO (Zinc oxide), AlN (Aluminium nitride).

Table 2. 2. Material properties of commonly used piezoelectric materials [48].

Property	**PZT**	**$LiNbO_3$**	**AlN**	**ZnO**
Piezoelectric constant(C/m^2)	e_{31}= -6.5 e_{33}= 23.33	e_{31}= 0.23 e_{33}= 1.33	e_{31}= -0.58 e_{33}= 1.55	e_{31}= -0.57 e_{33}= 1.32
Piezoelectric coefficient (pm/V)	d_{31} = -120 d_{31} = -170 d_{33} = 60–130	d_{31} = -7.4	d_{31} = -2.0 d_{33} = 3.9	d_{31} = -5.0 d_{33} = 5.9
Electromechanical coupling coefficient k^2	0.57–0.69	5.5	0.24	0.33
Elastic modulus (GPa)	68	203	308	201
Hardness (GPa)	8.0	–	17	5.0
Resistivity (Ω cm)	1 x 10^9	2x10^{10}	1x10^{11}	1x10^7
Thermal expansion (/˚C)	2 x 10^{-6}	1.5 x 10^{-5}	4.3 x 10^{-6}	6.5 x 10^{-6}
Acoustic velocity (m/s)	3900	3980	10127	5700
Dielectric loss angle tan δ (10^5 V/m)	0.01–0.03	–	0.003	0.01–0.1

2.8.1 Comparison between the PZT and AlN

PZT is widely used in inertial sensors application because of its high piezoelectric constant compare to other materials such as $LiNbO_3$, AlN, ZnO, and low manufacturing cost [24][41]. The high piezoelectric constant result in high charge sensitivity compare to other materials [49], but due to its low bang gap 3.2–3.7 eV the suitability for high temperature application decreases [50]. PZT contains lead and which pose a threat to environment because of its toxic properties.

While on the other hand the AlN a high band gap of 6eV which makes it a good choice for the high temperature application, and can maintain its piezoelectric properties at a temperature exceeding 1000◦C [51]. It has also gained an increasing importance because of its properties such as High Signal to Noise Ratio (SNR), post-CMOS compatibility [37], Small dielectric loss, and an environment friendly material which contain no lead [52].

3 Analytical analysis of accelerometer

This chapter is dealing with analytical analysis of the single cantilever beam 1-axis accelerometers design parameters, with the help of MATLAB the mathematical equations are simulated to get the optimized parameters of the single axis accelerometer. For tri-axial accelerometer the mathematical analysis is not possible because of the complexity of the design and the limitation of the coordinates. So, in this chapter we will only simulate the single axis accelerometer design parameters.

Single cantilever beam with proof mass as shown in figure 3.1 is the base of this mathematical equation derivation.

As we know

$$m = V_m \rho_{si} \tag{3.1}$$

$$F_z = m a_z \tag{3.2}$$

Where V_m is the volume and ρ_{Si} is density of the seismic mass (proof mass). ρ_{Si} = 2330 kg/m3

Curvature of the cantilever:

$$K = \frac{1}{\omega_c} = \frac{d\emptyset}{ds} \approx \frac{d^2 v}{dx^2} \tag{3.3}$$

ω_c is the radius of curvature and θ is the angle of rotation of the curve that is detected.

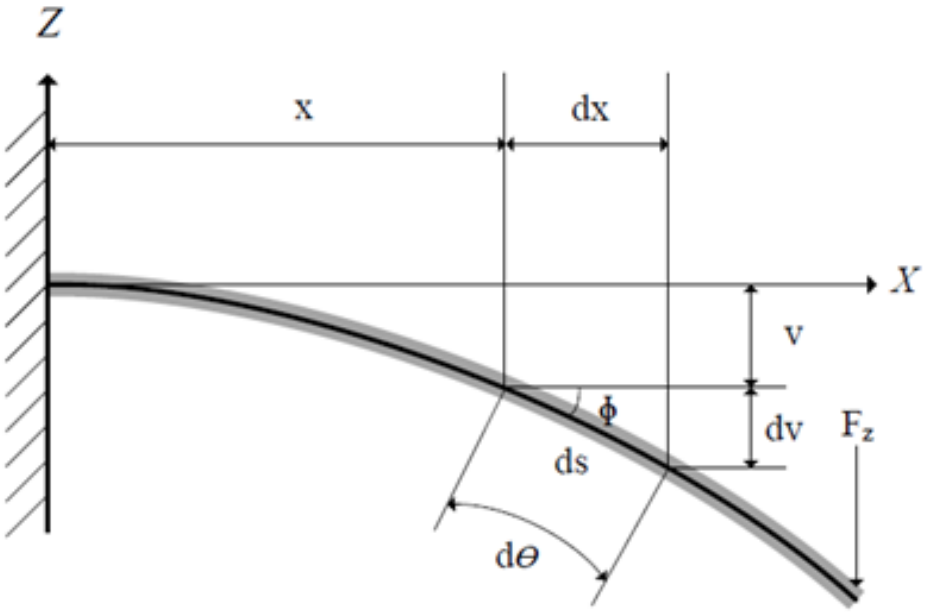

Figure 3. 1. Simple cantilever beam design of transducer

Design parameters are represented as l_c Length of the cantilever , t_c Thickness of the cantilever, w_c Width of the cantilever, l_p Length of the AlN, active layer, w_p Width of AlN, active layer, t_p Thickness of AlN (active layer), t_m Thickness of Si mass (proof mass), w_m Width of Si mass (proof mass), l_m Length of Si mass (proof mass), m Mass , and a_z acceleration.

Area moment of inertia I_y is given by

$$Iy = \int_A Z^2 \, dA \tag{3.4}$$

The bending moment M(x) in the beam at point x is given by,

$$M(x) = M_1 + R_1 x \qquad 0 \le x \le lc \tag{3.5}$$

where M1 is the reaction moment and R1 is the reaction force at x = lc.

$$\frac{d^2 v(x)}{dx^2} = -\frac{M_1 + R_1 x}{Y I_y} \tag{3.6}$$

For the uniaxial accelerometer the cantilever fixed at one end as V (0) = V‘0(0) = 0, the general deflection curve is derived

$$v(x) = -\frac{M_1}{2YI_y}x^2 - \frac{R_1}{6YI_y}x^3 \qquad 0 \le x \le lc \tag{3.7}$$

In the case of static deflection, the reaction force R_1 is equal to the applied force.

$$R_1 = F_z = ma_z \tag{3.8}$$

And the reaction moment equals to the sum of all moments.

$$M_1 = -F_z(l_c + \frac{l_m}{2}) \tag{3.9}$$

Hence deflection is given as below

$$v(x) = \frac{3(l_c + l_m/2)x^2 - x^3}{6YI_y}(ma_z) \tag{3.10}$$

The voltage generated "V" per acceleration is given by

$$V = -2.404 \times 10^2 \frac{Vm}{N} * \frac{ma_z}{8I_y l_p t_p}\left(t_p^2 l_c^2 + 2t_c t_p l_c^2\right) * t_p \tag{3.11}$$

The output voltage V per acceleration or charge Q generated per acceleration is

the sensitivity.

Voltage sensitivity is given by

$$S_{zV} = \frac{V}{a_z} \tag{3.12}$$

Charge sensitivity is given by

$$S_{zQ} = C_{aln} * \frac{V}{a_z} = \frac{Q}{a_z} \tag{3.13}$$

Capacitance C_{aln} of the AlN layer is given as,

$$C_{aln} = \frac{\omega_p l_p}{t_p} * \frac{d_{31}}{g_{31}} \tag{3.14}$$

And the Resonant frequency is given by the equation below

$$f_\circ = \frac{1}{2\pi}\sqrt{\frac{Y_{Si}I_y}{ml_c^3}}\sqrt{\frac{6z^2+6z+2}{8z^4+14z^3+(21/2)/z^2+4z+2/3}} \tag{3.15}$$

Where $z = c = l_c$ and c is half the length of the mass l_m.

3.1 Preliminary design parameters of single axis accelerometer

MATLAB is used in finding the optimum design parameters for single axis accelerometer. Some initial values of parameters were selected based on the research done in past from the literature review. To find out the optimum design parameters, I follow as simple analysis technique using the above-mentioned equations for deflection, sensitivity and frequency.

We keep one parameter as variable, the one which we want to optimize and fixed the rest of the parameters. Then we change that selected parameter over a range of values and check its results according to the changed values. Three parameters or optimization cases are selected to be optimized for different values, and deflection, voltage sensitivity and resonant frequency is calculated accordingly at each different value.

Case 1: Changing only l_c length of cantilever substrate layer (silicon layer).

Case 2: Changing beam length or both the cantilever substrate layer (silicon layer) l_c and piezoelectric layer (active layer) l_p.

Case 3: Changing the width of the piezoelectric layer (active layer) w_p.

Table 3. 1. Initial literature-based design parameters

Letter	Representation description	Values
l_c	Length of the cantilever (Silicon layer)	200 μm
t_c	Thickness of the cantilever (Silicon layer)	20 μm
w_c	Width of the cantilever (Silicon layer)	3000 μm
l_p	Length of the AlN (active layer)	200 μm
w_p	Width of AlN (active layer)	2500 μm
t_p	Thickness of AlN (active layer)	0.6 μm
l_m	Thickness of Si mass (proof mass)	570 μm
w_m	Width of Si mass (proof mass)	3000 μm
l_m	Length of Si mass (proof mass)	5000 μm
m	Mass	20 mg
a_z	Acceleration	9.8 m/s^2

3.2 Simulation results:

MATLAB is used to calculate the optimized parameters, equations mentioned above was used to calculate the results for all three selected cases of critical parameters and are reported in tables and plotted in form of line charts respectively here in section.

Case 1: Changing only l_c length of cantilever substrate layer (silicon layer).

Table 3.2 shows the recorded corresponding results of deflection of beam, voltage sensitivity and resonant frequency for different lengths of l_c cantilever layer (silicon layer), while all other parameters were kept unchanged. Calculated results for the deflection, voltage sensitivity and resonant frequency are plotted in figure 3.2, 3.3, 3.4, respectively.

Table 3. 2. Result of analysis of different length of l_c substrate layer (silicon layer).

No.	l_c length of beam substrate in μm	f◦ Resonant frequency in Hz	Deflection in nm	Voltage sensitivity S_{zv} in mV
1	150	781.90	14.9	-1.10
2	200	677.22	26.8	-1.90
3	250	605.77	42.3	-3.00
4	300	553.03	61.1	-4.30
5	350	512.04	84.4	-5.90

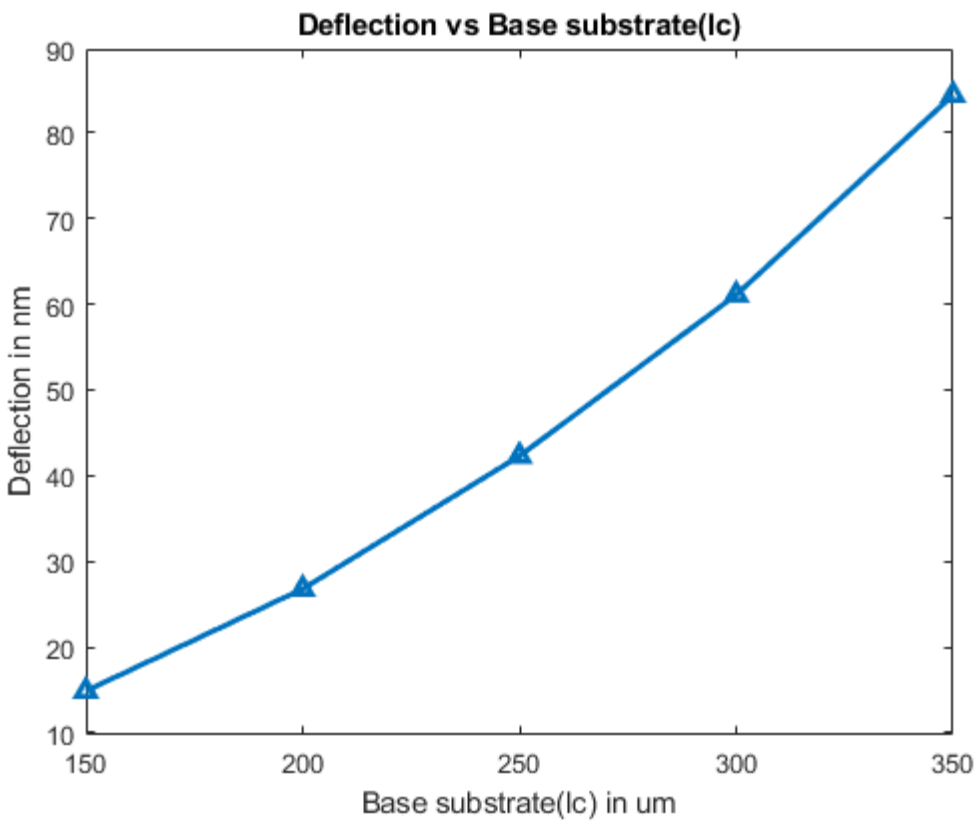

Figure 3. 2. Change in deflection with change in length of base substrate

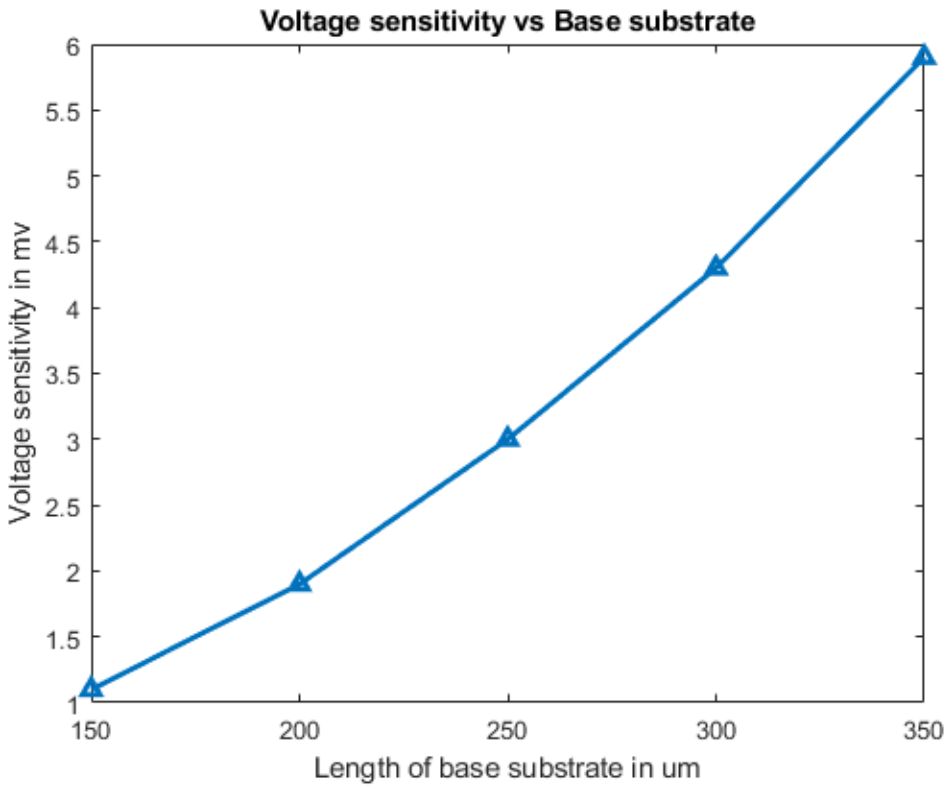

Figure 3. 3. Change in voltage sensitivity with change in length of base substrate

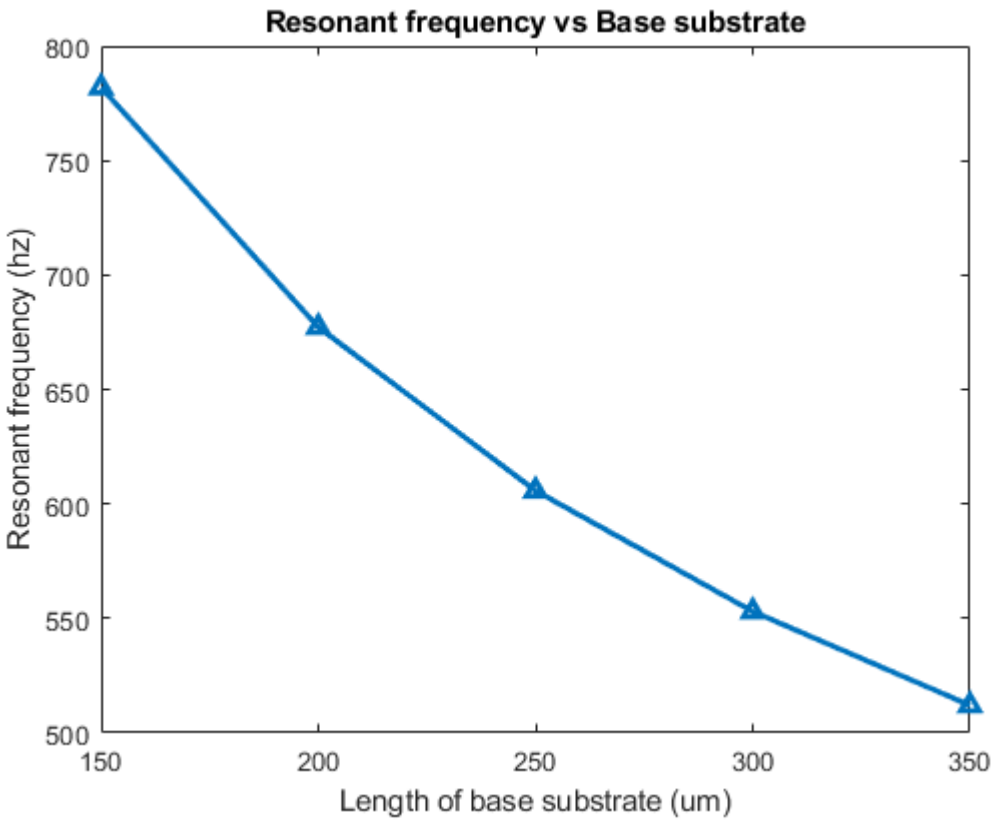

Figure 3. 4. Change in resonant frequency with change in length of base substrate

Case 2: Changing beam length or both the cantilever substrate layer (silicon layer) l_c and piezoelectric layer (active layer) l_p.

Result of the second case where the l_c substrate layer (Silicon layer) and l_p piezoelectric layer (active layer) are both changing and are having same values, while all other parameters were kept unchanged. Table 3.3 shows the recorded corresponding results of deflection of beam, voltage sensitivity and resonant frequency for this case and are plotted in figure 3.5, 3.6, 3.7, respectively.

Table 3. 3. Result of analysis at different lengths of both l_c substrate layer (silicon layer) and l_p piezoelectric (active layer).

No.	$\boldsymbol{l_c = l_p}$ **length of both parameters in** $\boldsymbol{\mu m}$	**f◦ Resonant frequency in Hz**	**Deflection in nm**	**Voltage sensitivity S_{zv} in mV**
1	150	781.90	14.9	-1.10
2	200	677.22	26.8	-1.40
3	250	605.77	42.3	-1.80
4	300	553.03	61.1	-2.20
5	350	512.04	84.4	-2.50

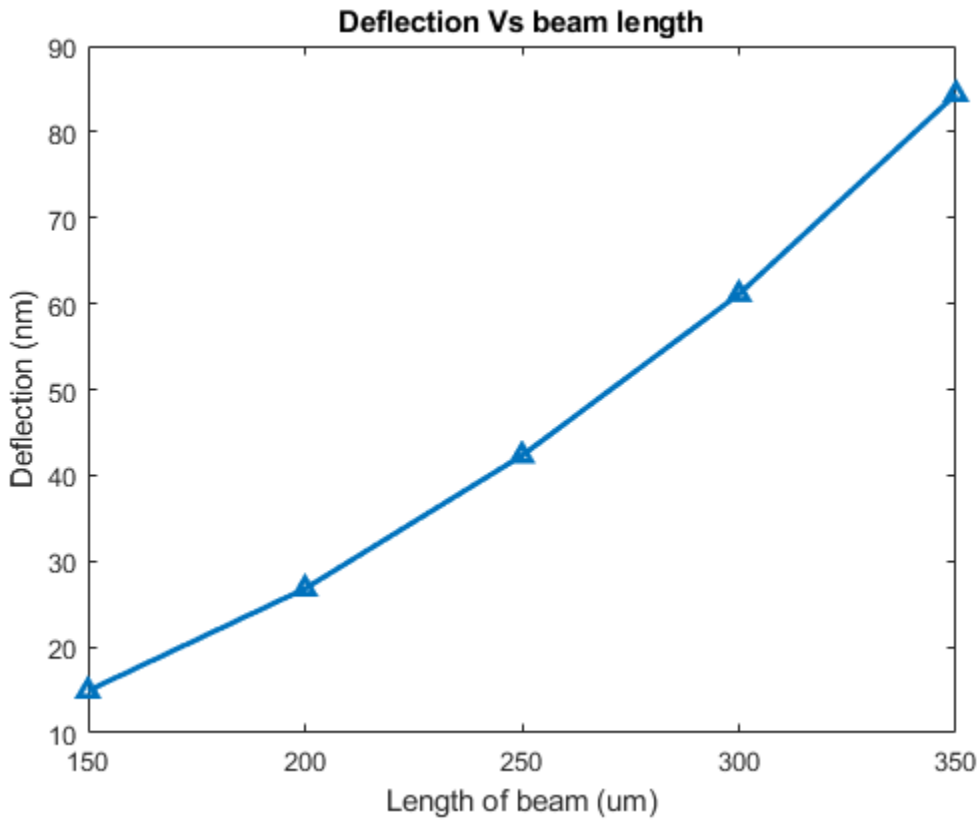

Figure 3. 5. Change in deflection with change in length of beam

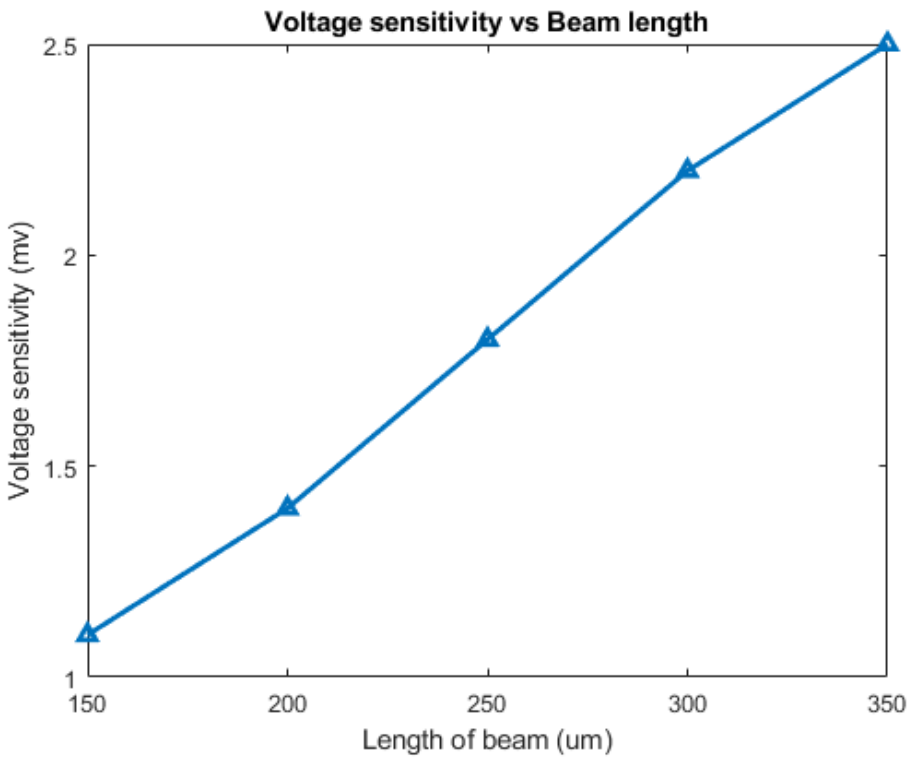

Figure 3. 6. Change in voltage sensitivity with change in length of beam

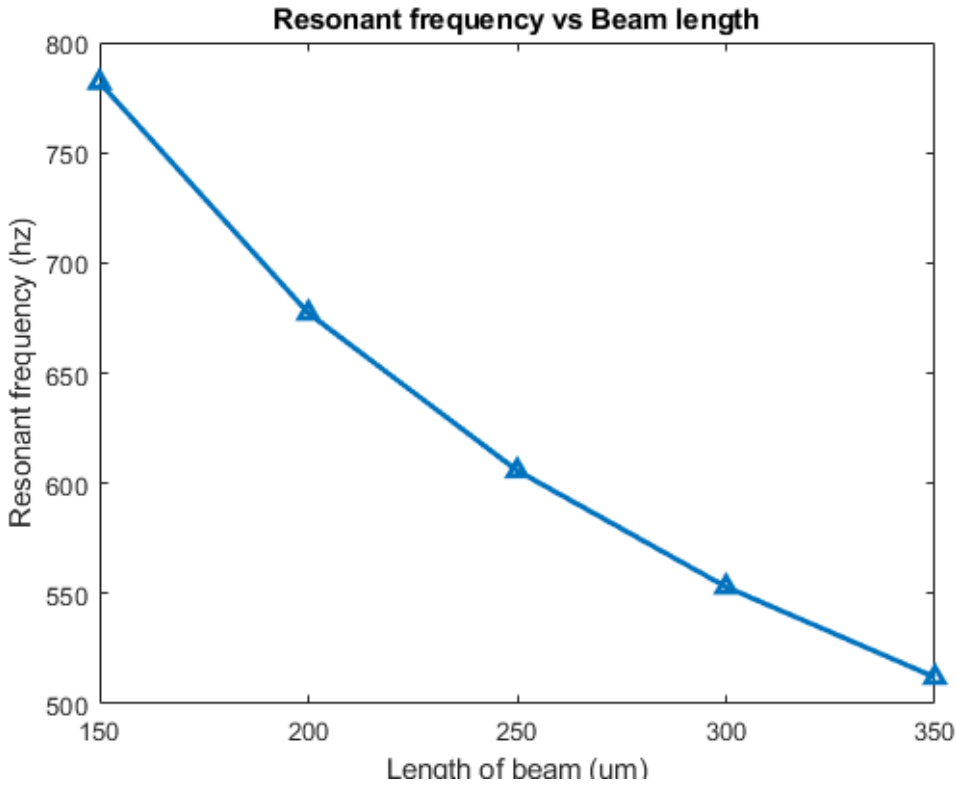

Figure 3. 7. Change in resonant frequency with change in length of beam

Case 3: Changing the width of the piezoelectric layer (active layer) w_p.

Changing the parameter w_p width of the piezoelectric layer (active) is the third case of the optimization. Calculated results for deflection of beam, voltage sensitivity and resonant frequency are recorded in the table 3.4 and are plotted in figure 3.8, 3.9, 3.10.

Table 3. 4. Result of analysis of different width of w_p width of piezoelectric (active layer).

No.	w_p width of piezoelectric layer in μm	f◦ Resonant frequency in Hz	Deflection in nm	Voltage sensitivity S_{zv} in mV
1	1000	781.90	14.9	-1.10
2	1500	677.22	14.9	-1.10
3	2000	605.77	14.9	-1.10
4	2500	553.03	14.9	-1.10
5	2980	512.04	14.9	-1.10

Plots of result is followed.

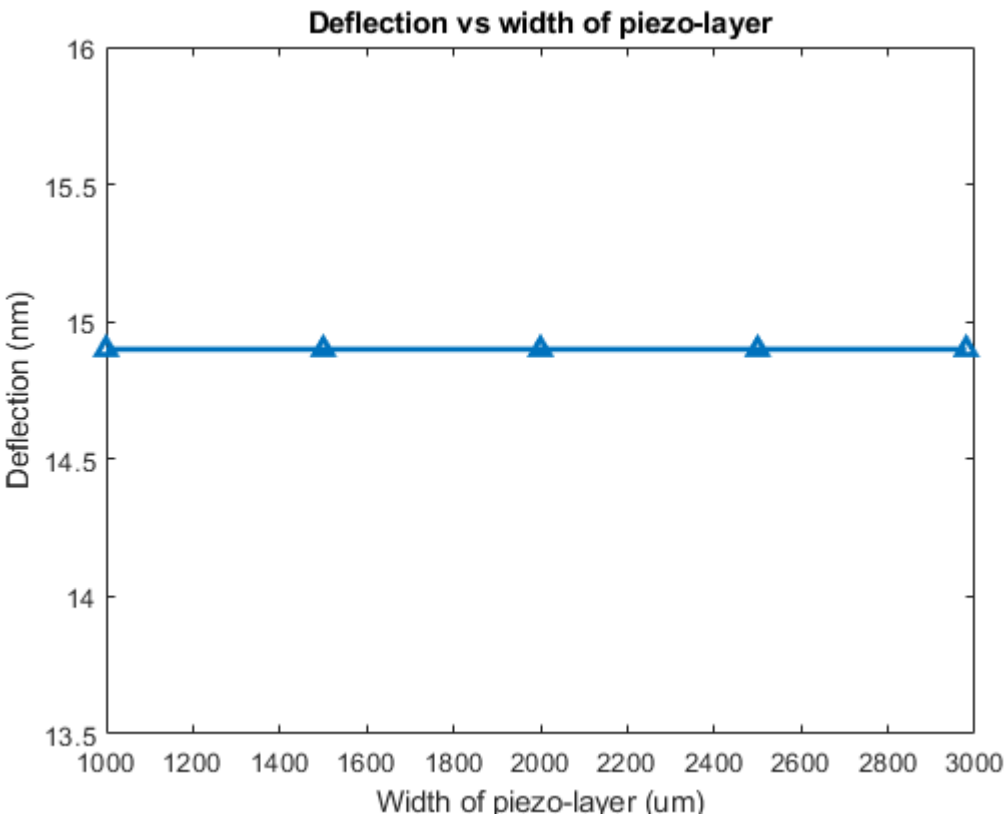

Figure 3. 8. Change in deflection with change in width of piezo layer

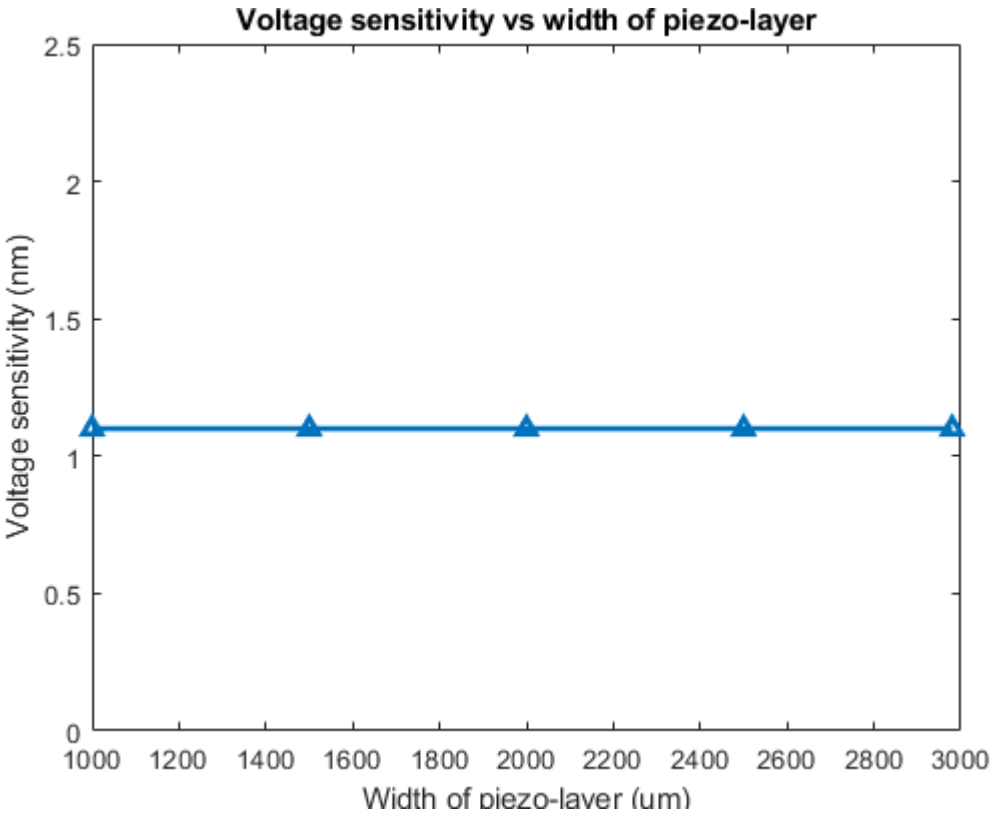

Figure 3. 9. Change in voltage sensitivity with change in width of piezo layer

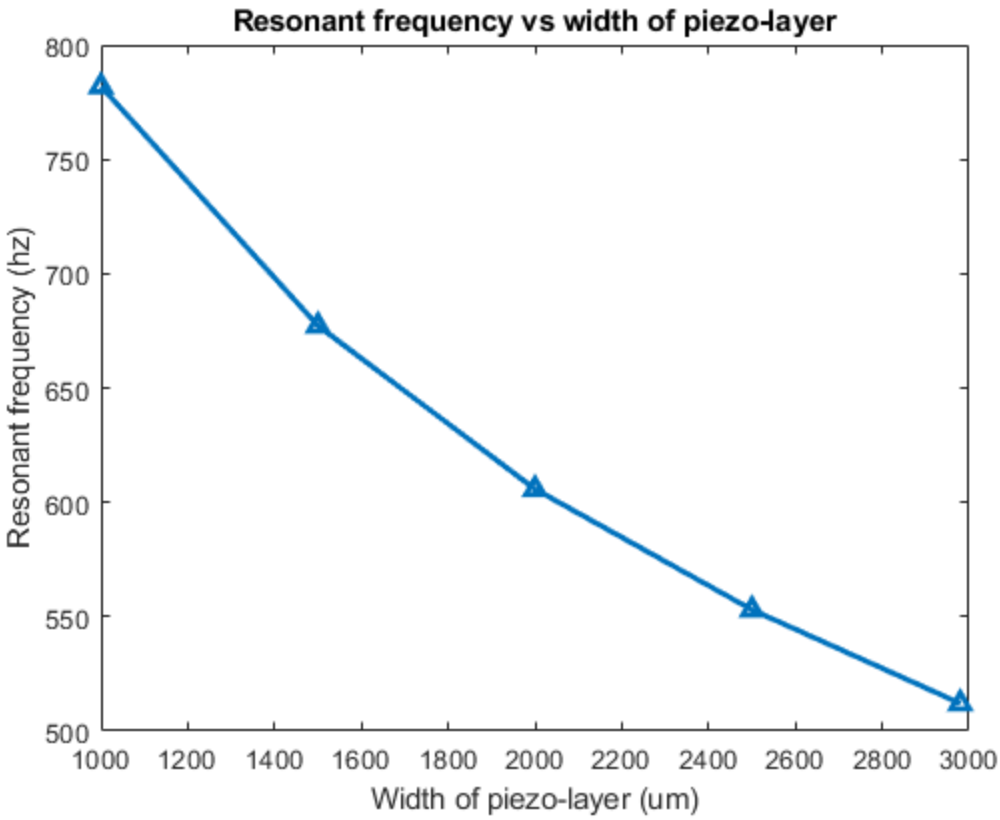

Figure 3. 10. Change in resonant frequency with change in width of piezo layer

4 Finite element model analysis

This chapter is about finite element model analysis of the of the both single and tri-axial accelerometers, COMSOL Multiphysics is used in this analysis. Three cases are considered for the analysis to verify and compare the result of FEM analysis with the analytical analysis done previous chapter for the single axis accelerometer design. While for the 3-axis accelerometer two cases are considered for the simulation and its analysis is performed in this chapter.

4.1 Single axis FEM analysis

Case 1: Changing only l_c length of cantilever substrate layer (silicon layer).

Case 2: Changing beam length or both the cantilever substrate layer (silicon layer) l_c and piezoelectric layer (active layer) l_p.

Case 3: Changing the width of the piezoelectric layer (active layer) w_p.

These are the same cases used in the analytical analysis and analysis are done for deflection, resonant frequency, and voltage sensitivity.

4.1.1 Geometrical structure designing and Meshing single axis accelerometer in COMSOL

Geometry of Single axis accelerometers were designed as shown in figure 4.1 in accordance with the optimum design parameters given in table 3.1. where the blue colour highlights the composite beam of Silicon (Si) as base substrate, Silicon dioxide (SiO_2) as buffer layer and Aluminium nitride (AlN) as active piezoelectric layer. Beam is attached to an anchor (support from one) and fixed from this side, while a seismic mass (proof mass) compose of Silicon (Si) is attached to other side of the beam which is free to move. For simulations the anchor (support) is neglected to avoid the complexities during the meshing process and the beam is selected to be fixed from one side instead of attaching it to an anchor and selecting the anchor as fixed object (which is the real-life design scenario).

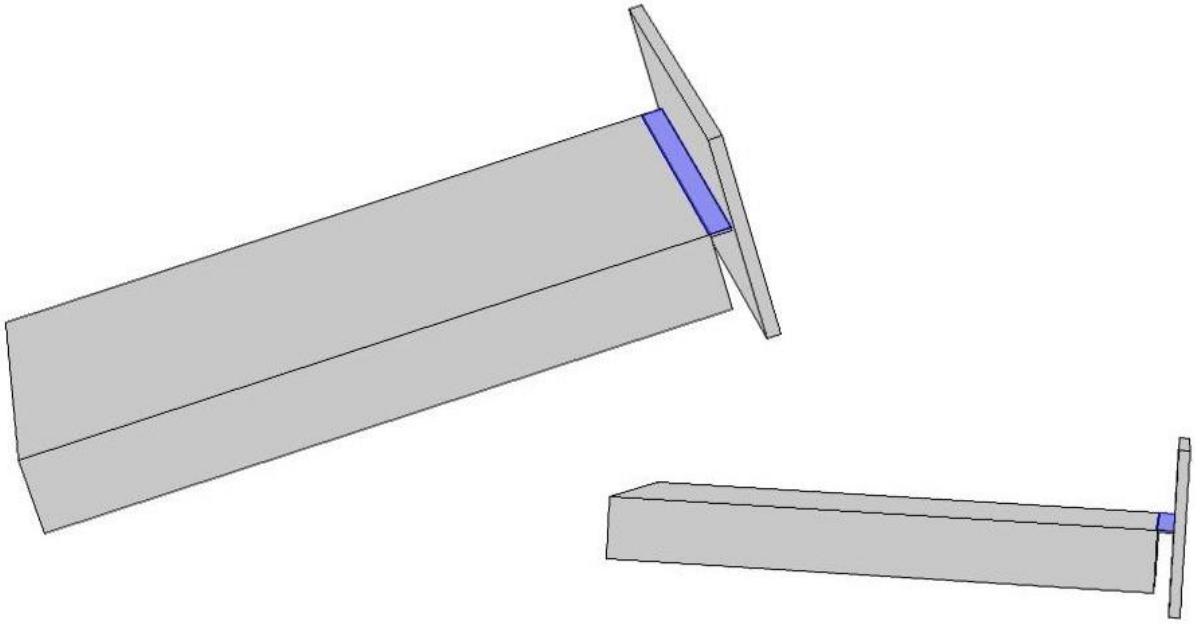

Figure 4. 1. Shows the design of single axis accelerometer

After finishing the geometory of the accelerometer, the process of add materials to its respective section begins with adding Silicon (Si) to the base substract of the beam and seismic mass, Silicon diaoxide (SiO_2) to buffer layer between the base substract and active layer (piezoelectric layer) and then Aluminum nidtride(AlN) to top layer of the beam.

Next step was to do the meshing of the geometory as shown in the figure 4.2. For mehsing user controlled mesh sequence type was selected with fine meshing size.

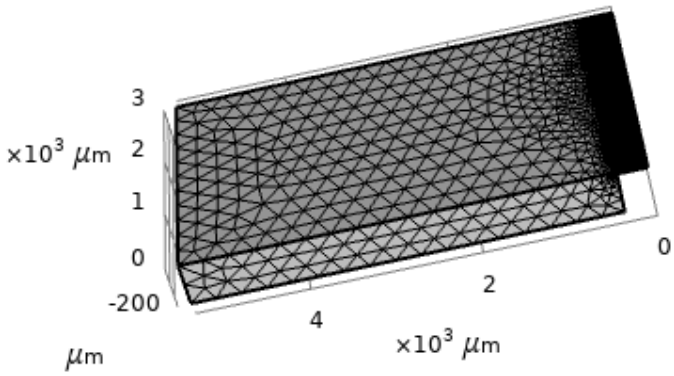

Figure 4. 2. Mesh of the single axis accelerometer in FEM analysis

4.1.2 Simulation's and its Results

FEM analysis are performed in three different cases of design parameters mentioned earlier and its effect on deflection, resonant frequency and voltage sensitivity is recorded for analysis purposes.

Case 1: Changing only l_c length of cantilever substrate layer (silicon layer)

Simulations are performed with acceleration of g (9.8 m/s^2) in all three-axis. And results are reported here for all three axes with its tables 3D plots and graph chart.

Deflection

Deflection is simulated with changing length of cantilever substrate l_c (Silicon layer). Table 4.1 shows the results for deflection, figure 4.4 shows 3D plotted and figure 4.3 shows the line chart of the values for deflection with respect to change in only l_c length of cantilever substrate layer (silicon layer).

Table 4. 1. Deflection recorded during simulation in all three axes (with acceleration g) of the changing l_c

No.	**l_c length of beam substrate in μm**	**Deflection in nm in Z-axis acceleration**	**Deflection in nm in X-axis acceleration**	**Deflection in nm in Y-axis acceleration**
1	150	8.895	0.0015	0.96
2	200	12.566	0.0019	1.33
3	250	16.093	0.0034	1.67
4	300	19.568	0.0050	2.05
5	350	23.559	0.0089	2.39

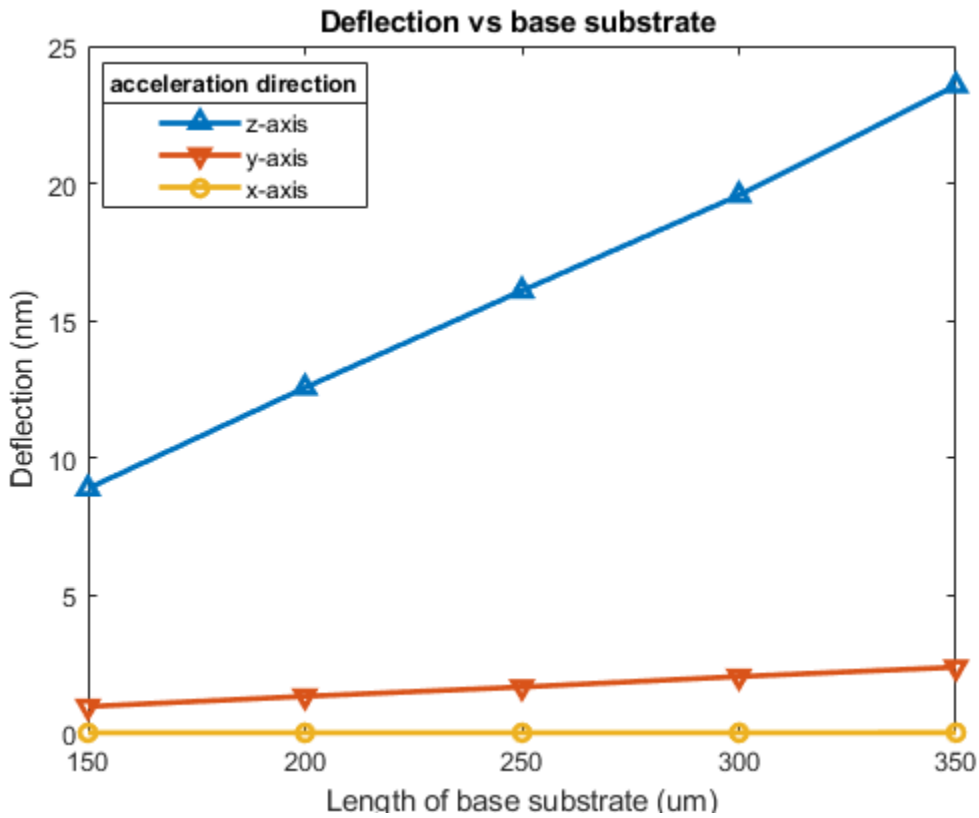

Figure 4. 3. Graph of deflection in diferent axes acceleration with changing l_c .

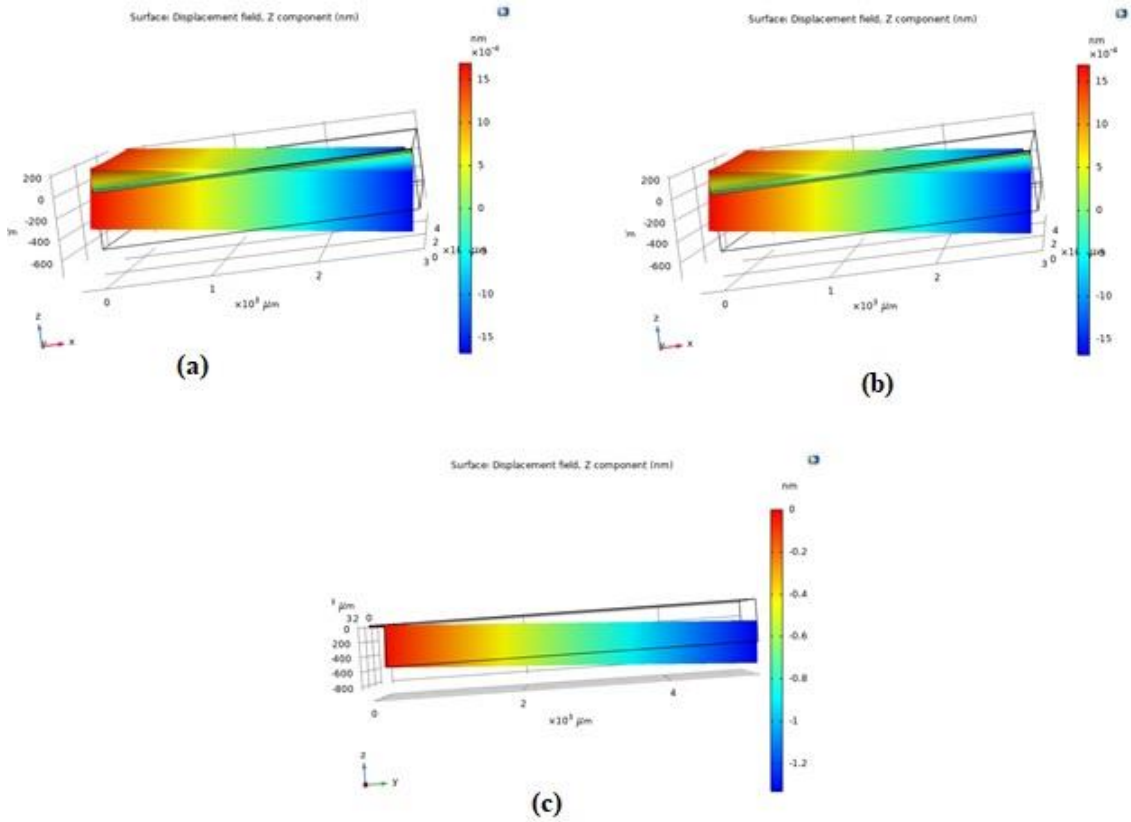

Figure 4. 4. Displacement to different direction acceleration (a) X-axis (b) Z-axis (c) Y-axis

Resonant frequency

In frequency analysis it is found that the direction of the acceleration applied had no effect on the resonant frequency and is same in all three directions. Table 4.2 shows the results for Resonant frequency, figure 4.6 shows all mentioned resonant frequencies plotted in 3D and figure 4.5 shows the line chart of the resonant frequencies with respect to change in only l_c length of cantilever substrate layer (silicon layer).

Table 4. 2. Resonant frequency recorded during simulation in all three axes acceleration g with changing l_c

No.	**l_c length of beam substrate in μm**	**Resonant frequency in Hz in Z-axis acceleration**	**Resonant frequency in Hz in X-axis acceleration**	**Resonant frequency in Hz in Y-axis acceleration**
1	150	619.55	619.55	619.55
2	200	525.98	525.98	525.98
3	250	463.48	463.48	463.48
4	300	417.59	417.59	417.59
5	350	382.27	382.27	382.27

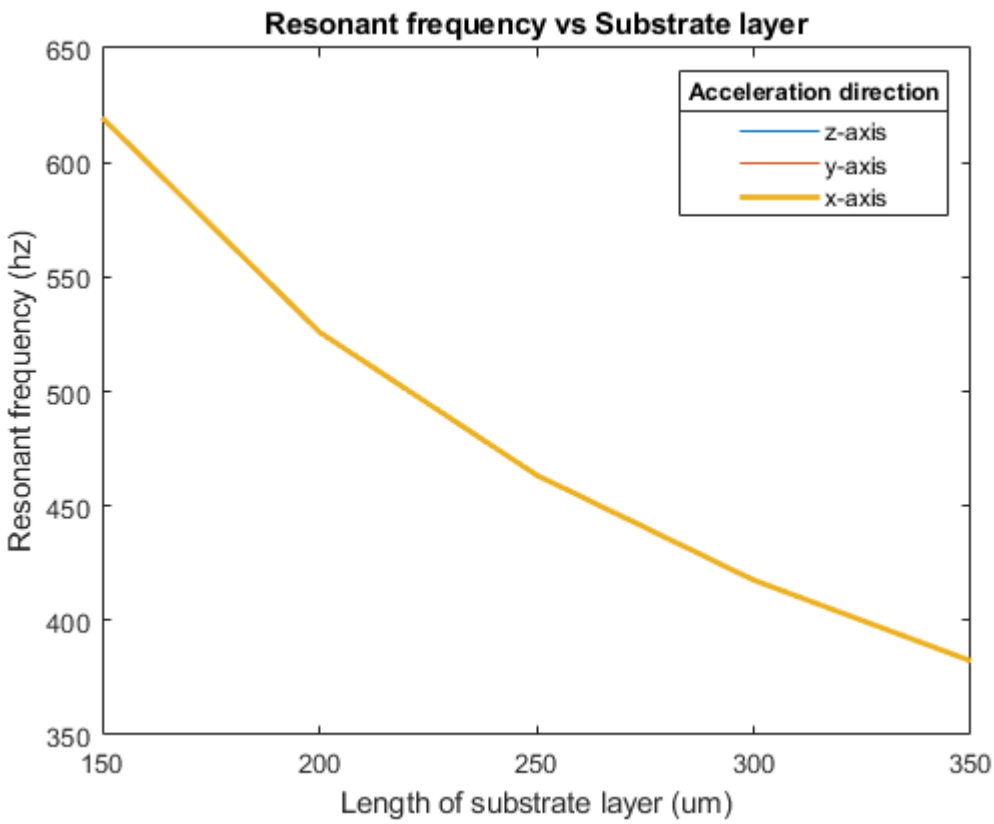

Figure 4. 5. Resonant frequency of in all three-direction acceleration with changing l_c.

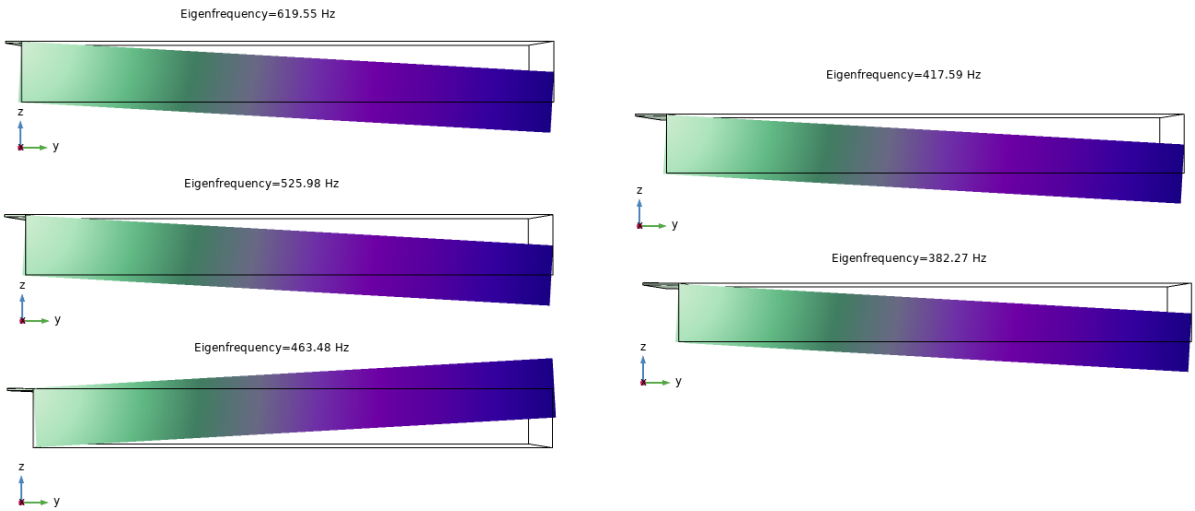

Figure 4. 6. 3D plots of resonant frequencies all mentioned lengths

Voltage sensitivity

Voltage sensitivity of accelerometer design is simulated with changing length of cantilever substrate l_c (Silicon layer). Table 4.3 shows the results for deflection, figure 4.7 ,4.8, 4.9 shows 3D plotted and figure 4.10 shows the line chart of the values for deflection with respect to change in only l_c length of cantilever substrate layer (silicon layer).

Table 4. 3. Generated voltage recorded during simulation in all three axes (with acceleration g) of the changing l_c

No.	**l_c length of beam substrate in μm**	**Voltage generated in (mv) by Z-axis acceleration**	**Voltage generated in (mv) by X-axis acceleration**	**Voltage generated in (mv) by Y-axis acceleration**
1	150	-0.892	-3.70E-07	-9.41E-02
2	200	-0.904	1.80E-06	-9.35E-02
3	250	-0.918	5.70E-06	-9.28E-02
4	300	-0.923	4.22E-06	-9.20E-02
5	350	-0.938	-1.25E-06	-9.15E-02

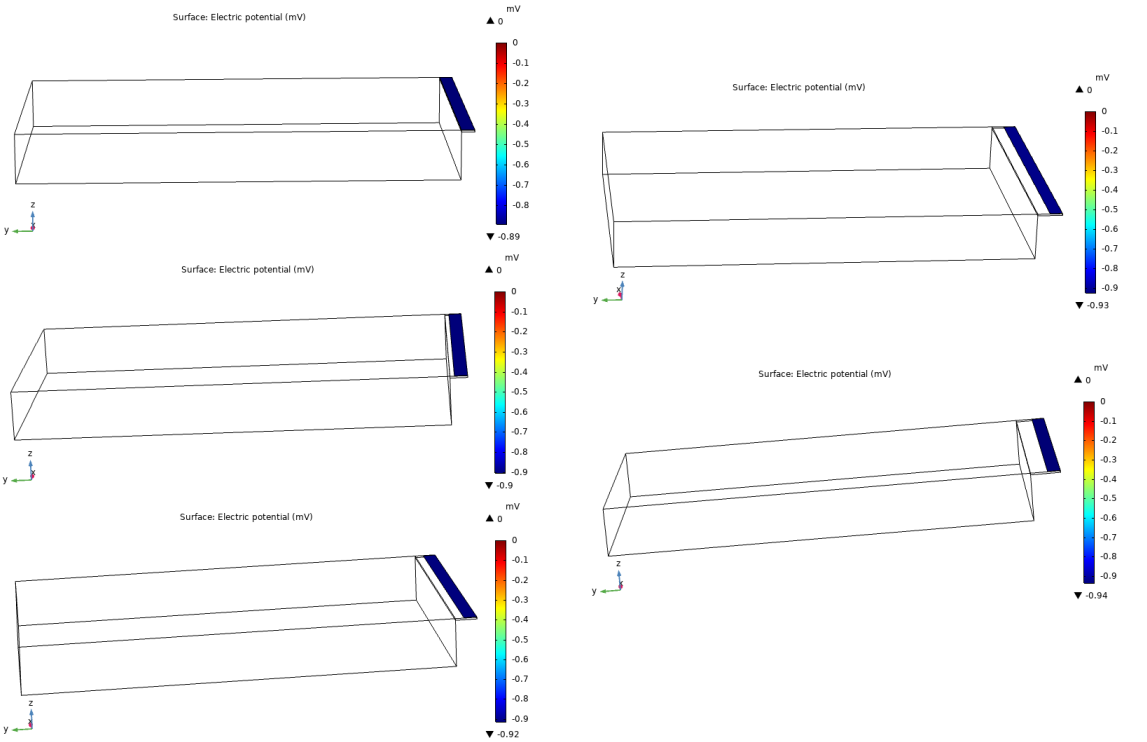

Figure 4. 7. Sensitivity at different length in z-axis acceleration

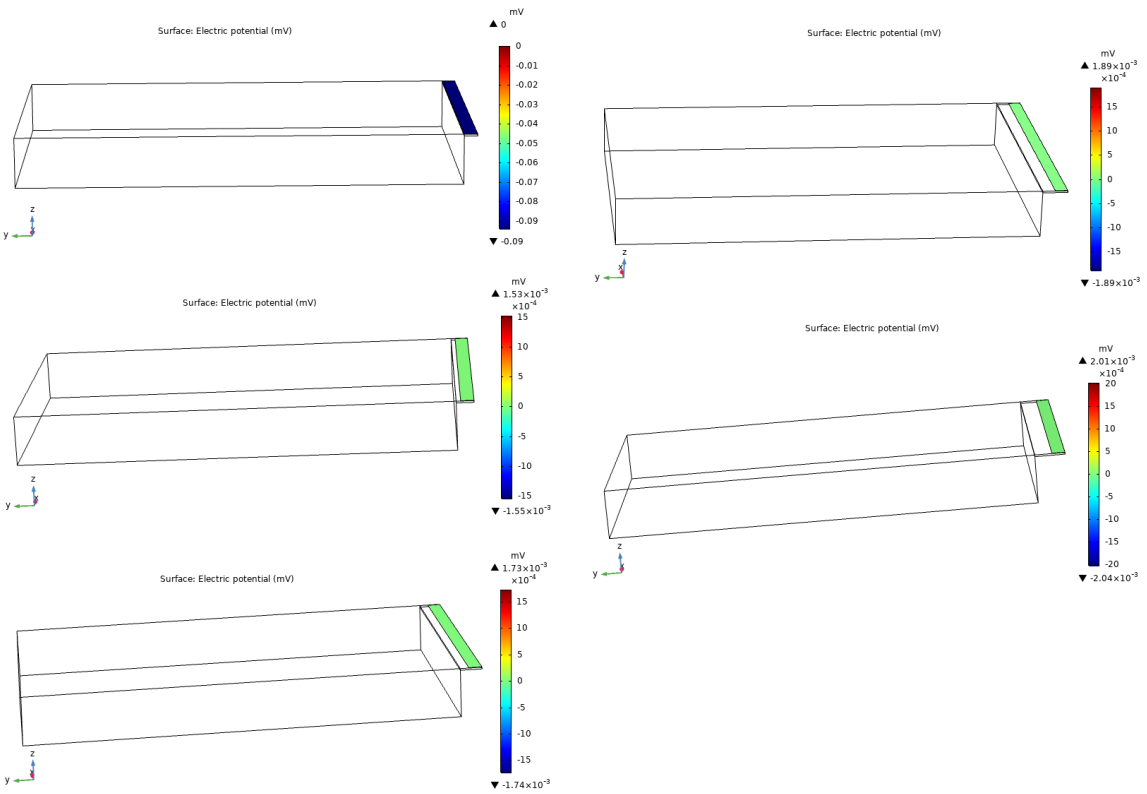

Figure 4. 8. Sensitivity at different length in y-axis acceleration

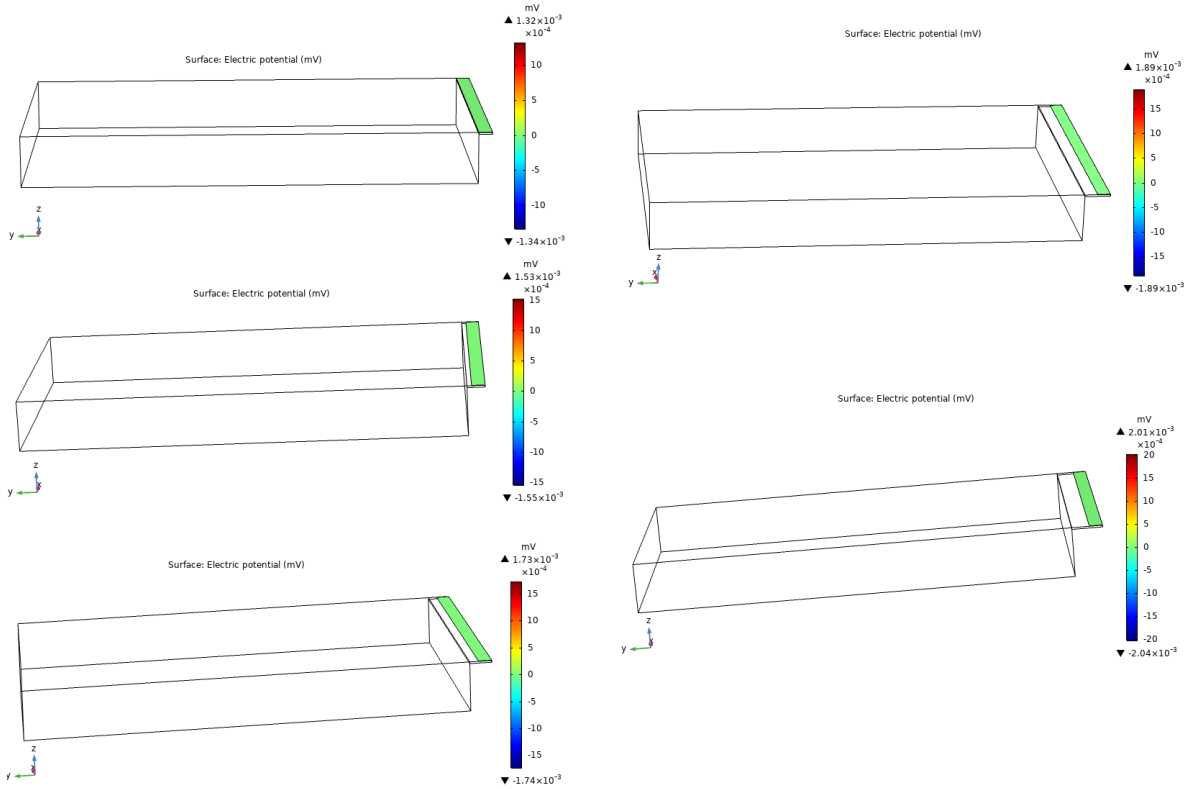

Figure 4. 9. Sensitivity at different length in x-axis acceleration

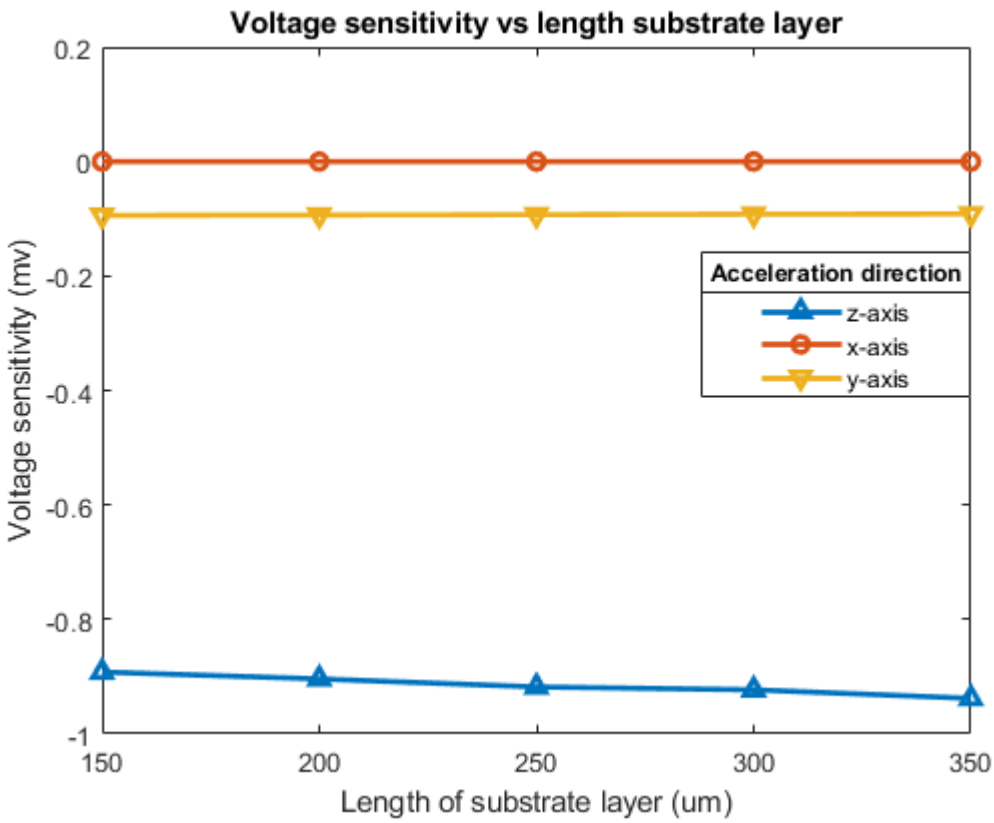

Figure 4. 10. Voltage generated in all three-direction acceleration with changing l_c.

Case 2: Changing beam length or both the cantilever substrate layer (silicon layer) l_c and piezoelectric layer (active layer) l_p.

Simulations are performed with acceleration of g (9.8 m/s^2) and in all three-directions. And results of deflection, frequency and voltage sensitivity are reported here for all three axes with its 3D plots and graph chart.

Deflection

Deflection is simulated with changing length of cantilever substrate l_c (Silicon layer) and piezoelectric layer (active layer) l_p. Table 4.4 shows the results for deflection, figure 4.12 (a)(b)(c) shows 3D plotted and figure 4.11 shows the line chart of the values for deflection while changing beam length or l_c length of cantilever substrate layer (silicon layer) and piezoelectric layer (active layer) l_p.

Table 4. 4. Deflection recorded during simulation in all three axes acceleration g with changing $l_c = l_p$ together or (beam length)

No.	$l_c = l_p$ in μm **Changing both**	**Deflection in nm in Z-axis acceleration**	**Deflection in nm in X-axis acceleration**	**Deflection in nm in Y-axis acceleration**
1	150	9.22	0.0012	0.987
2	200	12.09	0.0020	1.28
3	250	14.78	0.0030	1.55
4	300	17.50	0.0053	1.81
5	350	20.54	0.0078	2.09

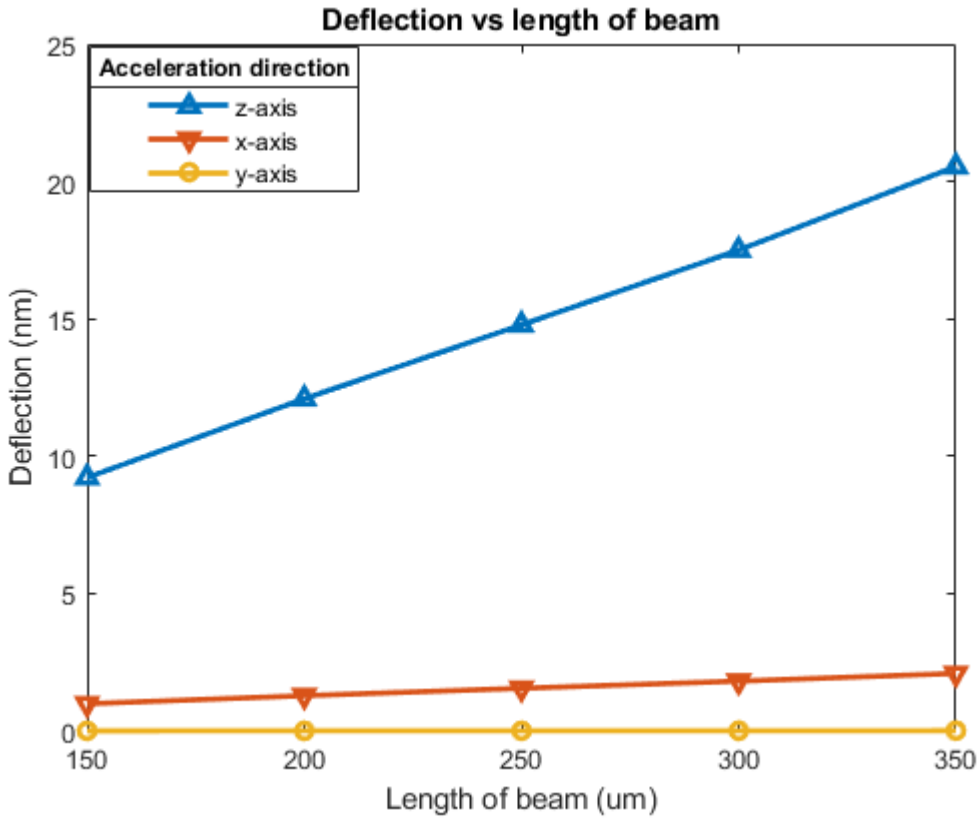

Figure 4. 11. Graph of deflection in diferent axes acceleration with changing $l_c = l_p$ (beam length)

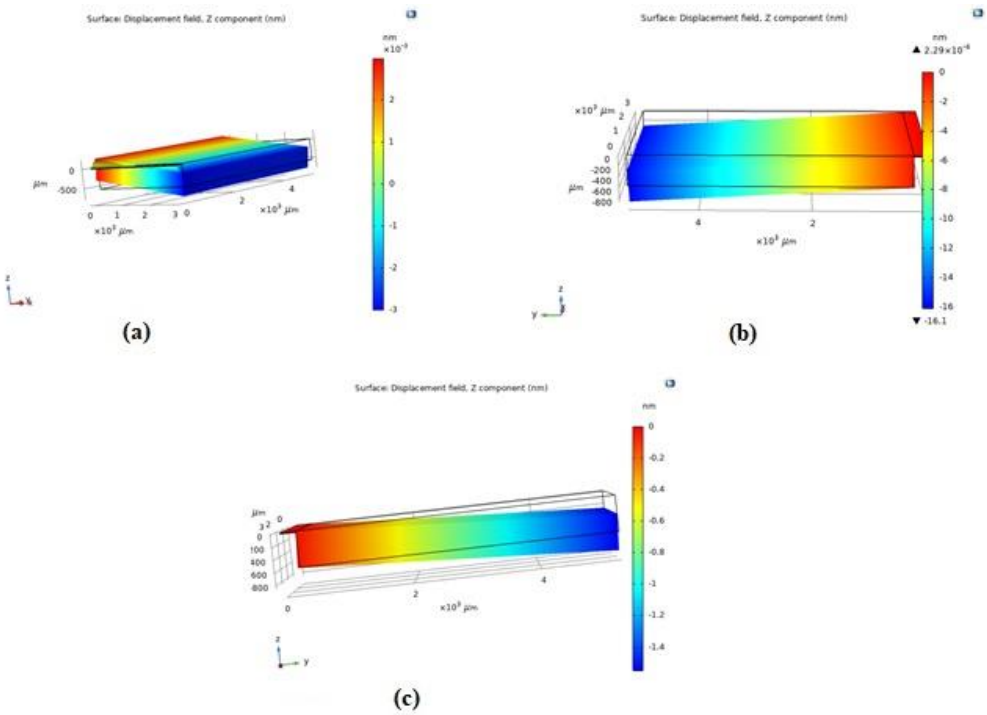

Figure 4. 12. Displacement to different direction acceleration (a) X-axis (b) Z-axis (c) Y-axis

Resonant frequency

In frequency analysis it is found that the direction of the acceleration applied had no effect on the resonant frequency and is same in all three directions. Table 4.5 shows the results for Resonant frequency, figure 4.13 shows 3D plotted of geometry at every frequency and figure 4.14 shows the line chart of the resonant frequencies with changing beam length or (l_c=$l_p$changing together).

Table 4. 5. Resonant frequency recorded during simulation in all three axes acceleration g with changing l_c =l_p together or (beam length)

No.	l_c = l_p in μm **Changing both**	**Resonant frequency in Hz in Z-axis acceleration**	**Resonant frequency in Hz in X-axis acceleration**	**Resonant frequency in Hz in Y-axis acceleration**
1	150	619.55	619.55	619.55
2	200	537.48	537.48	537.48
3	250	479.96	479.96	479.96
4	300	436.46	436.46	436.46
5	350	402	402	402

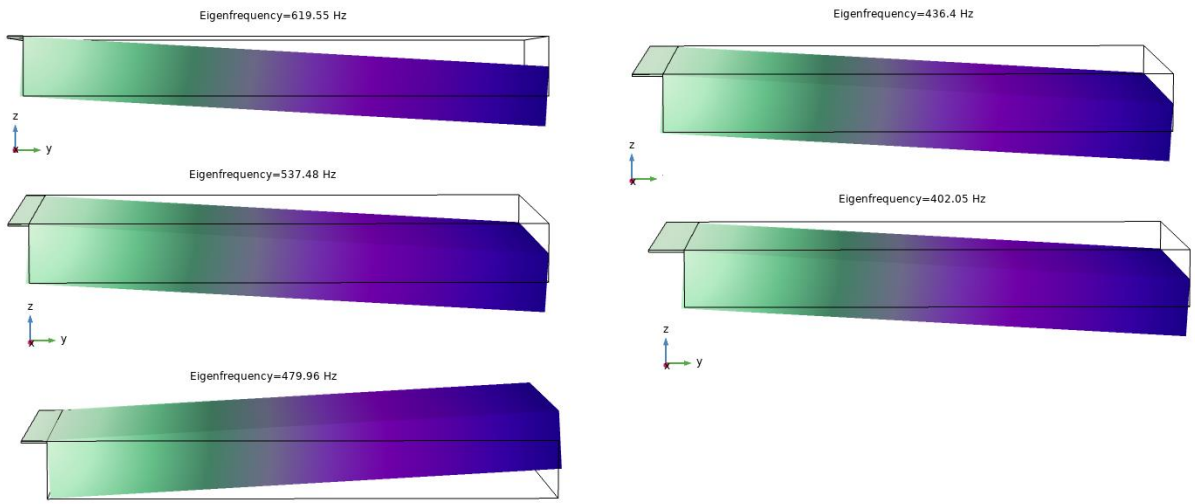

Figure 4. 13. Eigenfrequency at every length for z-axis acceleration

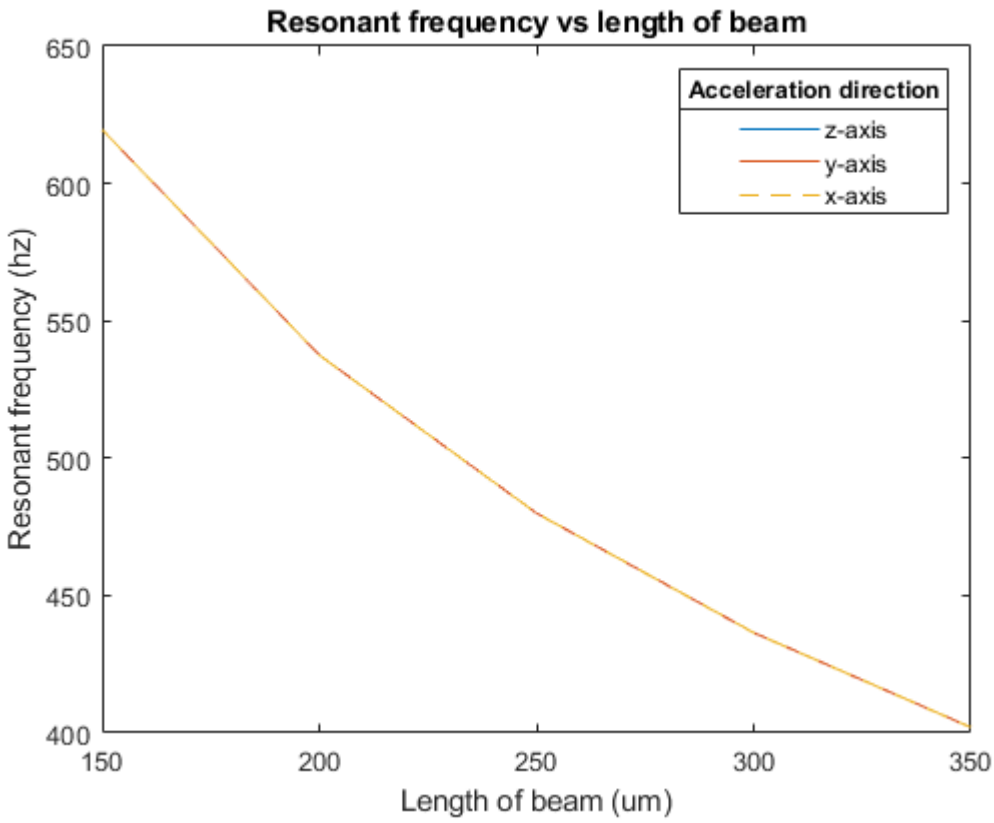

Figure 4. 14. Resonant in diferent axes acceleration with changing $l_c = l_p$ (beam length)

Voltage sensitivity

Design is simulated with changing length of cantilever substrate l_c (Silicon layer) and piezoelectric layer (active layer) l_p. Table 4.6 shows the results for deflection, figure 4.15 ,4.16,4.17 shows 3D plotted and figure 4.18 shows the line chart of the values for Voltage generated while changing beam length or l_c length of cantilever substrate layer (silicon layer) and piezoelectric layer (active layer) l_p.

Table 4. 6. Generated voltage recorded during simulation in all three axes acceleration g with changing $l_c = l_p$ together or (beam length)

No.	**l_c = l_p in μm Changing both**	**Voltage generated in (mv) by Z-axis acceleration**	**Voltage generated in (mv) by X-axis acceleration**	**Voltage generated in (mv) by Y-axis acceleration**
1	150	-0.892	3.70E-07	-0.094
2	200	-0.885	6.73E-07	-0.093
3	250	-0.883	2.79E-06	-0.091
4	300	-0.882	1.54E-06	-0.096
5	350	-0.881	-3.01E-07	-0.089

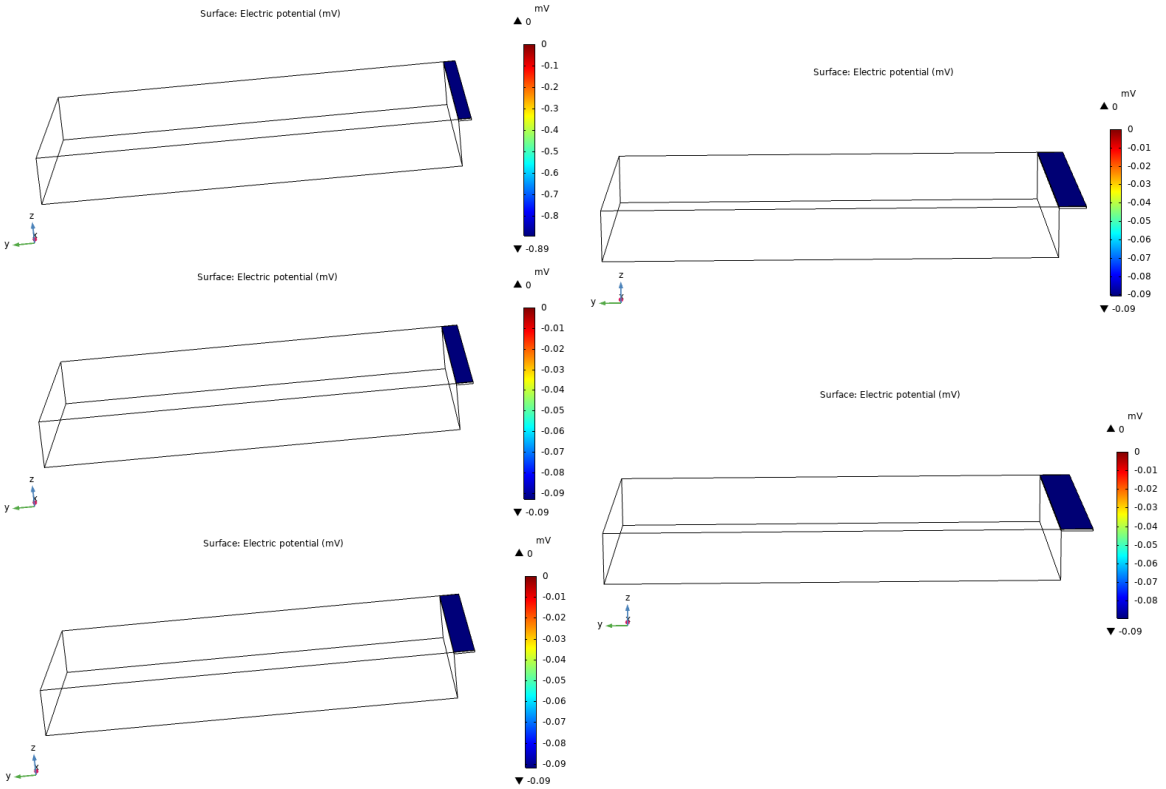

Figure 4. 15. Sensitivity at different length in z-axis acceleration

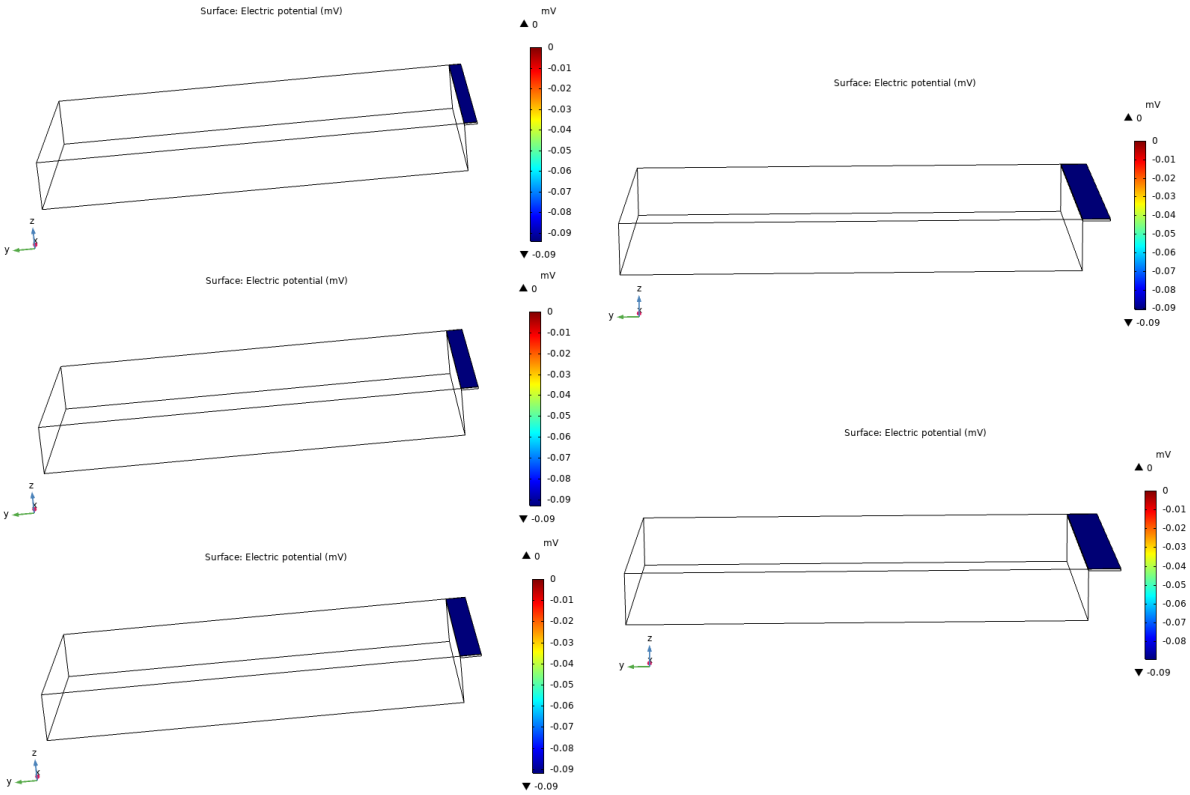

Figure 4. 16. Sensitivity at different length in Y-axis acceleration

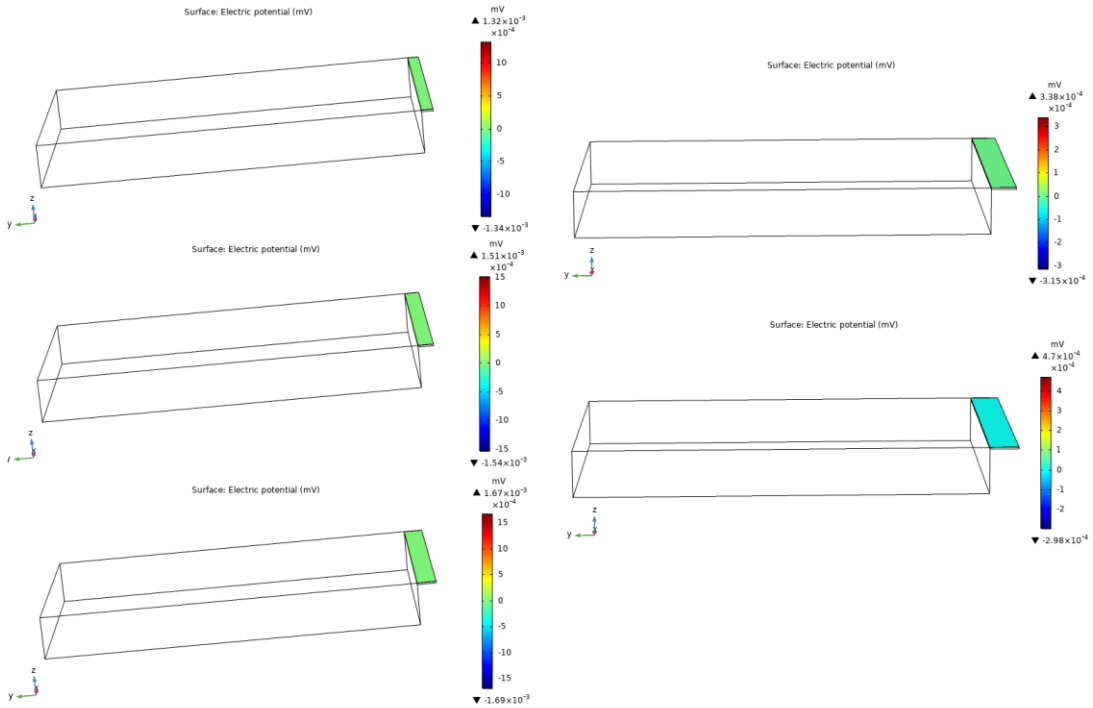

Figure 4. 17. Sensitivity at different length in X-axis acceleration

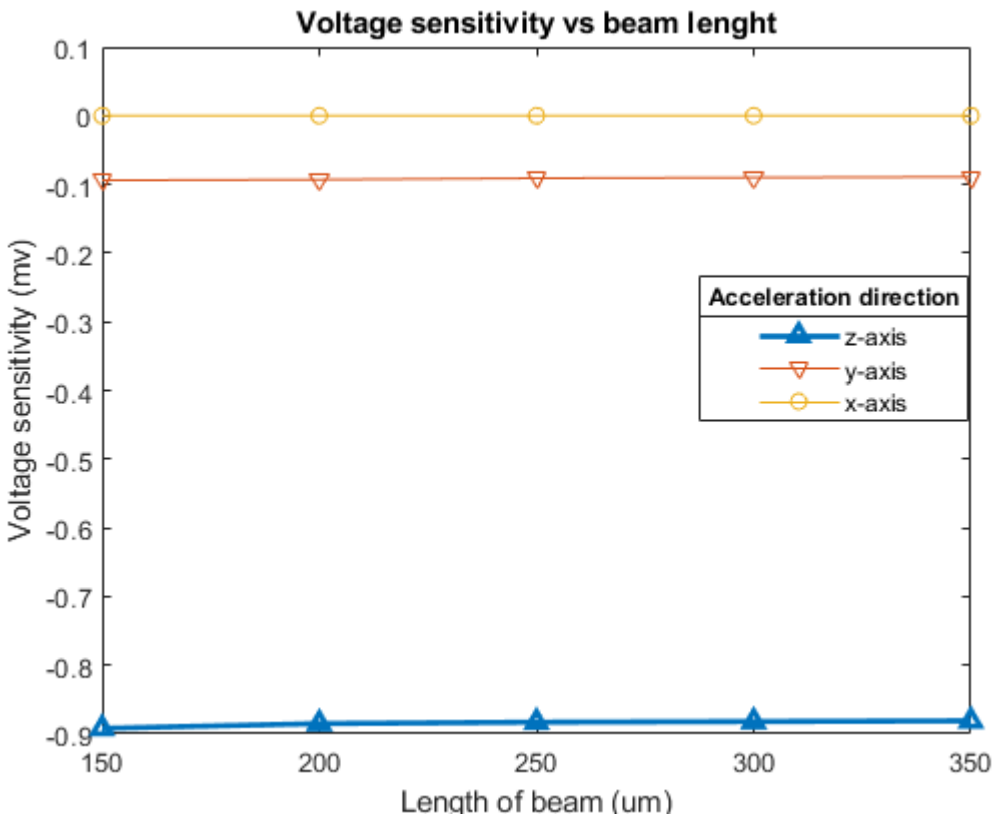

Figure 4. 18. Voltage generated in all three-direction acceleration with changing $l_c = l_p$ (beam length)

Case 3: Changing the width of the piezoelectric layer (active layer) w_p

Simulations are performed with acceleration of g (9.8 m/s^2) and in all three-directions. And results of deflection, frequency and voltage sensitivity are reported here for all three axes with its 3D plots and graph chart.

Deflection

Accelerometer is simulated with changing the width of the piezoelectric layer (active layer) w_p. Table 4.7 shows the results for deflection, figure 4.20 shows 3D plotted and figure 4.19 shows the line chart of the values for deflection while changing the width of the piezoelectric layer (active layer) w_p.

Table 4. 7. Deflection recorded during simulation in all three axes acceleration g with changing w_p (Width of active layer)

No.	w_p in μm	**Deflection in nm in Z-axis acceleration**	**Deflection in nm in X-axis acceleration**	**Deflection in nm in Y-axis acceleration**
1	1000	10.44	0.00135	1.12
2	1500	10.09	0.00132	1.08
3	2000	9.78	0.00132	1.04
4	2500	9.49	0.00130	1.01
5	2980	9.22	0.00124	0.98

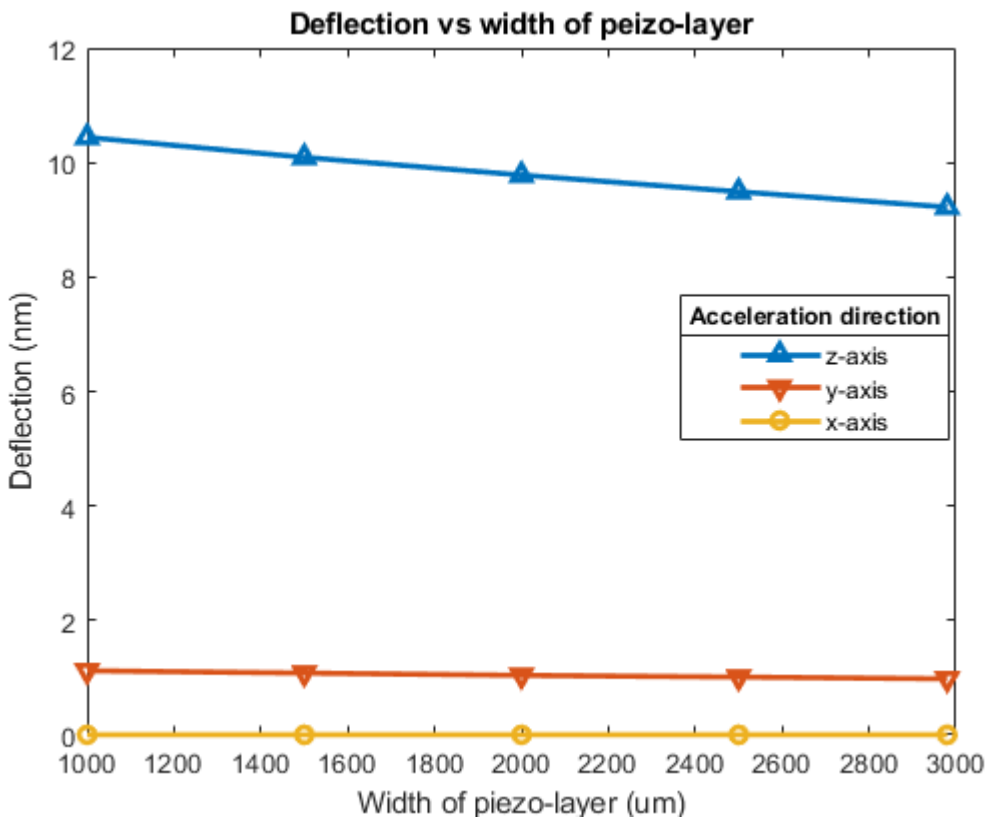

Figure 4. 19. Graph of deflection in diferent axes acceleration with changing w_p.

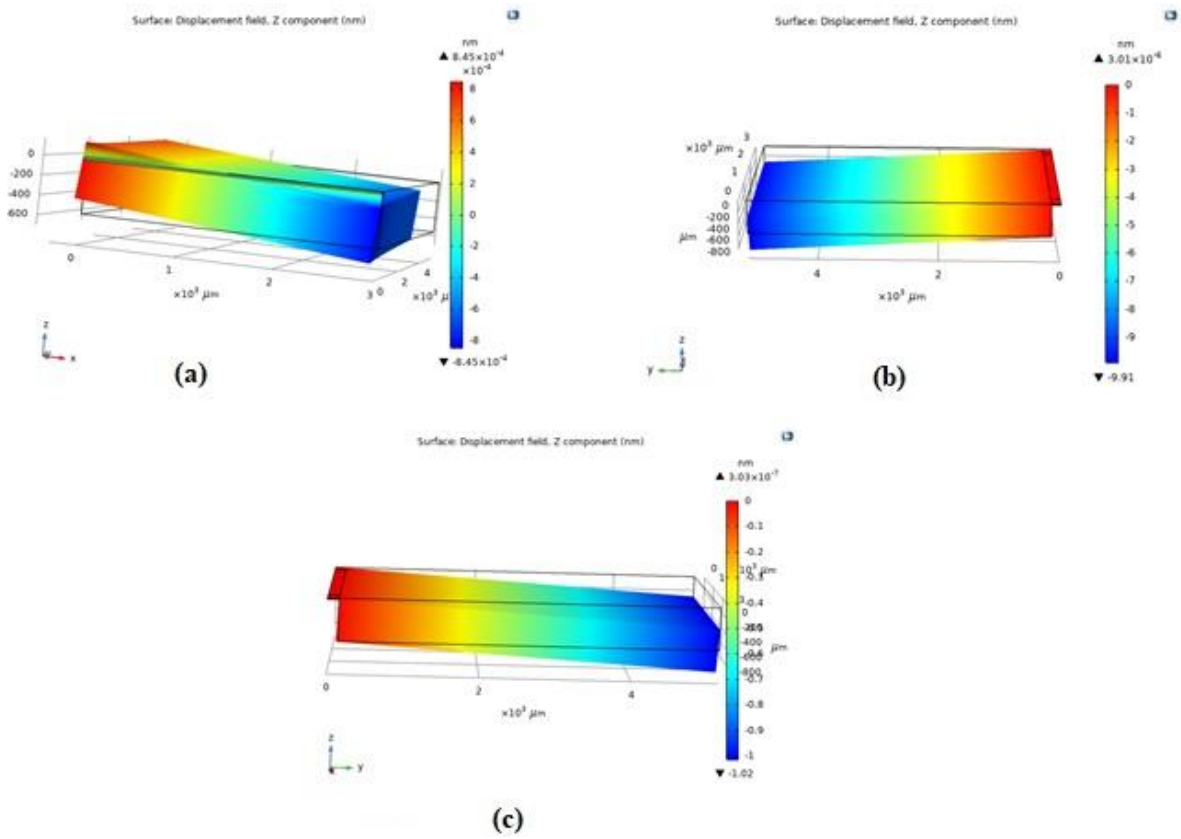

Figure 4. 20. Displacement to different direction acceleration (a) X-axis (b) Z-axis (c) Y-axis

Resonant frequency

In frequency analysis it is found that the direction of the acceleration applied had no effect on the resonant frequency and is same in all three directions. Table 4.8 shows the results for Resonant frequency, figure 4.21 shows 3D plotted geometry at all mentioned frequencies and figure 4.22 shows the line chart of the resonant frequencies with Changing the width of the piezoelectric layer (active layer) w_p.

Table 4. 8. Resonant frequency recorded during simulation in all three axes with acceleration g while changing w_p (Width of active layer)

No.	w_p in μm	**Resonant frequency in Hz in Z-axis acceleration**	**Resonant frequency in Hz in X-axis acceleration**	**Resonant frequency in Hz in Y-axis acceleration**
1	1000	586.66	586.66	586.66
2	1500	595.62	595.62	595.62
3	2000	603.83	603.83	603.83
4	2500	611.97	611.97	611.97
5	2980	619.55	619.55	619.55

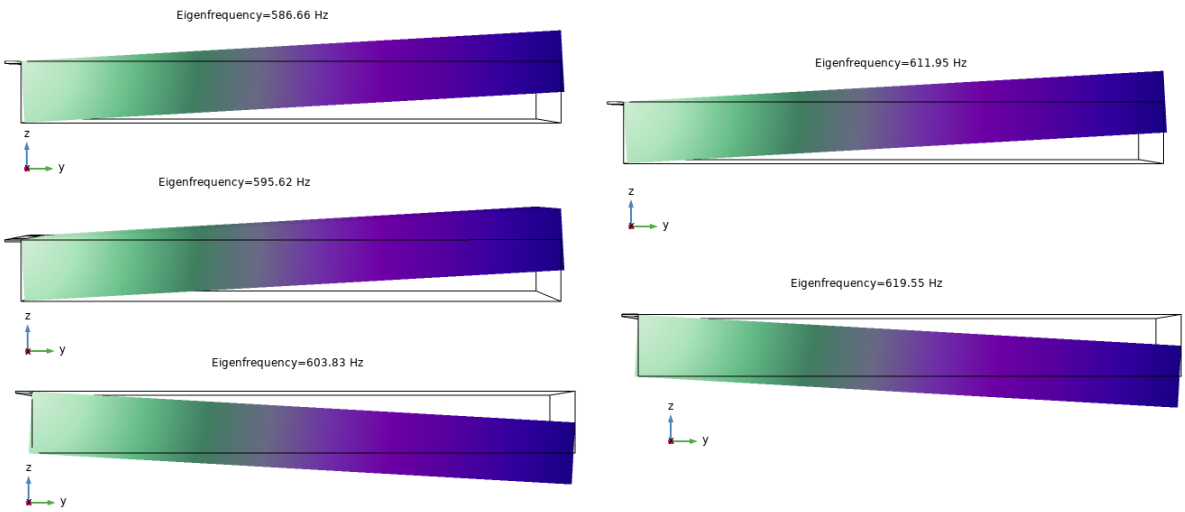

Figure 4. 21. Eigenfrequency at every length for z-axis acceleration

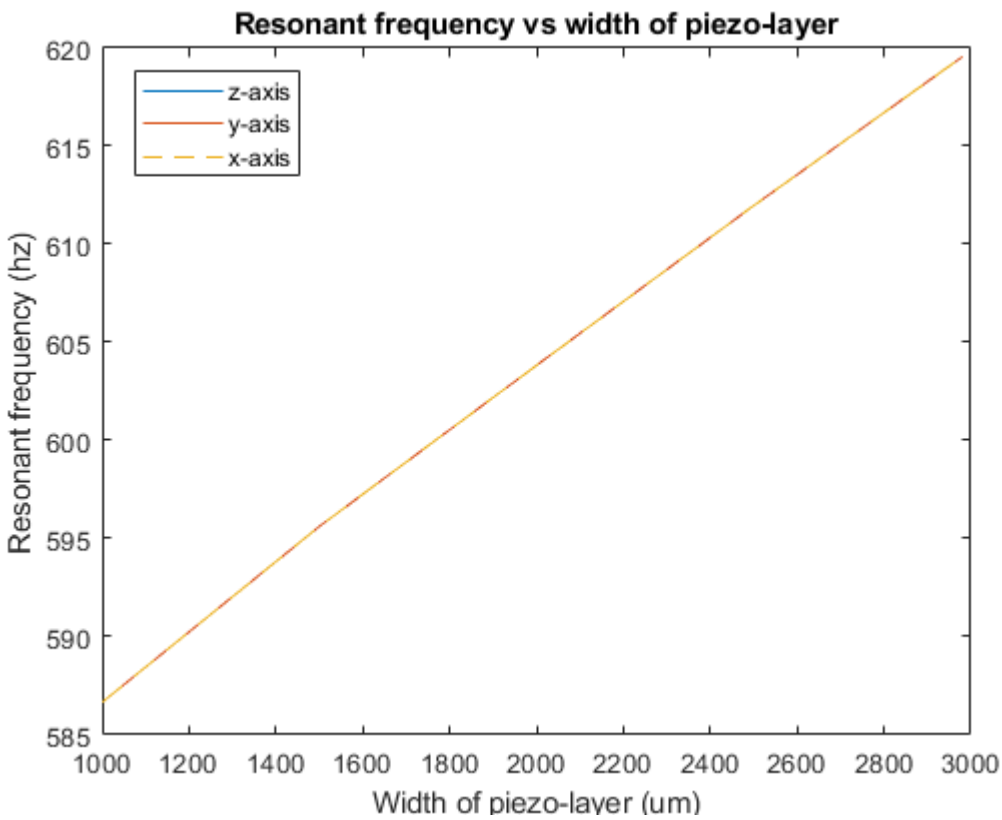

Figure 4. 22. Resonant frequency in diferent axes with acceleration of g while changing w_p.

Voltage sensitivity:

Accelerometer is simulated with changing the width of the piezoelectric layer (active layer) w_p. Table 4.9 shows the results for generated voltage, figure 4.23, 4.24, 4.25 shows 3D plotted and figure 4.26 shows the line chart of the values for generated voltage while changing the width of the piezoelectric layer (active layer) w_p.

Table 4. 9. Generated voltage recorded during simulation in all three axes with acceleration g while changing w_p (Width of active layer)

No.	w_p in μm	Voltage generated in (mv) by Z-axis acceleration	Voltage generated in (mv) by X-axis acceleration	Voltage generated in (mv) by Y-axis acceleration
1	1000	-1.04	2.63E-06	-0.1086
2	1500	-0.992	9.10E-07	-0.1047
3	2000	-0.959	9.10E-07	-0.101
4	2500	-0.925	-1.25E-06	-0.0975
5	2980	-0.892	-3.79E-07	-0.094

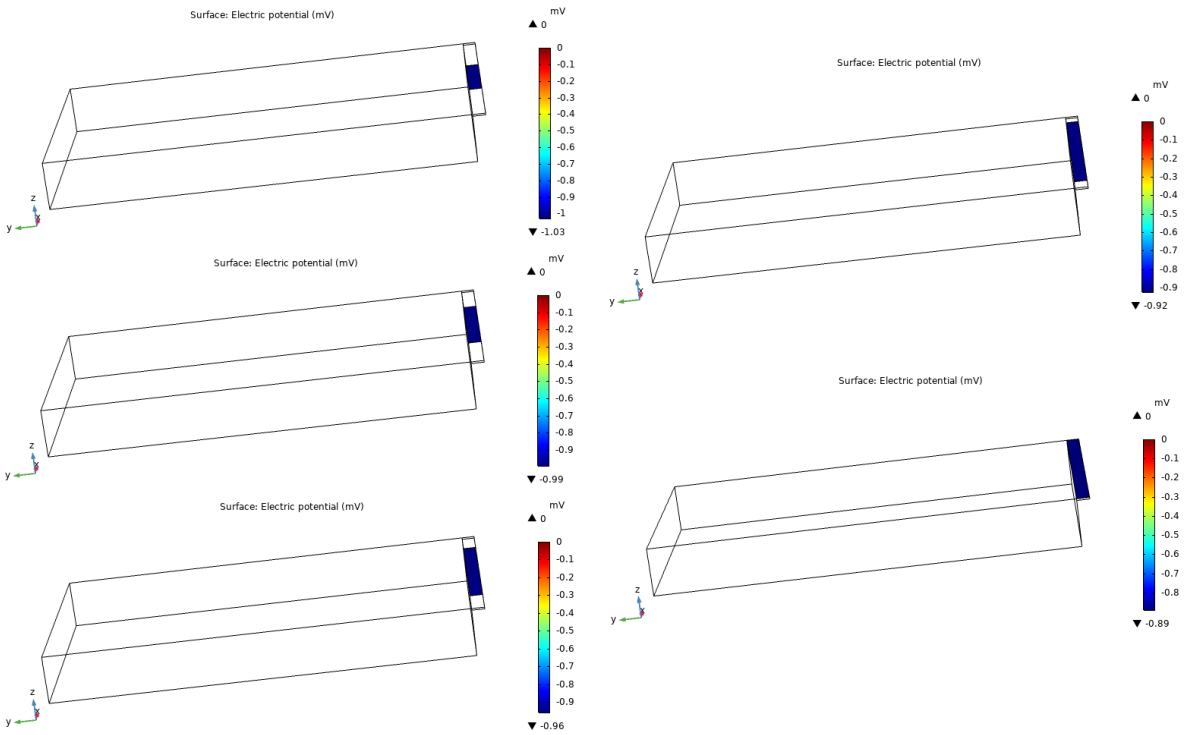

Figure 4. 23. Sensitivity at different piezo width in Z-axis acceleration

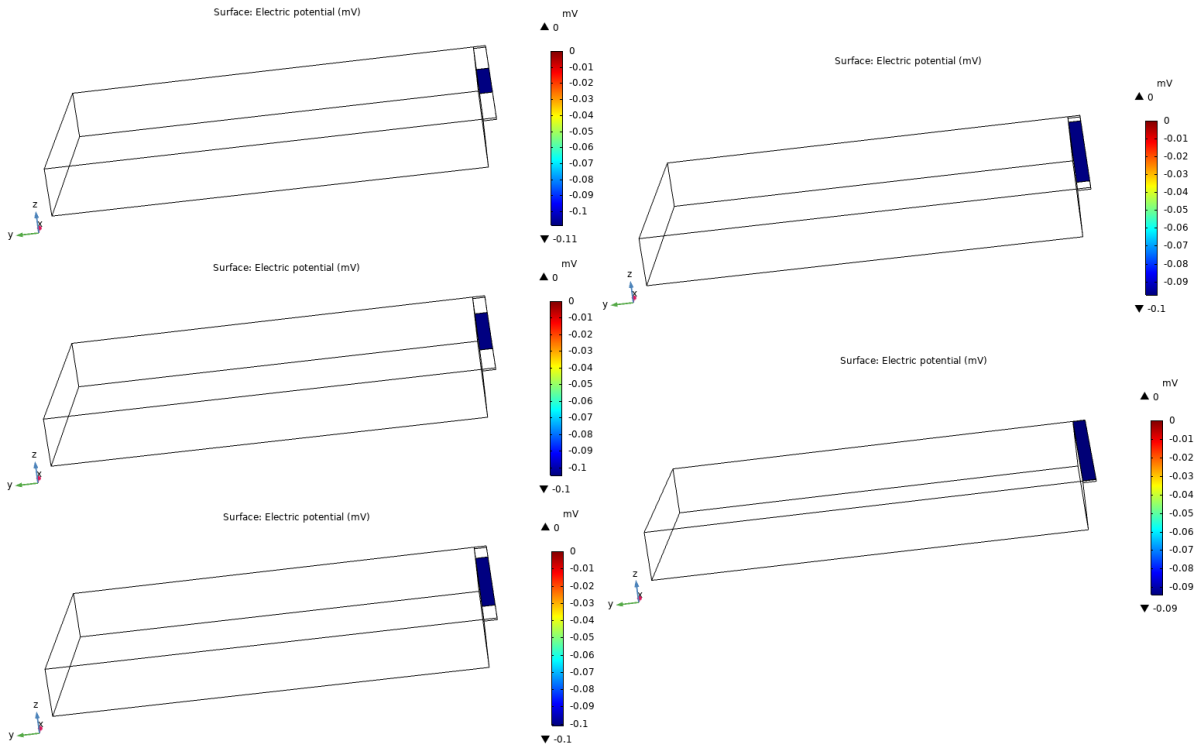

Figure 4. 24. Sensitivity at different piezo width in Y-axis acceleration

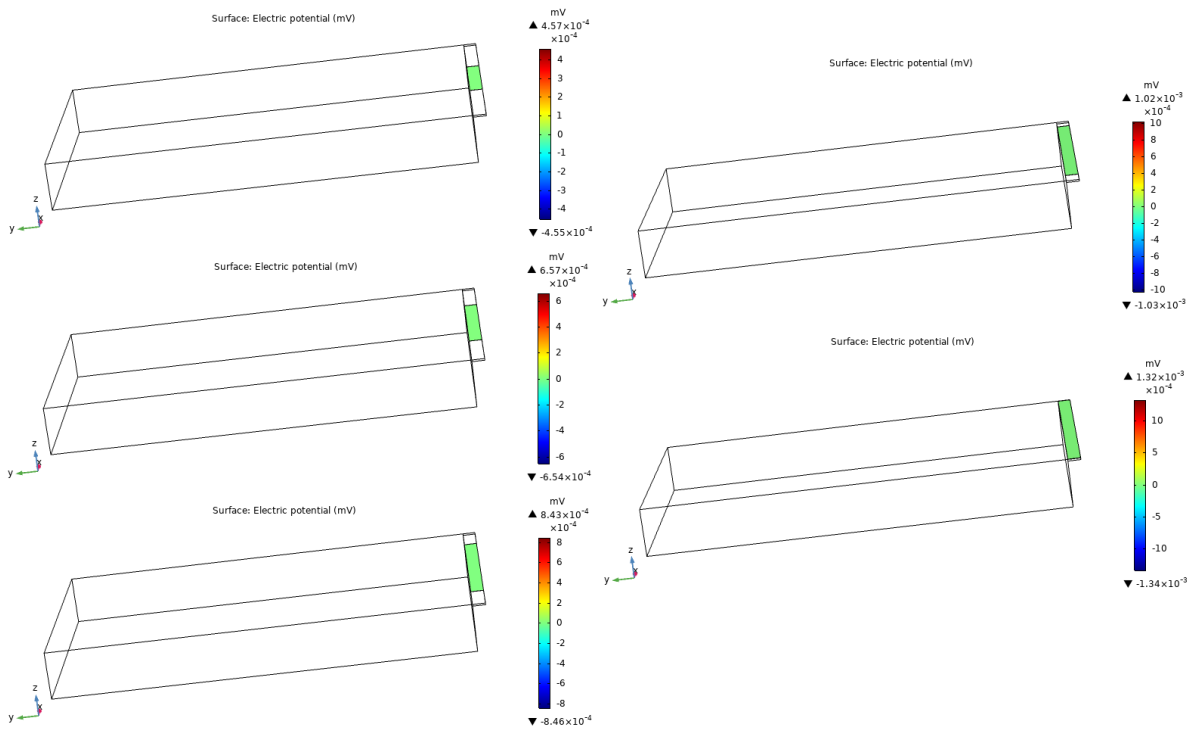

Figure 4. 25. Sensitivity at different piezo width in X-axis acceleration

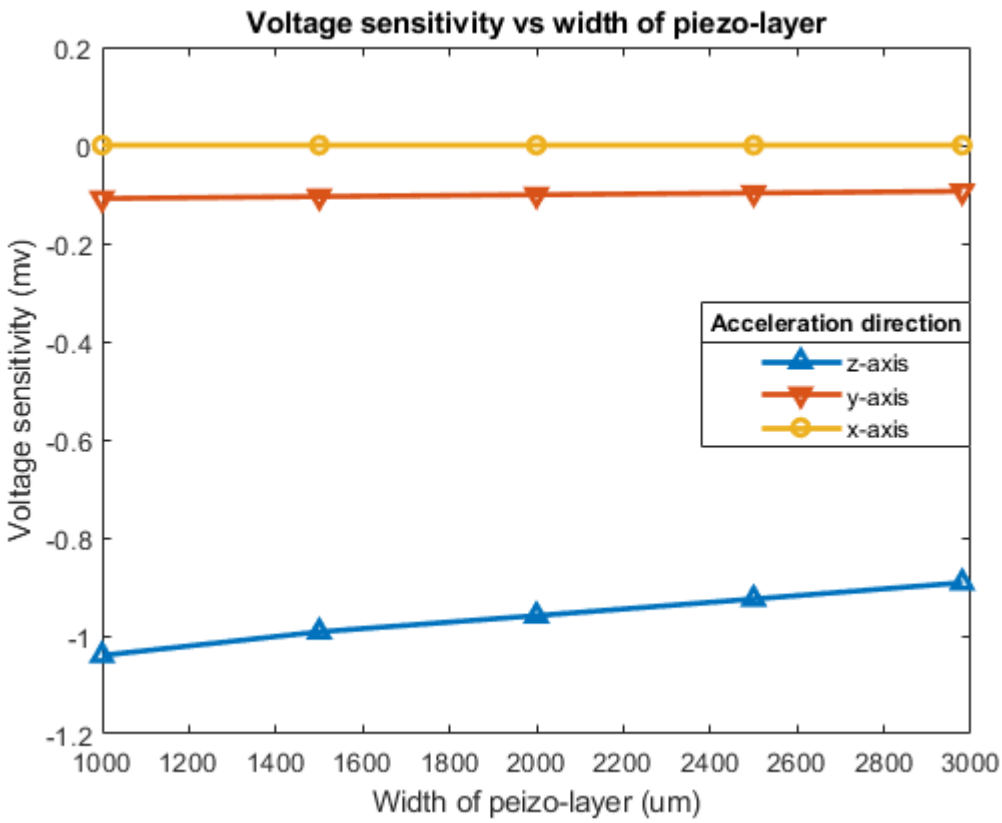

Figure 4. 26. Voltage generated in all three-direction with acceleration of g while changing w_p.

4.2 3-axis accelerometer FEM analysis

FEM analysis of 3- axis accelerometer was performed with the same COMSOL Multiphysics tool used for the single axis accelerometers FEM analysis. The approach of the simulation here was also the same. Some initial design parameter (table 4.10) was selected on the base of literature reviews and knowledge of the design parameters of the single axis accelerometer to be the base of the first geometrical design of our 3-axis accelerometer.

Two cases or scenario was selected for three-axis accelerometer to simulation on, with an acceleration of 1-g for X, Y, Z directions, respectively.

Case 1: Changing the length piezoelectric layer (active layer) l_p.

Case 2: Changing the width of the piezoelectric layer (active layer) w_p.

Table 4. 10. Initial selected parameters value for the 3-axis accelerometer based on the base of literature and knowledge of single axis accelerometer value.

Letter	Representation description	Values
l_c	Length of the cantilever (Silicon layer)	1000 μm
t_c	Thickness of the cantilever (Silicon layer)	15 μm
w_c	Width of the cantilever (Silicon layer)	2000 μm
l_p	Length of the AlN (active layer)	1000 μm
w_p	Width of AlN (active layer)	1980 μm
t_p	Thickness of AlN (active layer)	0.6 μm
l_m	Thickness of Si mass (proof mass)	570 μm
w_m	Width of Si mass (proof mass)	3000 μm
l_m	Length of Si mass (proof mass)	5000 μm
m	Mass	24 mg
a_z	Acceleration	9.8 m/s^2

4.2.1 Geometrical structure designing and Meshing tri-axial accelerometer in COMSOL

Three axis accelerometer design shown in figure 4.27, 4.28,4.29 the composition of the beams and seismic mass are same materials with same layers approach as per the single axis accelerometer, but with different dimensions and is design according to the initially selected parameters value as per table 4.10. Although one major change is the number of beams, now we are having four beams attached to all four sides of the seismic mass to be able to get the signal for 3-direction movement and which was only one in the case of the single axis accelerometer.

The figure 4.27 shows the design of the 3-axis accelerometer. where the blue colour highlights the composite beam with Silicon (Si) as base substrate, Silicon dioxide (SiO_2) as buffer layer and Aluminium nitride (AlN) as active piezoelectric layer.

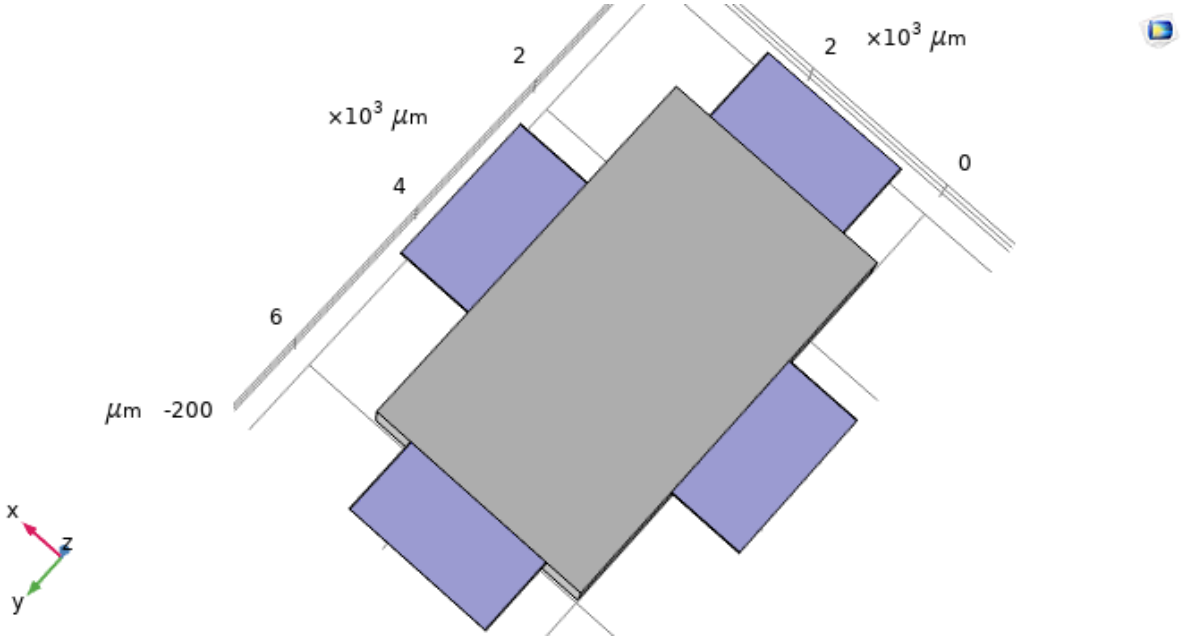

Figure 4. 27. 3-axis accelerometer design with composite beams highlighted in blue

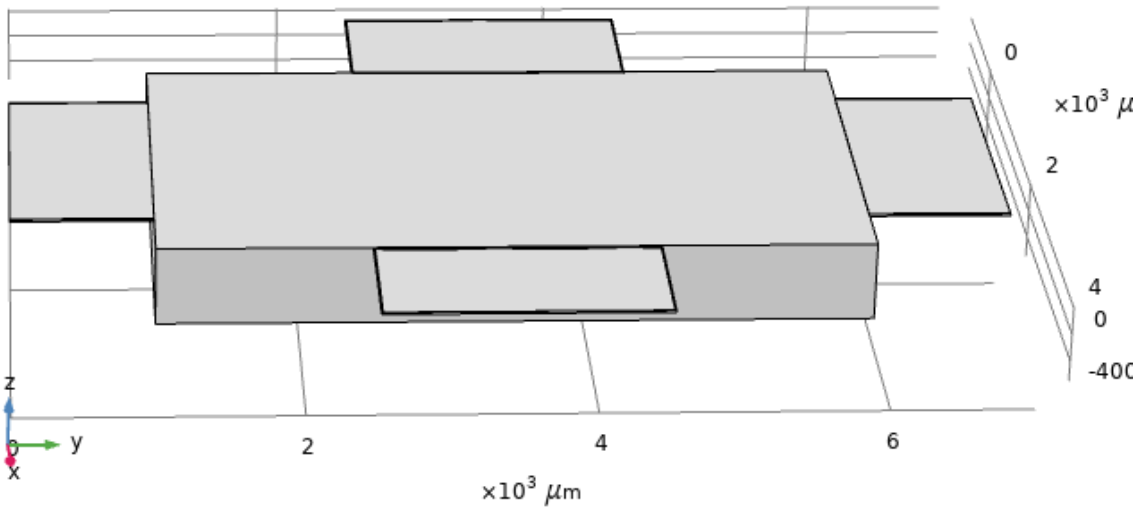

Figure 4. 28. 3-axis accelerometer design view top with and angle

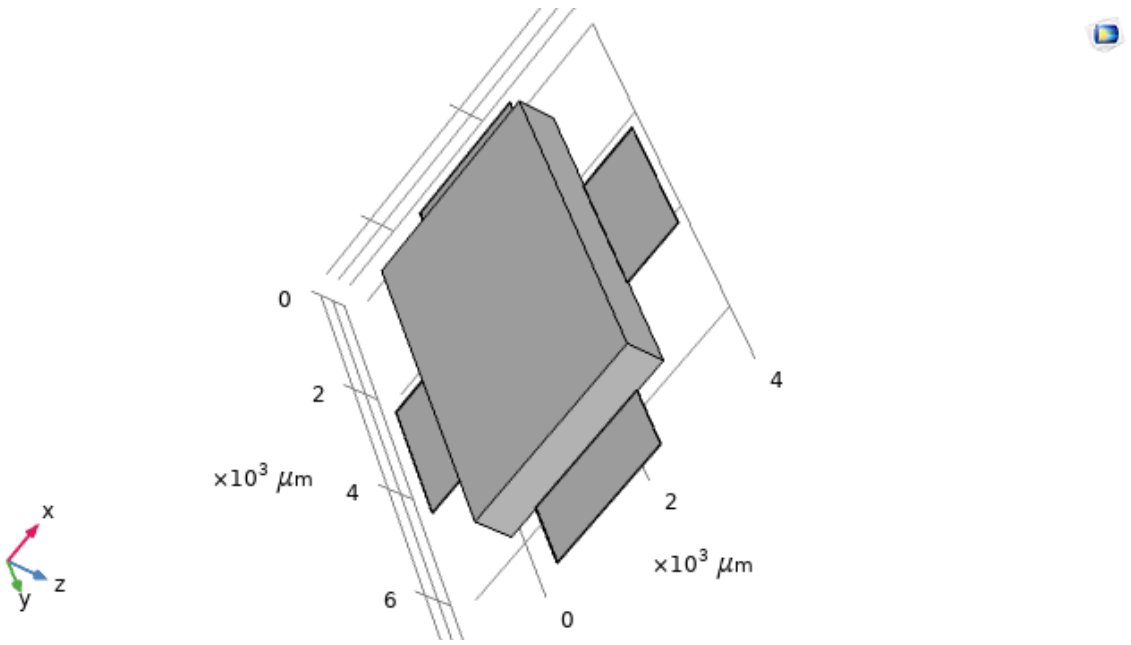

Figure 4. 29. 3-axis accelerometer design view from bottom with an angle

Once the geometry design stage of the 3-axis accelerometer was achieved, next step was to do the meshing of the geometry to perform the simulation and compute the response of our design. We need to perform the meshing every time we make change in any of the parameters in our design to simulate the changes and compute the respective results. For mehsing user controlled mesh sequence type was selected with fine meshing size. Figure 4.30(a), (b) shows a sample of meshing done for a particular design during our simulations of many different scenarios.

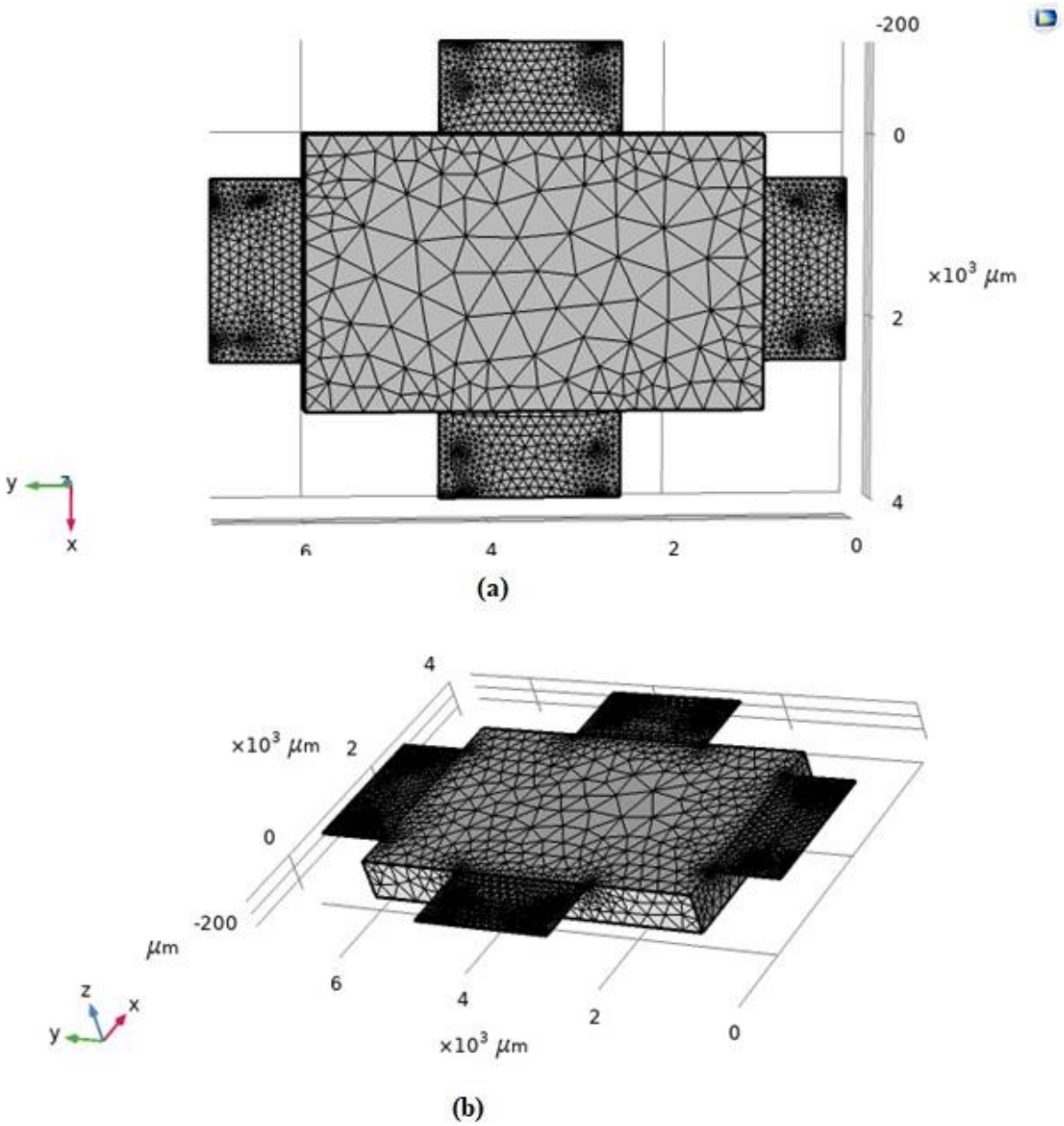

Figure 4. 30. (a)(b) Shows the geometry after meshing from two different angles

4.2.2 Simulation's and its Results

FEM analysis are performed in two different cases of design parameters mention earlier and its effect on deflection, resonant frequency and voltage sensitivity is recorded for analysis purposes, both cases are reported here.

Case 1: Changing the length piezoelectric layer (active layer) l_p.

Simulation were performed with changing the length active-layer only and acceleration of **g** applied from either X, Y, Z-direction (from one direction at time), the response of deflection, frequency and sensitivity to the change in beam length is measured and reported.

Deflection

Deflection in the beams were analysed after every change in the length of beams, with an applied acceleration of **g** from X, Y, Z directions, respectively. Table 4.11 shows the results for deflection, figure 4.31 shows 3D plotted and figure 4.32 shows line grape plot from the values reported in table.

Table 4. 11. Deflection against different beam lengths at different direction acceleration g applied.

No.	**Length of piezo layer in um**	**Deflection in nm in Z-axis acceleration**	**Deflection in nm in X-axis acceleration**	**Deflection in nm in Y-axis acceleration**
1	500	21.215	2.38	2.30
2	700	25.218	3.01	2.6469
3	900	18.34	2.17	2.1676
4	1000	3.408	0.1670	0.1326

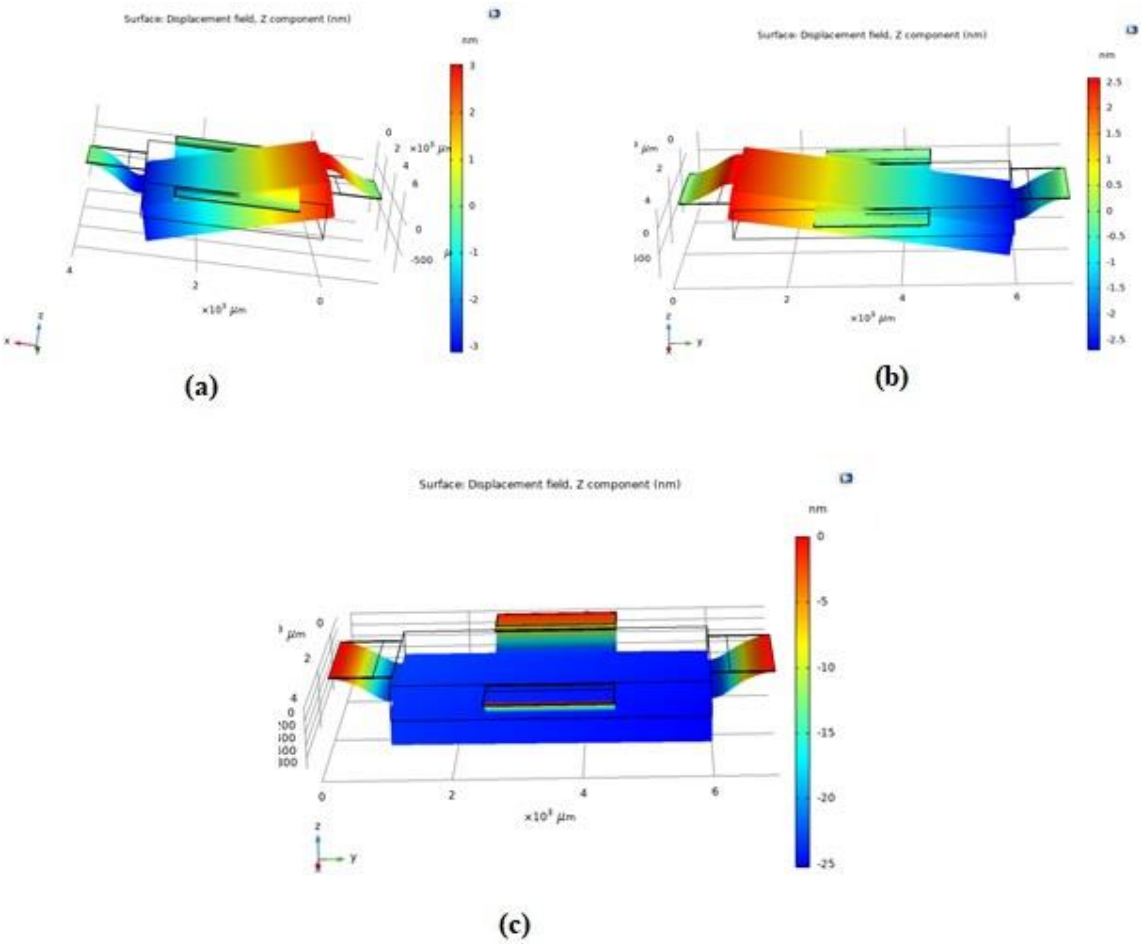

Figure 4. 31. (a)(b)(c): Shows deflection in X-axis Y-axis and Z-axis respectively

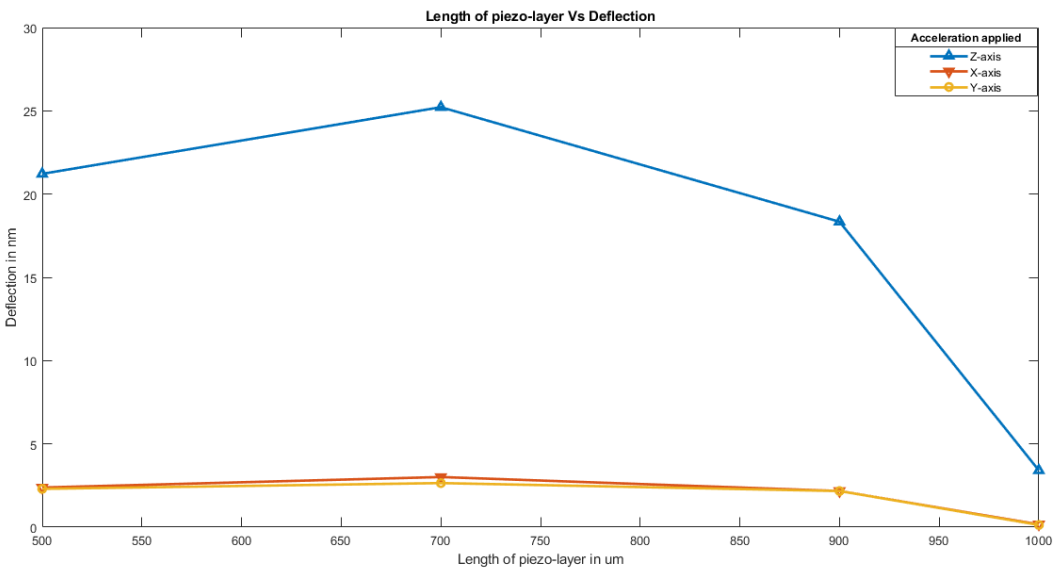

Figure 4. 32. Length of piezo-layer vs deflection in all 3-directions

Frequency

In frequency analysis it is found that the direction of the acceleration applied had no effect on the resonant frequency and is same in all three directions. Table 4.12 shows the results for Resonant frequency, figure 4.33 and figure 4.34 shows the line chart presentation of these and 3D plots of designs respectively with Changing the length piezoelectric layer (active layer) l_p.

Table 4. 12. Resonant frequency recorded during simulation in all three axes with acceleration of "g" while changing l_p (length of active layer)

No.	**Length of piezo layer in um**	**Resonant frequency in KHz in Z-axis acceleration**	**Resonant frequency in KHz in X-axis acceleration**	**Resonant frequency in KHz in Y-axis acceleration**
1	500	3.2165	Same	Same
2	700	4.1800	Same	Same
3	900	8.8530	Same	Same
4	1000	7.8427	Same	Same

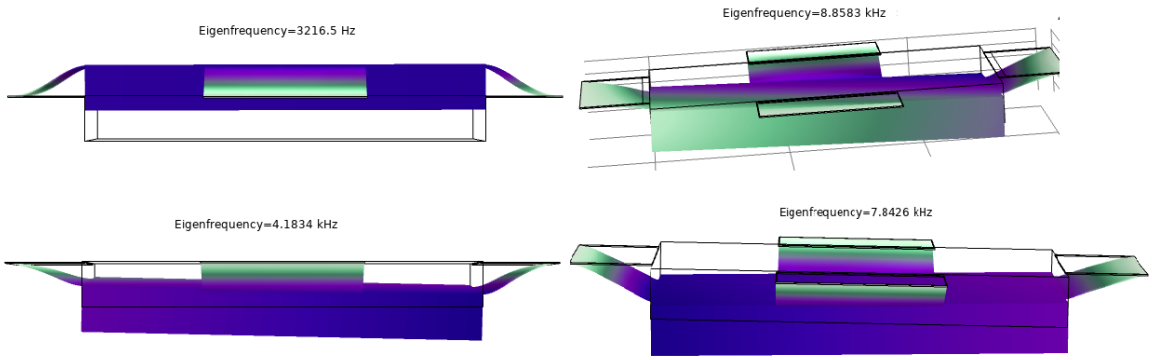

Figure 4. 33. 3D plots of the geometry at different eigenfrequencies

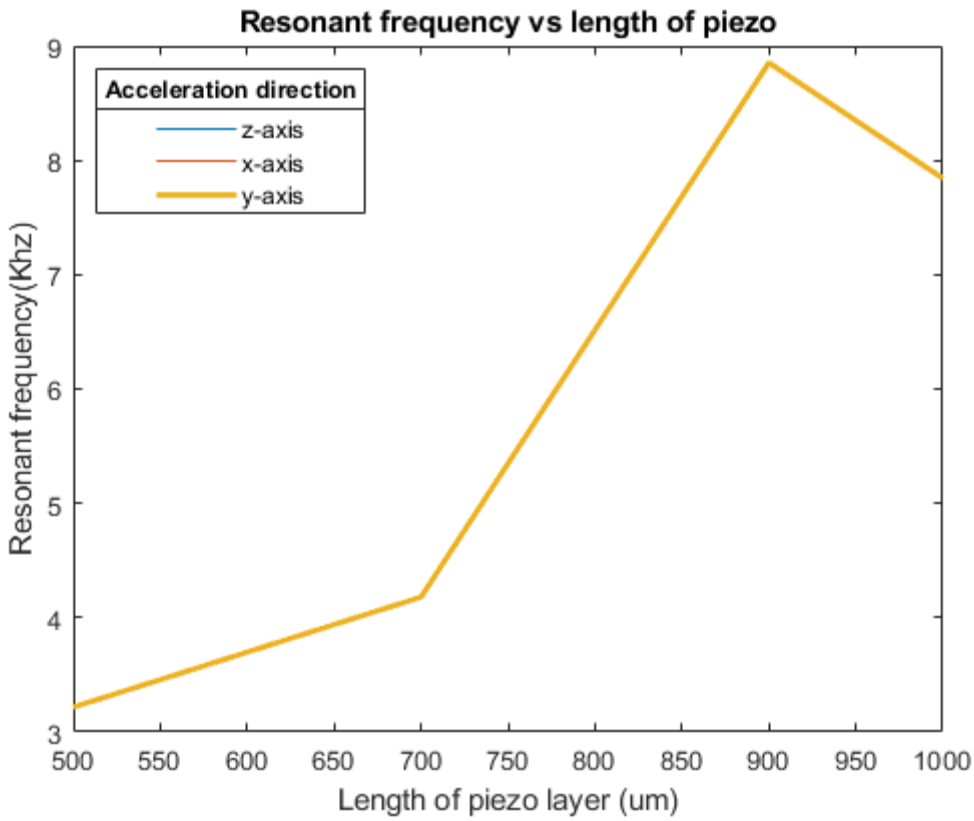

Figure 4. 34. Line chart of resonant frequency at different length of piezo layer

Voltage sensitivity

Accelerometer is simulated with Changing the length piezoelectric layer (active layer) l_p. To simulate the sensitivity of the 3-axis accelerometer we need to get the generated voltage signal from all 4 cantilever beams connected to seismic mass, Hence we named all 4 beams as X,X',Y,Y' as shown in figure 4.35 to be used as refence in further readings and kept the orientation of the geometry same throughout all sensitivity simulation phase. Table 4.13, 4.14, 4.15 shows the results for generated voltage at all 4 sensing beams with varying widths and different directional(x, y, z) acceleration of 1-g respectively . figure 4.36, 4.37, 4.38 shows 3D Electric potential plots for x, y, z direction acceleration respectively, and figure 4.39, 4.40, 4.41 shows the line chart for generated voltage while changing the length piezoelectric layer (active layer) l_p.

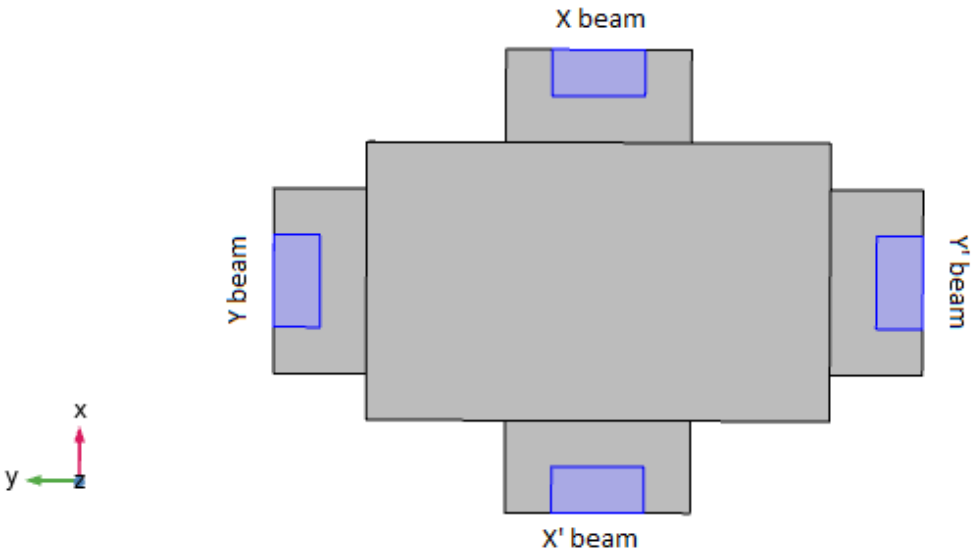

Figure 4. 35. Reference snap for sensing axis

Table 4. 13. Sensitivity recorded at all beams for x' axis acceleration of 1-g

l_p in um	X'-axis acceleration of 1 g applied (all voltages are in mV)			
	x-beam sensitivity	**x'-beam sensitivity**	**y-beam sensitivity**	**y'-beam sensitivity**
500	-0.6699	0.66784	-0.0042	0.00352
700	-0.4188	0.42525	-0.0027	-0.01202
900	-0.1711	0.18413	-0.0012	-0.00674
1000	-0.0437	0.04274	1.00e-4	-5.82e-4

Table 4. 14. Sensitivity recorded at all beams for y' axis acceleration of 1-g

l_p in um	Y'-axis acceleration of 1 g applied (all voltages are in mV)			
	x-beam sensitivity	**x'-beam sensitivity**	**y-beam sensitivity**	**y'-beam sensitivity**
500	-0.0053	-0.0085	-0.6774	0.6560
700	-0.0022	-0.0022	-0.4430	0.4347
900	-7.29e-4	0.0031	-0.1834	0.1817
1000	-4.51e-4	-3.78e-4	-6.21e-2	6.20e-2

Table 4. 15. Sensitivity recorded at all beams for z' axis acceleration of 1-g

l_p in um	Z'-axis acceleration of 1 g applied (all voltages are in mV)			
	x-beam sensitivity	**x'-beam sensitivity**	**y-beam sensitivity**	**y'-beam sensitivity**
500	-4.137	-4.1144	-5.2100	-4.9905
700	-2.6933	-2.07233	-3.3777	-3.3067
900	-1.0049	-1.0889	-1.1625	-1.1512
1000	-0.0287	-0.04325	-0.04567	-0.0691

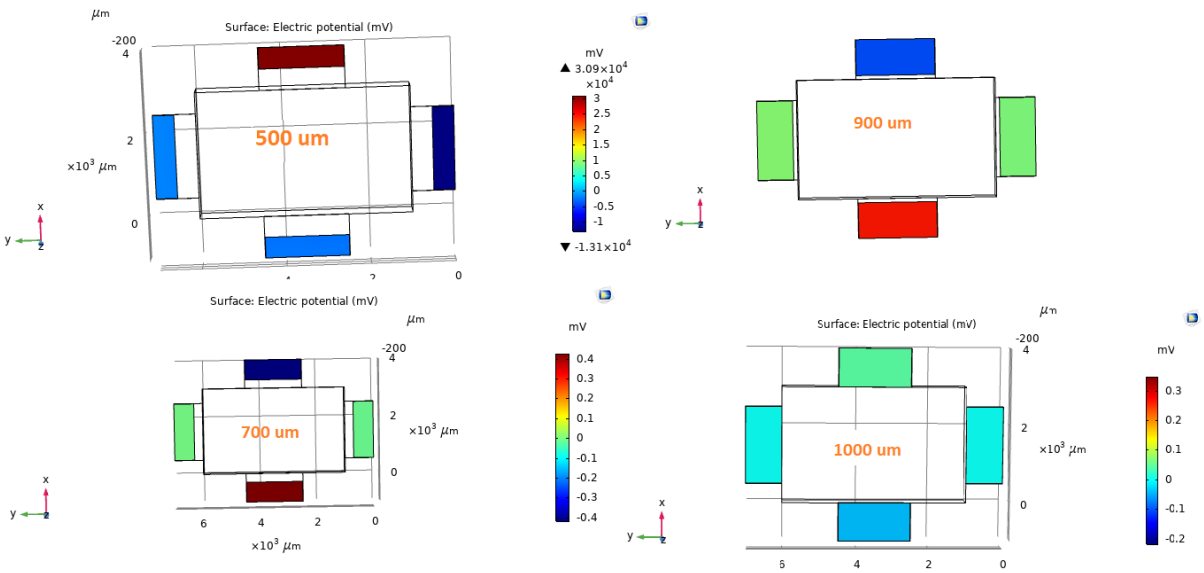

Figure 4. 36. 3D Electric potential plots for the x-direction acceleration applied

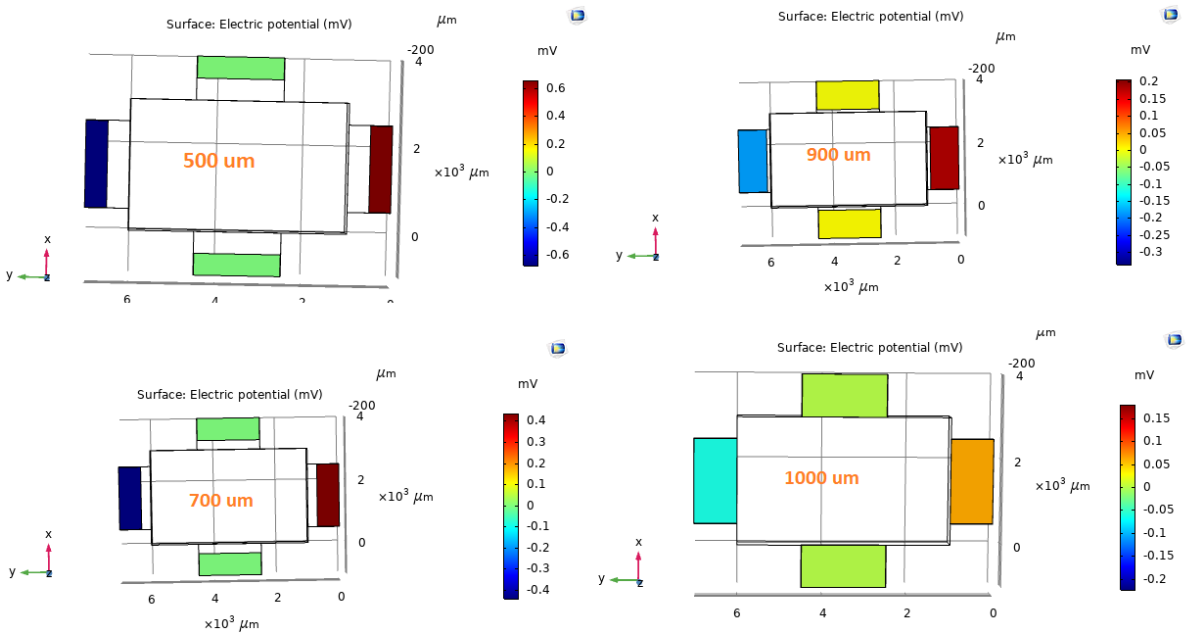

Figure 4. 37. 3D Electric potential plots for the y-direction acceleration applied

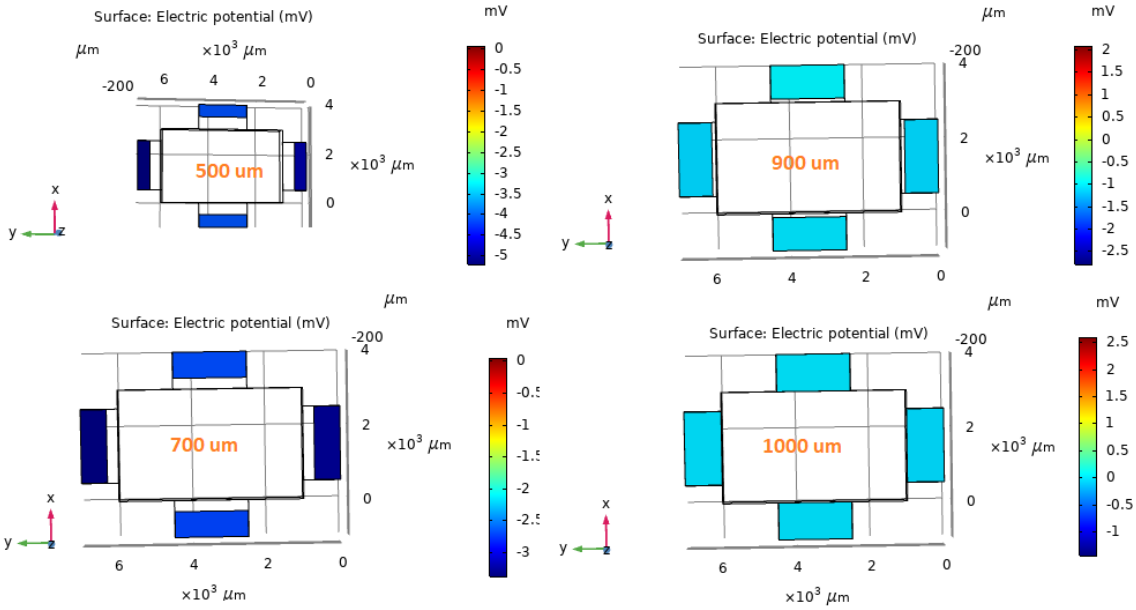

Figure 4. 38. 3D Electric potential plots for the Z-direction acceleration applied

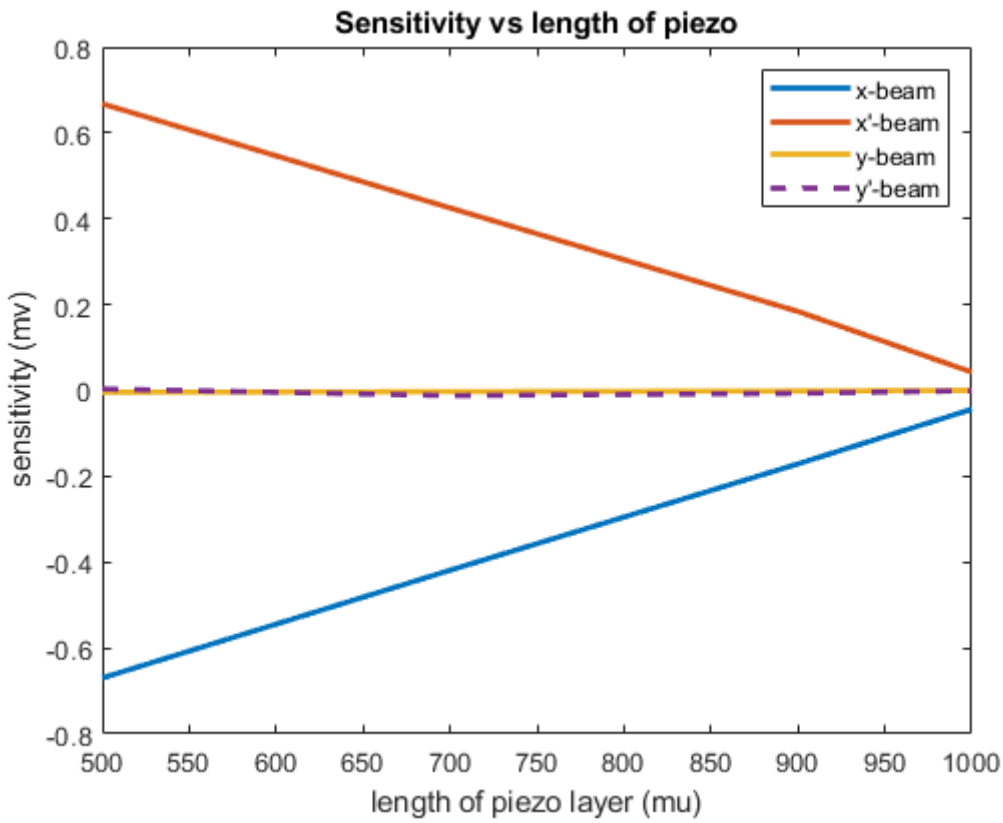

Figure 4. 39. Plot of Sensitivity recorded at all beams for x' axis acceleration of 1-g

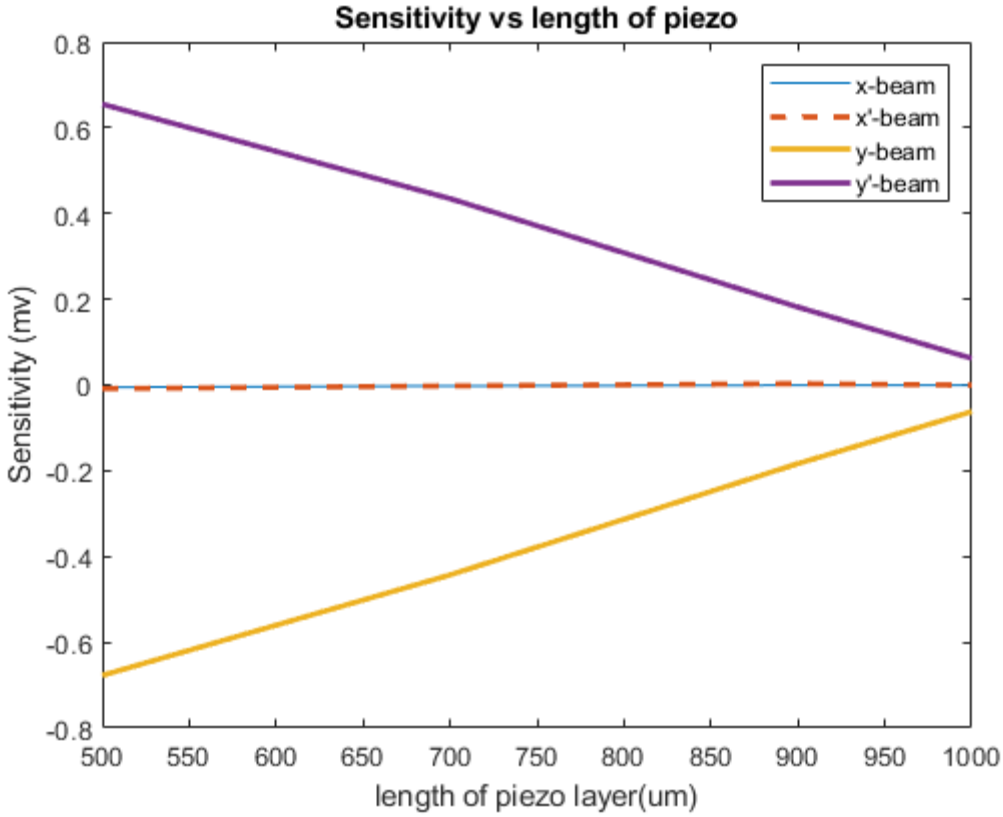

Figure 4. 40. Plot of Sensitivity recorded at all beams for y' axis acceleration of 1-g

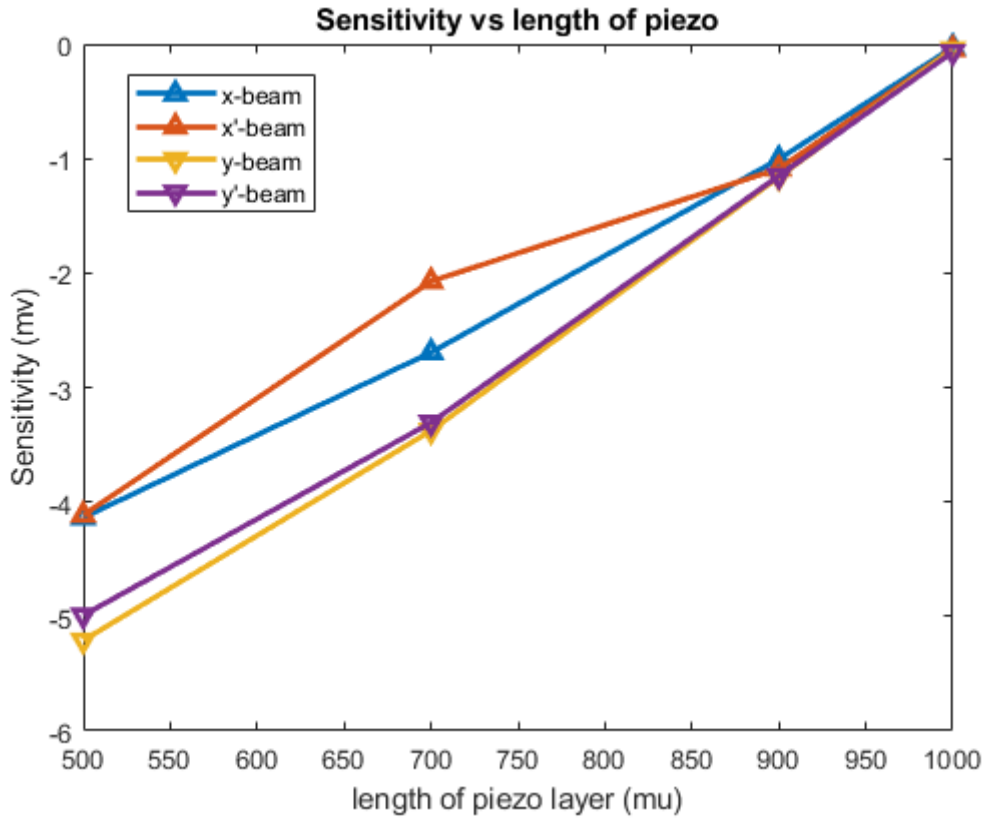

Figure 4. 41. Plot of Sensitivity recorded at all beams for Z' axis acceleration of 1-g

Case 2: Changing the width of the piezoelectric layer (active layer) w_p.

Simulation were performed with changing the width of the piezoelectric layer (active layer) w_p and an acceleration of **g** applied from either X, Y, Z-direction (from one direction at time), the response of deflection, frequency and sensitivity to the change in beam length is measured and reported.

Deflection

Deflection in the beams were analysed after every change in the width of w_p piezoelectric layer with an applied acceleration of **g** from X, Y, Z directions, respectively. Table 4.16 shows the results for deflection, figure 4.42 (a)(b)(c) shows 3D plots of design and figure 4.43 shows line grape plot for the deflection in all three directional accelerations.

Table 4. 16. Deflection against different piezo layer width at different direction acceleration g applied.

No.	**Width of piezo layer in um**	**Deflection in nm in Z-axis acceleration**	**Deflection in nm in X-axis acceleration**	**Deflection in nm in Y-axis acceleration**
1	500	38.01	5.39	4.46
2	1000	34.18	4.31	3.57
3	1500	31.34	4.30	3.68
4	1980	21.21	2.38	2.30

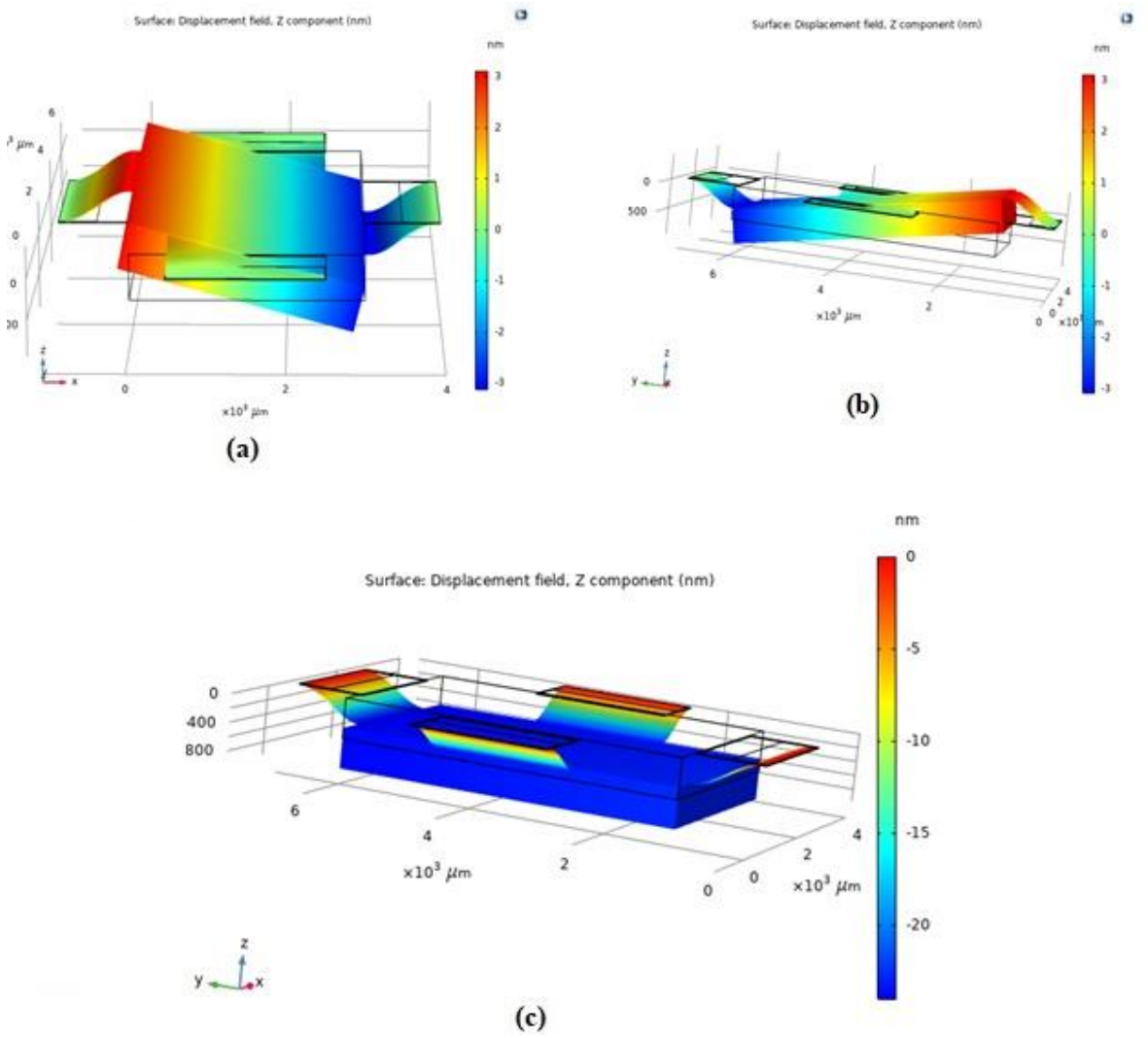

Figure 4. 42. (a)(b)(c): Shows deflection in x-axis, y-axis and z-axis respectively

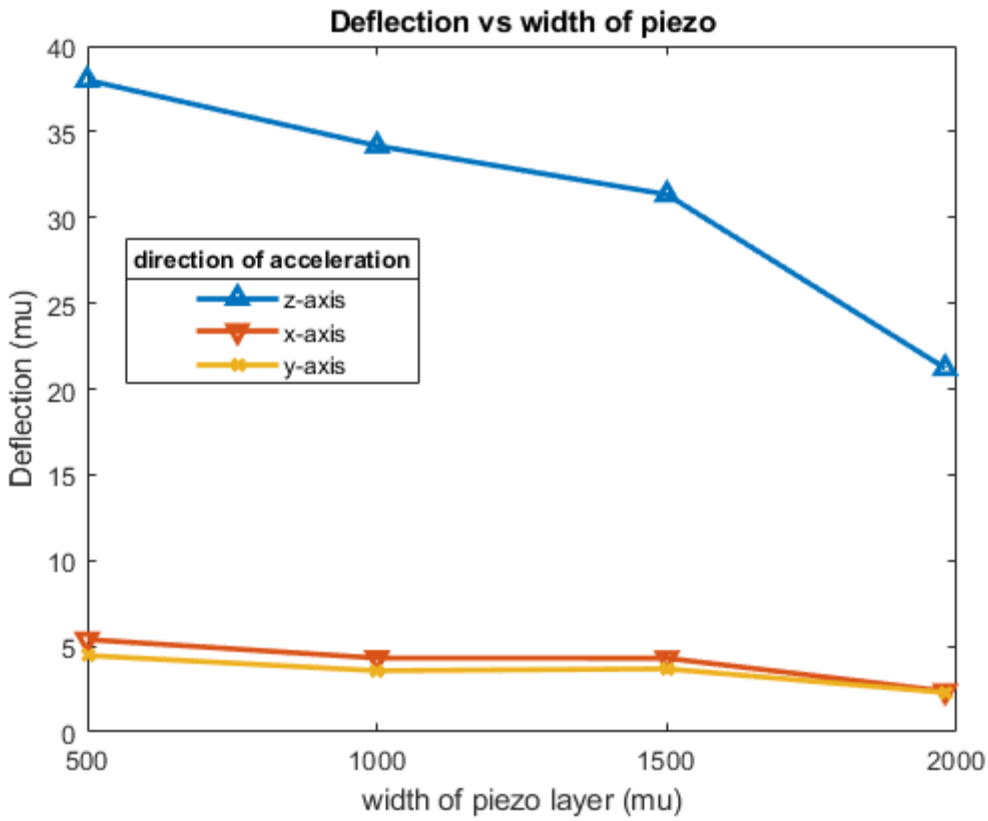

Figure 4. 43. Deflection at different piezo layer width with different direction acceleration 1-g applied.

Frequency

In frequency analysis it is found that the direction of the acceleration applied had no effect on the resonant frequency and is same in all three directions. Table 4.17 shows the results for Resonant frequency, figure 4.44 shows the 3D plots of design at different frequency and figure 4.45 shows the line chart of the resonant frequencies with Changing the width of the piezoelectric layer (active layer) w_p.

Table 4. 17. Resonant frequency recorded during simulation in all three axes with acceleration g while changing w_p (Width of active layer)

No.	Width of piezo layer in um	Resonant frequency in KHz in Z-axis acceleration	Resonant frequency in KHz in X-axis acceleration	Resonant frequency in KHz in Y-axis acceleration
1	500	2.5592	Same	Same
2	1000	2.6491	Same	Same
3	1500	2.731	Same	Same
4	1980	2.8512	Same	Same

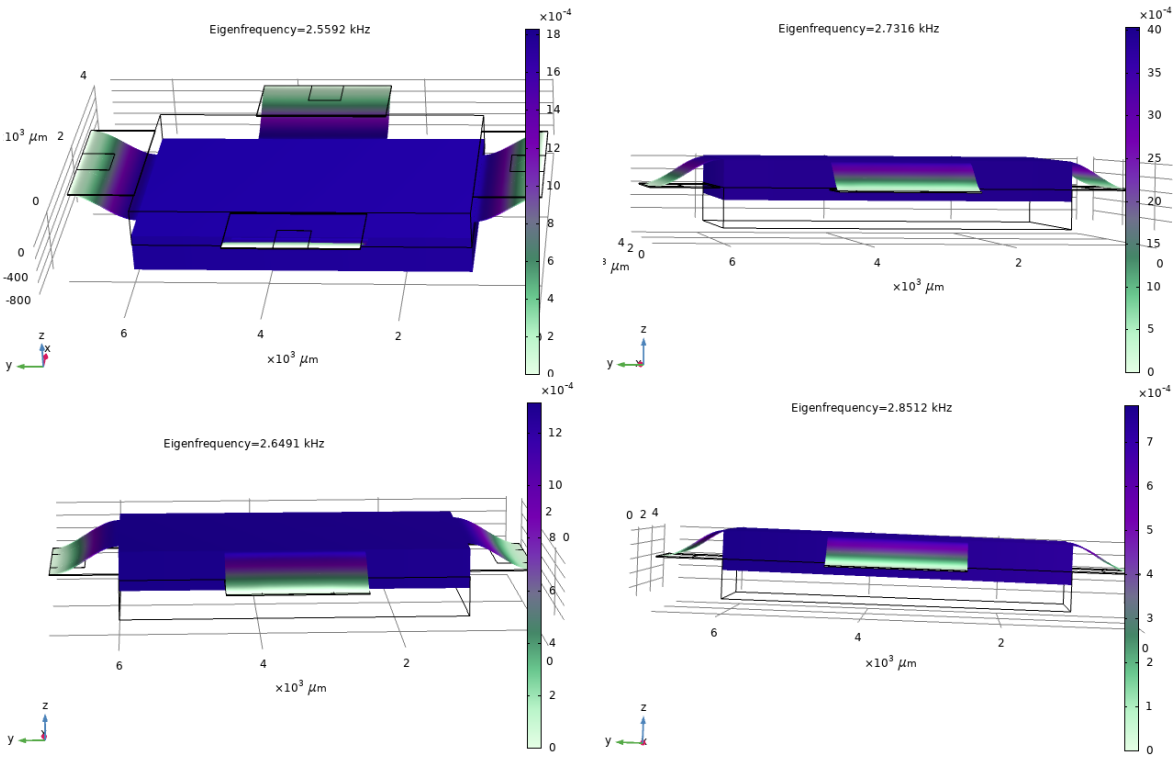

Figure 4. 44. 3D plots of the geometry at different eigenfrequencies

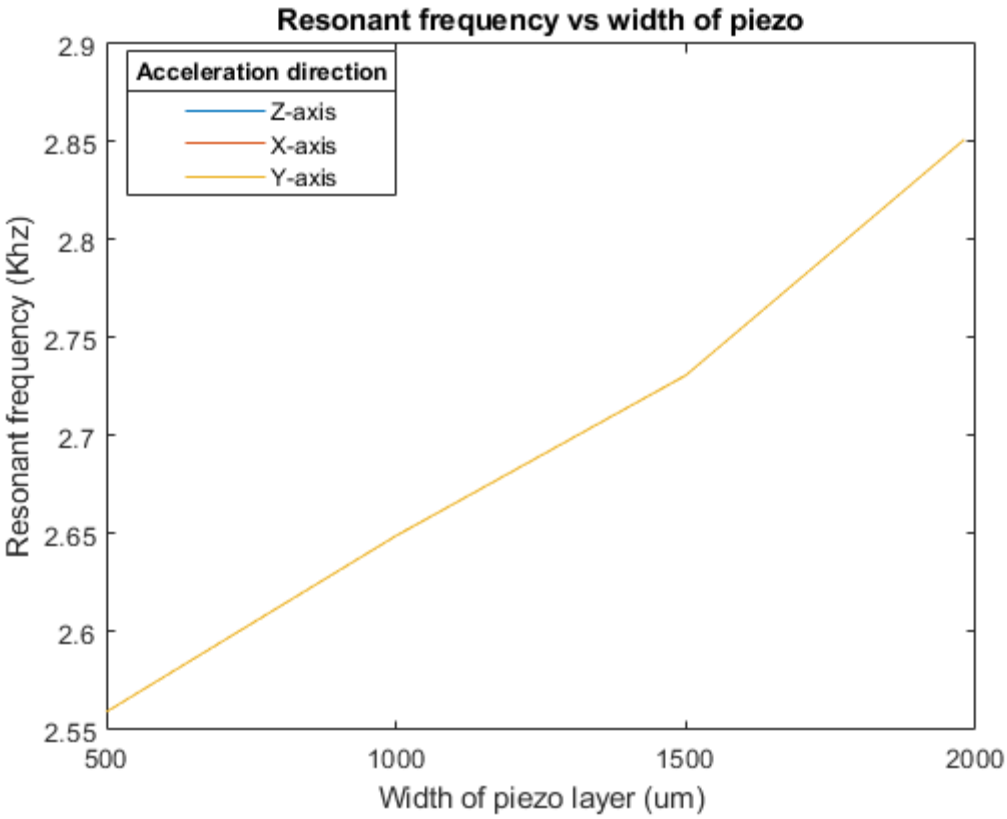

Figure 4. 45. Resonant frequency plot at all three axes acceleration of 1-g with changing width of the piezo layer

Voltage sensitivity

Accelerometer is simulated with changing the width of the piezoelectric layer (active layer) w_p.We will follow the same orientation that is discussed in voltage sensitivity analysis for the first case of the 3-axis accelerometer. Table 4.18, 4.19, 4.20 shows the results for generated voltage at all 4 sensing beams with varying widths and different directional (x, y, z) acceleration of 1-g respectively. figure 4.46, 4.47, 4.48.3 shows 3D plotted and figure 4.49, 4.50, 4.51 shows the line chart of the generated voltage while changing the width of the piezoelectric layer (active layer) w_p.

Table 4. 18. Sensitivity recorded at all beams for x' axis acceleration of 1-g

w_p in um	X'-axis acceleration of 1 g applied (all voltages are in mV)			
	x-beam sensitivity	**x'-beam sensitivity**	**y-beam sensitivity**	**y'-beam sensitivity**
500	-1.0945	1.0945	-0.00129	-0.00399
1000	-1.007	1.0493	0.00325	0.0068
1500	-0.90251	0.864411	-0.01509	-0.01099
1980	-0.66999	0.66784	-4.25e-3	3.52e-3

Table 4. 19. Sensitivity recorded at all beams for y' axis acceleration of 1-g

w_p in um	Y'-axis acceleration of 1 g applied (all voltages are in mV)			
	x-beam sensitivity	**x'-beam sensitivity**	**y-beam sensitivity**	**y'-beam sensitivity**
500	-0.00271	-6.83e-4	-1.0172	1.0145
1000	0.00676	-0.00113	-0.96849	0.95829
1500	1.41e-3	-0.00426	-0.85825	0.83458
1980	-5.33e-3	-8.56e-3	-6.77e-1	6.56e-1

Table 4. 20. Sensitivity recorded at all beams for z' axis acceleration of 1-g

w_p in um	Z'-axis acceleration of 1 g applied (all voltages are in mV)			
	x-beam sensitivity	x'-beam sensitivity	y-beam sensitivity	y'-beam sensitivity
500	-6.1112	-6.1296	-7.04756	-7.4500
1000	-5.7395	-5.9893	-7.1685	-7.1219
1500	-5.2718	-4.9978	-6.1921	-6.0324
1980	-4.137	-4.1144	-5.2100	-4.9905

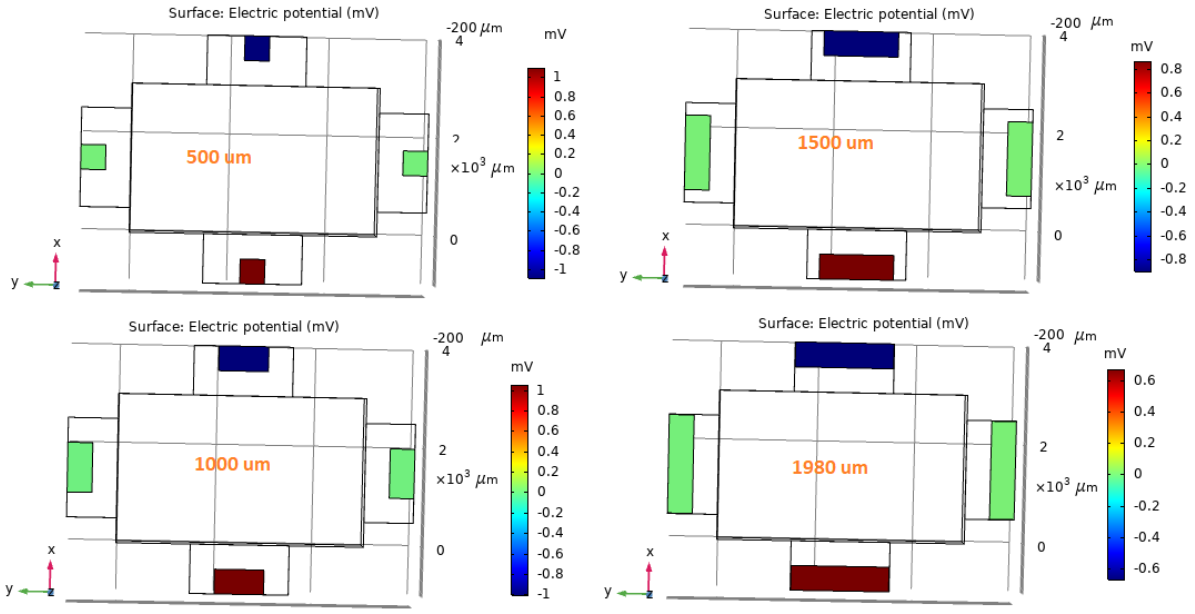

Figure 4. 46. 3D Electric potential plots for the X-direction acceleration applied

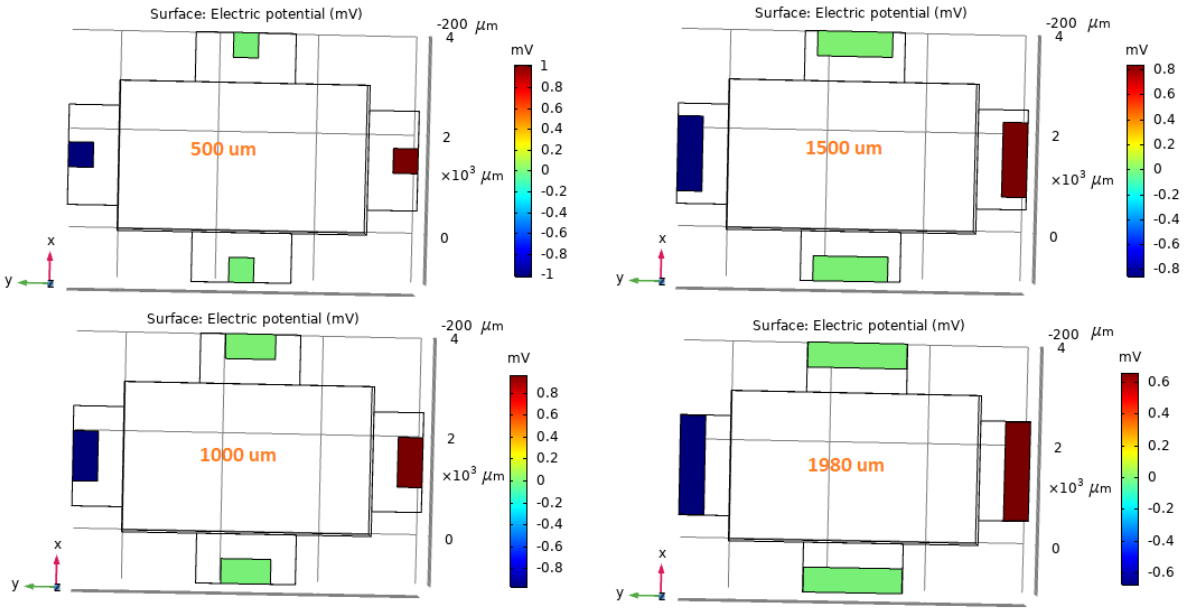

Figure 4. 47. 3D Electric potential plots for the Y-direction acceleration applied

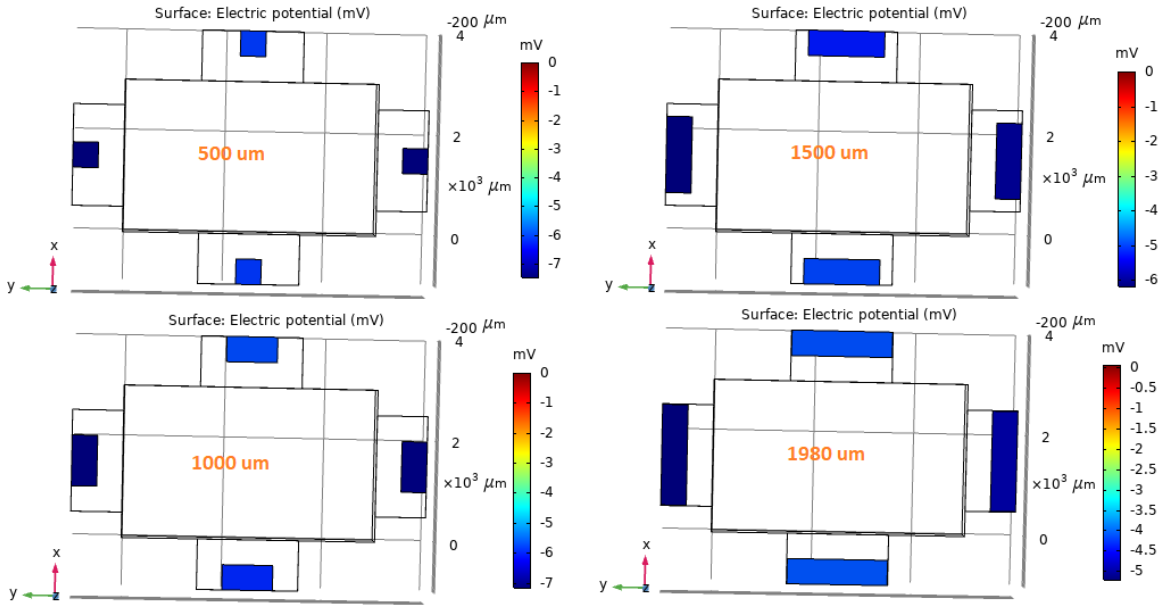

Figure 4. 48. 3D Electric potential plots for the Z-direction acceleration applied

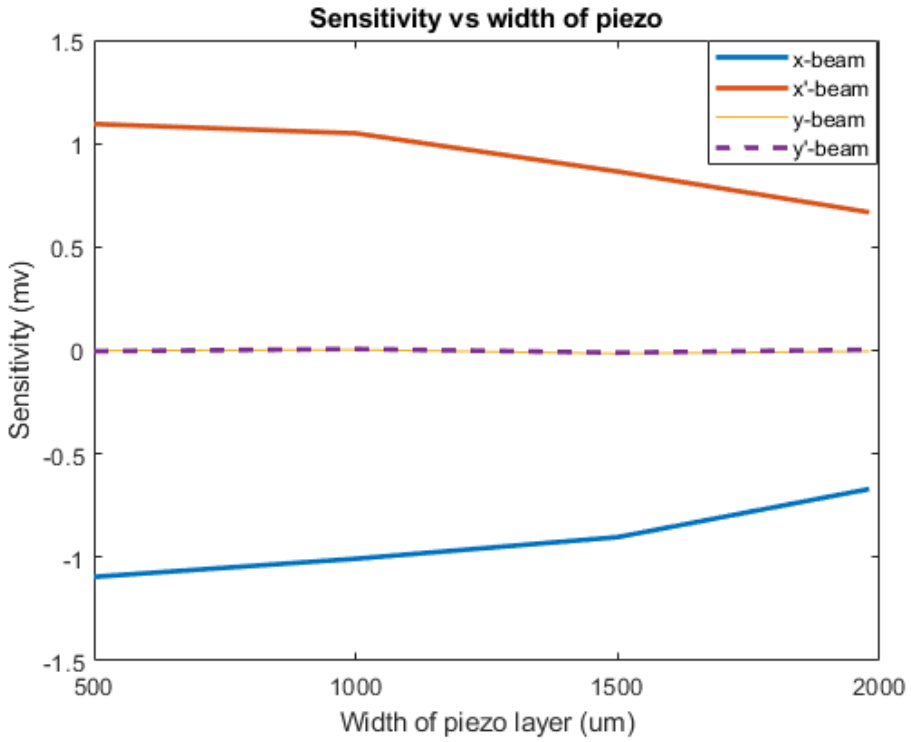

Figure 4. 49. Sensitivity recorded at all beams for x' axis acceleration of 1-g with changing width of piezo layer

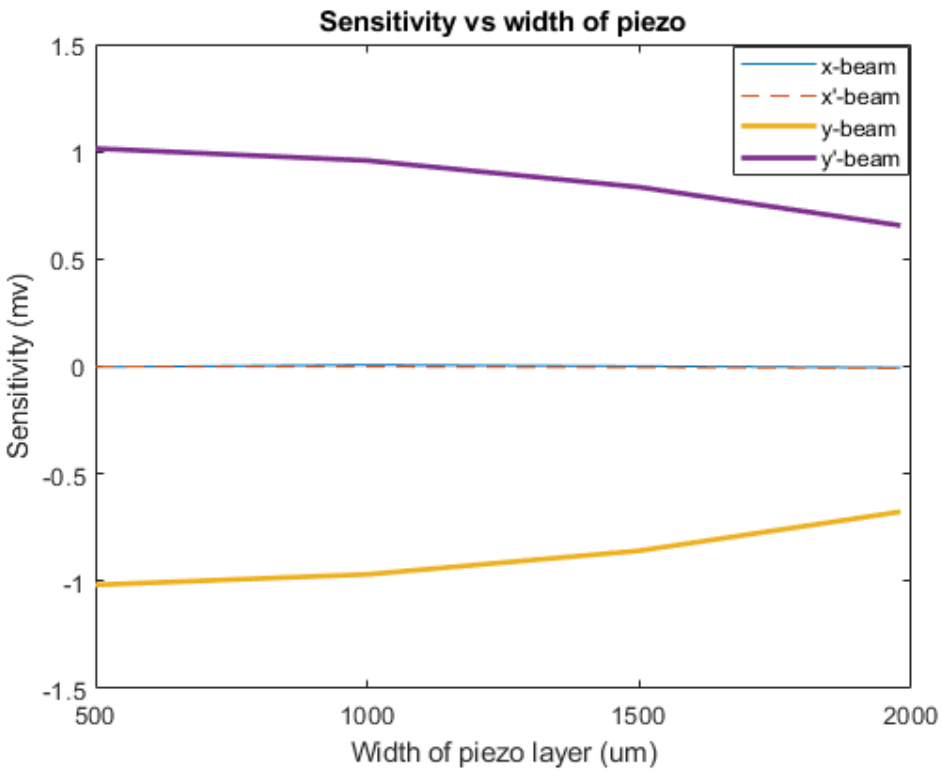

Figure 4. 50. Sensitivity recorded at all beams for y' axis acceleration of 1-g with changing width of piezo layer

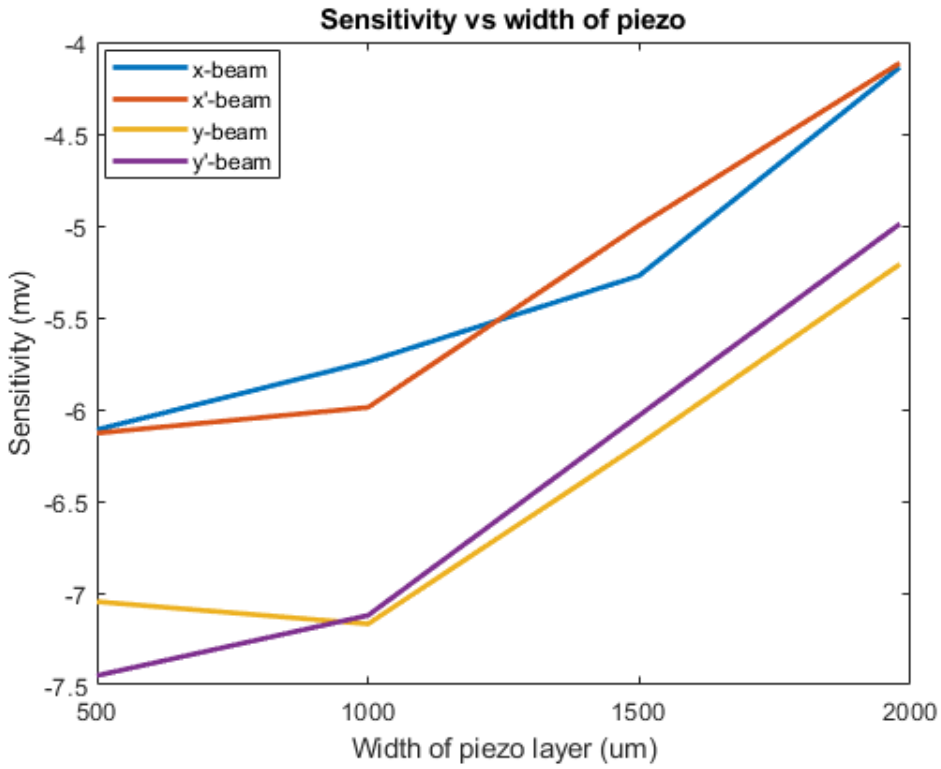

Figure 4. 51. Sensitivity recorded at all beams for z' axis acceleration of 1-g with changing width of piezo layer

5 Discussions of the mathematical and FEM models

After careful analysis and compilation of the data we got during all these different designs mathematical and FEM models analysis, the design parameters which gives us the best sensitivity along the sensing axis were noted and optimized parameters were finalized.

5.1 Single axis accelerometer optimization:

For single axis accelerometer a simple Unimorph structure of piezoelectric beam connected with a mass were selected. Analytical simulation of the design was performed with the help of MATLAB and finite element model analysis were performed using COMSOL Multiphysics.

Initial design parameters shown in table 3.1 were selected based on the lecture reviews, three parameters which are more important for the design and play a more important role in performance of the accelerometers, were selected for optimization, respectively. These parameters were

(1) l_c length of the beam substrate layer (silicon layer only).

(2) Length of the complete beam (substrate + isolation + active).

(3) w_p Width of the active layer (piezo layer).

All these three selected parameters were simulated for its different lengths and widths, while keeping the other parameters values fixed as per the table 3.1. Results obtained from mathematical modelling and FEM model simulation at different values from selected interval were then examined for the effect it has on the deflection, sensitivity and resonance frequency of the accelerometer. All three cases mentioned cases are discussed simultaneous.

Case 1

In the first case considering the "l_c length of the beam substrate layer (silicon layer only)" gives us some improvement in deflection and sensitivity with increase in length of this parameter. But the improvement in the results (table 4.1, 4.2, 4.3) that we get when compared with the cost which we pay in term of increase in the length of the "l_c" or in other term 50um increase in the size of the whole design is not significant improvement.

These simulations were performed for the optimization of this design at sensing axis (z-axis) when acceleration of "1 g" were applied in Z-axis direction. It is very important for an accelerometer to have good efficiency (sensitivity) across the sensing axis and zero (theoretically) or near zero in non-sensing axis (x-axis, y-axis). Line chart figures 4.10 and 4.3 shows the comparison of the voltage sensitivity and deflection for all three axes, and we see that the sensitivity and deflection lines for the non-sensing axis (x-axis and y-axis) are zero or every low compare to the line representing the sensing axis(z-axis). From this analysis we easily conclude that the design is good this regard, and we get a single at the sensing axis only.

Results attained from the mathematical modelling shown in table 3.2, shows a significant increase in deflection and voltage sensitivity with any increase in the beam substrate layer. And if compared with the results attained from the simulation of FEM models of the design in COMSOL there is a big disagreement between the results of both analysis although both are having same increasing pattern which is an indication of the accuracy FEM models analysis. This difference between the values is because of the number of the numeric equations used to perform the analysis in COMSOL is very high and in analytical(mathematical) analysis it is based on just one equation. From the mathematical analysis we cannot get any information on the acceleration from x and y axis and it give only on dimensional analysis.

Because of all these mentioned lacks in mathematical analysis, the reliable, more accurate and complete analysis is the FEM analysis and hence our decision of the design will mostly be based on the FEM models simulations results. And as we do not get any persuading improvement in result in this case by increasing the length of Lc, we did not change the initial selected value as per table 3.1 and go on to study l_c with the l_p in second scenario for simulation of the single axis accelerometer.

Case 2

"Length of the complete beam (substrate +isolation + active)" was considered for the second case of the single axis accelerometer simulation where we do change the length of the whole beam or in other words parameter l_c and l_p are kept at same length. The simulations were performed in the same environment and with same parameter values (table 3.1), but this time the length of the whole composite beam is changing with the same values, so if we increase the length of the beam it means both the "l_c" and "l_p" length increase with same value.

After studying of the results (table 4.4 4.6) we attained from the FEM models simulation performed for the second scenario of single axis accelerometer. It is observed that the effect of the increase in length of the beam had resulted in increase of the deflection of design. and continued an approximate 2.8um increase in deflection with every 50um increase in length of the beam starting from 150um (initial guess) till 350um.

While on other side when we examined the result attained for voltage sensitivity, we observed an extremely small but a decrease in generated signal from 200um till 350um with every increase of 50um, but we noticed slight increase in signal when we decrease the length from 200um to 150um. Acceleration from none sensing axis (x-axis and y-axis) were also simulated in this case, which are reported in the same table 4.4,4.6 and are also plot in line chart 4.3,4.10 for clear demonstration and all are found to approximately zero or very low compare to the sensing axis(z-axis).

From mathematical model analysis the results shown in table 3.3, if we make comparison with the FEM analysis this time the results for the deflections are in the same increasing pattern but the for the generated voltage, we noticed that the pattern is also not exactly matching. Beside the other reasons mentioned in the first case there are possibilities that the mathematical equations used for this modelling is lacking some other parameters which can cause these problems and with a better and more complex equation model this result might improve.

So, from the study of the results of the second scenario based upon the FEM analysis we concluded that we could decrease the length of the beam from 200um to 150um and we can reduce the size of the device, use of material and cost also, while having a good impact on the performance.

Case 3

"w_p or width of the active layer (piezo layer) was the parameter that was simulated in third scenario of the single axis accelerometer design optimization. All other parameters were kept fixed to value according to the table 3.1, but the values of "l_p" length of piezo and "l_c" length of substrate or in other words length of the beam which was 200um in table 3.1 were reduced to 150um as we optimized in the second case of our analysis that it promises good results.

The design was simulated with different width of the piezo-layer and achieved results were reported in the table 4.7,4.9. After thorough study of the extracted results of the simulation, it is noticed that increase in the initial value 2500 um (from table 3.1) of the width of piezo-layer results in a decrease in the efficiency of the device while any decrease in the width of the piezo-layer cause an increase in efficiency. Hence, we get the best result at 1000um width of the piezo layer.

For the non-sensing axis acceleration, the very same procedure to first two cases were followed and found to be zero or very less in comparison to the sensing axis signals, which can also be seen from the line chart figures 4.19, 4.26. Mathematical analysis for third case is not really of any help as we do not have any representation for w_p in modelled equation and hence it has no effect on the results.

From third case we get the conclusion that we need to reduce the width of the piezo layer from 2500um to 1000um to get good efficiency and reduce the use of the piezo material and hence a decrease in the overall cost of the device. After all this simulations and analysis of the results we can now finalise our design parameters, the final optimized table of the design parameters would be

Table 5. 1. Final optimized parameters for single axis accelerometer.

Letter	Representation description	Values
l_c	Length of the cantilever (Silicon layer)	150 μm
t_c	Thickness of the cantilever (Silicon layer)	20 μm
w_c	Width of the cantilever (Silicon layer)	3000 μm
l_p	Length of the AlN (active layer)	150 μm
w_p	Width of AlN (active layer)	1000 μm
t_p	Thickness of AlN (active layer)	0.6 μm
l_m	Thickness of Si mass (proof mass)	570 μm
w_m	Width of Si mass (proof mass)	3000 μm
l_m	Length of Si mass (proof mass)	5000 μm
m	Mass	20 mg
a_z	Acceleration	9.8 m/s^2
f	Frequency	586 Hz
V	Voltage sensitivity	1.04 mv
d	deflection	10.44 nm

5.2 Three-axis accelerometer optimization

For the optimization of the 3-axis accelerometer parameters two major parameters "l_p" length of the piezo layer and "w_p" width of the piezo layer were selected to be simulated at different value of the parameters and its impact on the efficiency of the accelerometers to be examined. The reliabilities and ineffectiveness of mathematical model analysis performed for the single axis accelerometer, and considering the complexity of the design of the 3-axis accelerometer is was almost impossible to model an equation for this design and which is can be used to perform this complex analysis, or maybe if possible it is beyond the scope of the thesis. So, for three axis accelerometer analysis we only relied on the FEM model-based analysis and no mathematical modelling is performed for this design.

Case 1

Changing "l_p" length of the piezo layer: In the first case, accelerometer was designed at different lengths of the piezo layer "l_p" with all other parameter used according to the table 4.10 and was simulated under the different directional acceleration applied. The attained result for the deflection in design are reported in table 4.11 and plotted as line chart in figure 4.32. while studying the attained results we noticed a significant increase in the deflection when we increase the length of piezo layer from 500um to 700um. But after that any further increase in the length of the ‘’l_p’’was causing sharp decrease in the deflection efficiency of the design for all three-axis acceleration simulation, this sharp decrease is also very clearly visible on the line chart plotted in figure 4.32.

For the sensitivity analysis we need to get signal from all four beam of the design to identify the direction of the acceleration. For that purpose, we named every beam with an individual name x, x’, y, y' as shown in the figure 4.35, and kept the same orientation of the design for whole analysis of sensitivity of three axis for both cases.

While studying the effect of the change in "l_p" on the sensitivity of the generated voltage, it is noticed that decrease in the initially selected length "l_p =1000um"(table 4.10) of the piezo layer had caused increase in the sensitivity of the design, the pattern is same for all three axis directional accelerations and we get the best sensitivity at the length of 500 um.

For the acceleration from x'-axis, our sensing beams(terminals) are x and x' and we get strong signal at these two terminals which are approximately equal in magnitudes but are opposite in direction as reported in table 4.13 and line chart plotted figure 4.39, while we get no signal at the non-sensing axis(terminals) y, y'. Similarly, for the acceleration from y' direction we get strong signal at y, y' beams(terminals) and no signal at x, x' beams, as reported in table 4.14 and plotted in line chart figure 4.40. But for the acceleration from Z'-axis we get a strong signal on all four beams(terminals) namely x, x', y, y', as reported in table 4.15 and plotted in line chart figure 4.41.

So, from analysis of the first case of the three-axis accelerometer we can conclude that the length of the "l_p" which was choosed to be 1000um initially should be reduced to get 500um to get better performance and reduce the size and cost of the device at same time.

Case 2

Changing "w_p" width of piezo layer: In the second case of the simulation for the tri-axial accelerometer, the geometry was design according to the table 4.10, but for the "l_p" " length of the piezo layer the value was used as per the finding of the first case. Starting with the discussion of deflection's results attained during the simulation while changing the width of the piezo layer, we notice an increase in the deflection with decrease in the width of the piezo layer for all three-axis directional acceleration applied as reported in table 4.16. Initial value for "w_p" from table 4.10 which was the 1980um but if we decrease the width, we get better efficiency, smaller size and less cost. The achieved results are plotted in line chart figure 4.43 and the 3D geometry plot for all three directions are shown in figure 4.42.

For the study of the generated voltage sensitivity in this case, again we use figure 4.35 as reference for the beams(terminal) signal and use the same orientation of the geometry. Examining the tables 4.18,4.19,4.20 for x, y, z axis directional acceleration, yet again we see the same increasing pattern for the sensitivity with any decrease in the width of the piezo layer. We get the best efficiency for all three-axis acceleration at width of 500um.

Figures 4.49, 4.50, 4.51 shows us the line chart of the signal we get at every terminal(beam) for each different acceleration, and it clearly shows a strong signal at x, x' for x-axis acceleration, at y, y' for y-axis acceleration and for the z-axis acceleration a strong signal at all four beams(terminal) x, x', y, y'. From the second simulation case we get the conclusion that width of the piezo layer should also be fixed at the 500um instead of the 1980um which was initially guess of the parameter. So, now we can have the final optimized table of the triaxial accelerometer.

Table 5. 2. Final optimized parameters for three-axis accelerometer.

Letter	Representation description	Values
l_c	Length of the cantilever (Silicon layer)	500 μm
t_c	Thickness of the cantilever (Silicon layer)	15 μm
w_c	Width of the cantilever (Silicon layer)	2000 μm
l_p	Length of the AlN (active layer)	500 μm
w_p	Width of AlN (active layer)	500 μm
t_p	Thickness of AlN (active layer)	0.6 μm
l_m	Thickness of Si mass (proof mass)	570 μm
w_m	Width of Si mass (proof mass)	3000 μm
l_m	Length of Si mass (proof mass)	5000 μm
m	Mass	24 mg
a_z	Acceleration	9.8 m/s^2
f	Frequency	2.5KHz
v_x	Voltage sensitivity at terminal x, x' with X-axis acceleration	1.09 mv
v_y	Voltage sensitivity at terminal y, y' with Y-axis acceleration	1.01 mv
v_z	Voltage sensitivity at terminal x, x' and y, y' with Z-axis acceleration	6.11 mv (x, x') 7.4 mv (y, y')
d_x	Deflection with x-axis acceleration	38.01 nm
d_y	Deflection with y-axis acceleration	5.39 nm
d_z	Deflection with z-axis acceleration	4.46 nm

6 Conclusion and Future Work

Accelerometers are electromechanical inertial sensors which has many useful applications in the field of consumer electronics, smart electronics systems, military equipment and some life critical applications in medical field. The main goal of this work was to design and optimise piezoelectric material base MEMS single and three axis accelerometers. Because the research was supposed to be performed on the piezoelectric materials which do not pose any harm to human health, the selection of the AlN (aluminium nitride) a Lead (pb) free piezoelectric was one of the important and critical decision of this research.

This work can be divided into to two main categories, single axis accelerometer design and optimization and tri-axial accelerometer design and optimization, although both types of accelerometers optimizations and design process are tightly linked to each other. Three critical design parameters were selected for single axis and two for the tri-axial accelerometer. Total of 23 geometrical structures were design; 15 geometrical structures were design for single axis and rest of 8 were design for the 3-axis during the whole simulations process.

For single axis accelerometer both mathematical and FEM analysis were performed, while for the three-axis accelerometer only the FEM analysis were performed, due to the complexity of geometrical design and ineffective of the mathematical analysis for the single axis it was not performed for case of three axis accelerometer. Chosen critical parameters were optimised with gravitational acceleration (gravity force), and optimised design parameters were identified with the help of the reported simulations. For single axis accelerometer the critical design parameters length of beam (substrate + active layer) l_c,l_p are 150 μm and width of the beam active layer w_p is 1000 μm , voltage sensitivity on sensing axis was 1.04mv, deflection in beam was 10.44nm and 586Hz eigenfrequency was recorded.

Tri-axial accelerometer critical design parameters length of each beam (substrate + active layer) l_c,l_p was 500 μm and the width of the beam active layer w_p is 500 μm. Deflection for x, y, z axis acceleration of g was 38.01 nm, 5.39 nm, 4.46nm, as the voltage signal for the x, y axis acceleration is only on their respective sensing beams so it was recorded to be 1.09 mv and 1.01 mv and for y axis acceleration both directional beams collect a signal hence we got 6.11 mv at x-directional and 7.40 mv at y-directional beams, while the eigenfrequency was recorded to be 2.5 KHz.

6.1 Future Work

The research has optimized all the design parameters for the single and three axis accelerometers. The results from this thesis can be used in the fabrication of the test devices in ordered to verify the examine the outcomes. Also, as for now the 6-axis accelerometer is made of the integration of the 3-axis accelerometer and 3-axis gyroscope, there is a need for research for standalone 6-axis accelerometer, for that the 3-axis design presented in this thesis can be a starting point.

Bibliography

[1] F. Chollet and H. Liu, *A (not so) short introduction to MEMS*, no. September. 2011.

[2] D. Sparks *et al.*, "Embedded MEMS-based concentration sensor for improved active fuel cell performance," *TRANSDUCERS EUROSENSORS '07 - 4th Int. Conf. Solid-State Sensors, Actuators Microsystems*, pp. 1911–1914, 2007, doi: 10.1109/SENSOR.2007.4300532.

[3] J. M. Darmanin *et al.*, "Development of a High-G Shock Sensor Based on MEMS Technology for Mass-Market Applications," *Inert. 2019 - 6th IEEE Int. Symp. Inert. Sensors Syst. Proc.*, pp. 2019–2022, 2019, doi: 10.1109/ISISS.2019.8739763.

[4] C. Maj and M. Szermer, "Influence of Fringing Fields on Parallel Plate Capacitance for Capacitive MEMS Accelerometers," *2020 IEEE 16th Int. Conf. Perspect. Technol. Methods MEMS Des. MEMSTECH 2020 - Proc.*, pp. 82–85, 2020, doi: 10.1109/MEMSTECH49584.2020.9109500.

[5] H. Yanazawa and K. Homma, "Growing market of MEMS and technology development in process and tools specialized to MEMS," *2017 IEEE Electron Devices Technol. Manuf. Conf. EDTM 2017 - Proc.*, vol. 1, no. 2, pp. 143–144, 2017, doi: 10.1109/EDTM.2017.7947543.

[6] M. K. Mishra, V. Dubey, P. M. Mishra, and I. Khan, "MEMS Technology: A Review," *J. Eng. Res. Reports*, vol. 4, no. 1, pp. 1–24, 2019, doi: 10.9734/jerr/2019/v4i116891.

[7] T. K. Sethuramalingam and A. Vimalajuliet, "Design of MEMS based capacitive accelerometer," *ICMET 2010 - 2010 Int. Conf. Mech. Electr. Technol. Proc.*, no. Icmet, pp. 565–568, 2010, doi: 10.1109/ICMET.2010.5598424.

[8] Z. Mohammed, I. (Abe) M. Elfadel, and M. Rasras, "Monolithic multi degree of freedom (MDoF) capacitive MEMS accelerometers," *Micromachines*, vol. 9, no. 11, pp. 1–20, 2018, doi: 10.3390/mi9110602.

[9] C. Sun, M. Tsai, Y. Liu, and W. Fang, "Implementation of a Monolithic Single," *IEEE*

Trans. Electron Devices, vol. 57, no. 7, pp. 1670–1679, 2010.

[10] R. Amarasinghe, D. V. Dao, T. Toriyama, and S. Sugiyama, "Development of miniaturized 6-axis accelerometer utilizing piezoresistive sensing elements," *Sensors Actuators, A Phys.*, vol. 134, no. 2, pp. 310–320, 2007, doi: 10.1016/j.sna.2006.05.044.

[11] A. Albarbar, S. Mekid, A. Starr, and R. Pietruszkiewicz, "Suitability of MEMS accelerometers for condition monitoring: An experimental study," *Sensors*, vol. 8, no. 2, pp. 784–799, 2008, doi: 10.3390/s8020784.

[12] M. Yu *et al.*, "A Two-Axis MEMS Piezoresistive In-Plane Accelerometer with Pure Axially Deformed Microbeams," *Proc. IEEE Sensors*, vol. 2018-October, pp. 4–7, 2018, doi: 10.1109/ICSENS.2018.8589746.

[13] K. Hari, I. R. Praveenkrishna, and V. Seena, "Piezoresistive Si MEMS accelerometer with novel nonplanar flexures for low cross axis sensitivity," *2016 3rd Int. Conf. Emerg. Electron. ICEE 2016*, pp. 5–8, 2017, doi: 10.1109/ICEmElec.2016.8074618.

[14] S. K. Reguieg, Z. Ghemari, and T. Benslimane, "Extraction of the relative sensitivity model and improvement of the piezoelectric accelerometer performances," *2018 Int. Conf. Signal, Image, Vis. their Appl. SIVA 2018*, pp. 1–5, 2019, doi: 10.1109/SIVA.2018.8661159.

[15] G. L. Luo and D. A. Horsley, "Piezoelectric Micromachined Ultrasonic Transducers with Corrugated Diaphragms Using Surface Micromachining," *2019 20th Int. Conf. Solid-State Sensors, Actuators Microsystems Eurosensors XXXIII, TRANSDUCERS 2019 EUROSENSORS XXXIII*, no. June, pp. 841–844, 2019, doi: 10.1109/TRANSDUCERS.2019.8808774.

[16] R. Mukherjee, J. Basu, P. Mandal, and P. K. Guha, "A review of micromachined thermal accelerometers," *J. Micromechanics Microengineering*, vol. 27, no. 12, 2017, doi: 10.1088/1361-6439/aa964d.

[17] T. Liu, C. Chu, M. H. Li, and C. Liu, "CMOS-MEMS THERMAL-PIEZORESISTIVE OSCILLATORS WITH HIGH TRANSDUCTION EFFICIENCY FOR MASS SENSING APPLICATIONS Institute of NanoEngineering and MicroSystems , National Tsing Hua University , Hsinchu , Taiwan Department of Power Mechanical Engineering

, Nati," *TRANSDUCERS 2017 - 19th Int. Conf. Solid-State Sensors, Actuators Microsystems*, pp. 452–455, 2017, [Online]. Available: https://doi.org/10.1109/TRANSDUCERS.2017.7994084%0Ahttps://ieeexplore.ieee.org/document/7994084.

[18] E. L. W. Gardner, T. A. Vincent, A. De Luca, and F. Udrea, "Comparison of Thermo-Resistive and Thermo-Electronic Transduction Methods in Thermal Flow Sensors," *2019 20th Int. Conf. Solid-State Sensors, Actuators Microsystems Eurosensors XXXIII, TRANSDUCERS 2019 EUROSENSORS XXXIII*, no. June, pp. 2084–2087, 2019, doi: 10.1109/TRANSDUCERS.2019.8808660.

[19] H. Zhang *et al.*, "Theoretical and experimental study on optical fiber microseismic accelerometer based on cantilever beam structure," *2019 18th Int. Conf. Opt. Commun. Networks, ICOCN 2019*, no. 3, pp. 2019–2021, 2019, doi: 10.1109/ICOCN.2019.8934417.

[20] M. Ahmadian, K. Jafari, and M. J. Sharifi, "Novel graphene-based optical MEMS accelerometer dependent on intensity modulation," *ETRI J.*, vol. 40, no. 6, pp. 794–801, 2018, doi: 10.4218/etrij.2017-0309.

[21] Y. Bao, F. Zhou, T. W. Lebrun, and J. J. Gorman, "A photonic MEMS accelerometer with a low-finesse hemispherical microcavity readout," *Int. Conf. Opt. MEMS Nanophotonics*, pp. 5–6, 2017, doi: 10.1109/OMN.2017.8051490.

[22] E. Soltanian, K. Jafari, and K. Abedi, "A novel differential optical MEMS accelerometer based on intensity modulation, using an optical power splitter," *IEEE Sens. J.*, vol. 19, no. 24, pp. 12024–12030, 2019, doi: 10.1109/JSEN.2019.2936752.

[23] A. Abbasi, "Application of Piezoelectric Materials and Piezoelectric Network for Smart Roads," *Int. J. Electr. Comput. Eng.*, vol. 3, no. 6, pp. 857–862, 2013, doi: 10.11591/ijece.v3i6.4588.

[24] M. Jean, F. Rouchon, M. M. Ronkowski, M. L. Petit, I. Lyon, and M. Slawomir Wiak, "Concept, implementation and analysis of the piezoelectric resonant sensor/actuator for measuring the aging process of human skin," 2016, [Online]. Available: http://oatao.univ-toulouse.fr/16248/1/Sienkiewicz_Lukasz.pdf.

[25] S. Priya, “Advances in energy harvesting using low profile piezoelectric transducers,” *J. Electroceramics*, vol. 19, no. 1, pp. 165–182, 2007, doi: 10.1007/s10832-007-9043-4.

[26] J. Fialka and P. Benes, “Comparison of methods for the measurement of piezoelectric coefficients,” *IEEE Trans. Instrum. Meas.*, vol. 62, no. 5, pp. 1047–1057, 2013, doi: 10.1109/TIM.2012.2234576.

[27] S. B. Kim, H. Park, S. H. Kim, H. C. Wikle, J. H. Park, and D. J. Kim, “Comparison of MEMS PZT cantilevers based on d31 and d 33 modes for vibration energy harvesting,” *J. Microelectromechanical Syst.*, vol. 22, no. 1, pp. 26–33, 2013, doi: 10.1109/JMEMS.2012.2213069.

[28] L. J. Gong, B. Ju, G. J. Xiao, and Z. H. Feng, “Equivalent circuit for unloaded triple-layer piezoelectric cantilevers,” *Proc. 2014 Symp. Piezoelectricity, Acoust. Waves Device Appl. SPAWDA 2014*, no. February 2016, pp. 345–350, 2014, doi: 10.1109/SPAWDA.2014.6998596.

[29] S. H. Kim, S. Ju, C. H. Ji, and S. J. Lee, “Equivalent circuit model of an impact-based piezoelectric energy harvester,” *J. Phys. Conf. Ser.*, vol. 557, no. 1, 2014, doi: 10.1088/1742-6596/557/1/012094.

[30] J. Lu *et al.*, “Piezoelectric MEMS devices and its application as bio-chemical sensors,” *8th Annu. IEEE Int. Conf. Nano/Micro Eng. Mol. Syst. IEEE NEMS 2013*, vol. 1, no. 2, pp. 163–166, 2013, doi: 10.1109/NEMS.2013.6559705.

[31] D. L. DeVoe and A. P. Pisano, “Surface micromachined piezoelectric accelerometers (PiXLs),” *J. Microelectromechanical Syst.*, vol. 10, no. 2, pp. 180–186, 2001, doi: 10.1109/84.925733.

[32] Q. Zou, W. Tan, E. S. Kim, and G. E. Loeb, “Single- and triaxis piezoelectric-bimorph accelerometers,” *J. Microelectromechanical Syst.*, vol. 17, no. 1, pp. 45–57, 2008, doi: 10.1109/JMEMS.2007.909100.

[33] S. Naduvinamani and N. C. Iyer, “Design and simulation of PZT based MEMS piezoelectric accelerometer,” *Int. Conf. Electr. Electron. Optim. Tech. ICEEOT 2016*, pp. 3715–3721, 2016, doi: 10.1109/ICEEOT.2016.7755403.

[34] J. Yang *et al.*, “A T-Shape Aluminum Nitride Thin-Film,” vol. 28, no. 5, pp. 776–781, 2019.

[35] H. Zhou, R. H. Han, M. H. Xu, and H. Guo, “Study of a piezoelectric accelerometer based on d33 mode,” *Proc. 2016 Symp. Piezoelectricity, Acoust. Waves Device Appl. SPAWDA 2016*, pp. 61–65, 2017, doi: 10.1109/SPAWDA.2016.7829957.

[36] Y. Wang, H. Ding, X. Le, and J. Xie, “A MEMS piezoelectric in-plane resonant accelerometer with two-stage micro-leverage mechanism,” *2016 IEEE 11th Annu. Int. Conf. Nano/Micro Eng. Mol. Syst. NEMS 2016*, pp. 455–459, 2016, doi: 10.1109/NEMS.2016.7758289.

[37] G. Vigevani, F. T. Goericke, A. P. Pisano, I. I. Izyumin, and B. E. Boser, “Microleverage DETF Aluminum Nitride resonating accelerometer,” *2012 IEEE Int. Freq. Control Symp. IFCS 2012, Proc.*, pp. 754–757, 2012, doi: 10.1109/FCS.2012.6243634.

[38] M. Y. Chao, A. Ali, S. Ghosh, and J. E. Lee, “AN ALUMINUM NITRIDE ON SILICON RESONANT MEMS ACCELEROMETER Department of Electronic Engineering , City University of Hong Kong , Kowloon , HONG KONG State Key Lab of Millimeter Waves , City University of Hong Kong , Kowloon , HONG KONG,” vol. 2, pp. 8–11, 2017.

[39] R. H. Han, J. Y. Wang, M. H. Xu, and H. Guo, “Design of a tri-axial micro piezoelectric accelerometer,” *Proc. 2016 Symp. Piezoelectricity, Acoust. Waves Device Appl. SPAWDA 2016*, pp. 66–70, 2017, doi: 10.1109/SPAWDA.2016.7829958.

[40] C. C. Hindrichsen, N. S. Almind, S. H. Brodersen, O. Hansen, and E. V. Thomsen, “Analytical Model of a PZT Thick-Film Triaxial Accelerometer for Optimum Design,” *IEEE Sens. J.*, vol. 9, no. 4, pp. 419–429, 2009, doi: 10.1109/JSEN.2009.2014412.

[41] X. Gong, C.-T. Chen, W.-J. Wu, and W.-H. Liao, “A high sensitivity piezoelectric MEMS accelerometer based on aerosol deposition method,” vol. 1097026, no. March 2019, p. 89, 2019, doi: 10.1117/12.2514224.

[42] L. P. Wang *et al.*, “Design, fabrication, and measurement of high-sensitivity piezoelectric microelectromechanical systems accelerometers,” *J. Microelectromechanical Syst.*, vol. 12, no. 4, pp. 433–439, 2003, doi:

10.1109/JMEMS.2003.811749.

[43] M. B. E.Varadrajan, “Design and Simulation of Unimorph Piezoelectric E nergy H arvesting S ystem,” *2013 COMSOL Conf. Bangalore*, pp. 1–6, 2013.

[44] R. H. Olsson, K. E. Wojciechowski, M. S. Baker, M. R. Tuck, and J. G. Fleming, “Post-CMOS-compatible aluminum nitride resonant MEMS accelerometers,” *J. Microelectromechanical Syst.*, vol. 18, no. 3, pp. 671–678, 2009, doi: 10.1109/JMEMS.2009.2020374.

[45] L. P. Wang *et al.*, “Sputtered AlN thin films for piezoelectric MEMS devices,” *Proc. IEEE Sensors*, pp. 10–13, 2006, doi: 10.1109/ICSENS.2007.355705.

[46] N. Sinha *et al.*, “Piezoelectric aluminum nitride nanoelectromechanical actuators,” *Appl. Phys. Lett.*, vol. 95, no. 5, 2009, doi: 10.1063/1.3194148.

[47] Иые, “No Titleывмывмыв,” *Ятыатат*, vol. вы12у, no. 235, p. 245, 2007.

[48] M. A. Fraga, H. Furlan, R. S. Pessoa, and M. Massi, “Wide bandgap semiconductor thin films for piezoelectric and piezoresistive MEMS sensors applied at high temperatures: An overview,” *Microsyst. Technol.*, vol. 20, no. 1, pp. 9–21, 2014, doi: 10.1007/s00542-013-2029-z.

[49] C. G. Hindrichsen, R. Lou-Møller, K. Hansen, and E. V. Thomsen, “Advantages of PZT thick film for MEMS sensors,” *Sensors Actuators, A Phys.*, 2010, doi: 10.1016/j.sna.2010.05.004.

[50] M. D. Durruthy-Rodríguez, J. Costa-Marrero, M. Hernández-García, F. Calderón-Piñar, and J. M. Yañez-Limón, “Photoluminescence in ‘hard’ and ‘soft’ ferroelectric ceramics,” *Appl. Phys. A Mater. Sci. Process.*, vol. 98, no. 3, pp. 543–550, 2010, doi: 10.1007/s00339-009-5501-y.

[51] E. Silveira, J. A. Freitas, S. B. Schujman, and L. J. Schowalter, “AlN bandgap temperature dependence from its optical properties,” *J. Cryst. Growth*, vol. 310, no. 17, pp. 4007–4010, 2008, doi: 10.1016/j.jcrysgro.2008.06.015.

[52] F. Gerfers *et al.*, “Sputtered AlN Thin Films for Piezoelectric MEMS Devices - FBAR Resonators and Accelerometers,” *Solid State Circuits Technol.*, no. January, 2010, doi:

10.5772/6887.

Appendix 1 – Non-exclusive licence for reproduction and publication of a graduation thesis[1]

I Waqas Rashid

1. Grant Tallinn University of Technology free licence (non-exclusive licence) for my thesis "Piezoelectric Based MEMS Accelerometer Design and Optimization", supervised by Mehadi Hassan Ziko (Ph.D.).
   1.1. to be reproduced for the purposes of preservation and electronic publication of the graduation thesis, incl. to be entered in the digital collection of the library of Tallinn University of Technology until expiry of the term of copyright;
   1.2. to be published via the web of Tallinn University of Technology, incl. to be entered in the digital collection of the library of Tallinn University of Technology until expiry of the term of copyright.
2. I am aware that the author also retains the rights specified in clause 1 of the non-exclusive licence.
3. I confirm that granting the non-exclusive licence does not infringe other persons' intellectual property rights, the rights arising from the Personal Data Protection Act or rights arising from other legislation.

04.01.2021

1 The non-exclusive licence is not valid during the validity of access restriction indicated in the student's application for restriction on access to the graduation thesis that has been signed by the school's dean, except in case of the university's right to reproduce the thesis for preservation purposes only. If a graduation thesis is based on the joint creative activity of two or more persons and the co-author(s) has/have not granted, by the set deadline, the student defending his/her graduation thesis consent to reproduce and publish the graduation thesis in compliance with clauses 1.1 and 1.2 of the non-exclusive licence, the non-exclusive license shall not be valid for the period.